IN SILICO STUDIES OF CANNABINOIDS TARGETING COX-2 AND CB2 RECEPTORS FOR ANTI-INFLAMMATORY DRUG DESIGN

BY

WATCHARIN KUMAEUM

A THESIS SUBMITTED IN PARTIAL FULFILLMENT OF THE REQUIREMENTS FOR THE DEGREE OF MASTER OF SCIENCE (CHEMISTRY)

DEPARTMENT OF CHEMISTRY

FACULTY OF SCIENCE AND TECHNOLOGY

THAMMASAT UNIVERSITY

ACADEMIC YEAR 2024

IN SILICO STUDIES OF CANNABINOIDS TARGETING COX-2 AND CB2 RECEPTORS FOR ANTI-INFLAMMATORY DRUG DESIGN

BY

WATCHARIN KUMAEUM

A THESIS SUBMITTED IN PARTIAL FULFILLMENT OF THE REQUIREMENTS FOR THE DEGREE OF MASTER OF SCIENCE (CHEMISTRY)

DEPARTMENT OF CHEMISTRY

FACULTY OF SCIENCE AND TECHNOLOGY

THAMMASAT UNIVERSITY

ACADEMIC YEAR 2024

THAMMASAT UNIVERSITY
FACULTY OF SCIENCE AND TECHNOLOGY

THESIS

BY

WATCHARIN KUMAEUM

ENTITLED

IN SILICO STUDIES OF CANNABINOIDS TARGETING COX-2 AND CB2 RECEPTORS FOR ANTI-INFLAMMATORY DRUG DESIGN

was approved as partial fulfillment of the requirements for the degree of Master of Science (Chemistry)

on November 26, 2024

Chairman _____
(Associate Professor Yuthana Tantirungrotechai, Ph.D.)

Member and Advisor _____
(Assistant Professor Panichakorn Jaiyong, Ph.D.)

Member _____
(Associate Professor Piyarat Nimmanpipug, Ph.D.)

Dean _____
(Associate Professor Supet Jirakajohnkool, Ph.D.)

Thesis Title	IN SILICO STUDIES OF CANNABINOIDS TARGETING COX-2 AND CB2 RECEPTORS FOR ANTI-INFLAMMATORY DRUG DESIGN
Author	Watcharin Kumaeum
Degree	Master of Science (Chemistry)
Department/Faculty/University	Chemistry Faculty of Science and Technology Thammasat University
Thesis Advisor	Assistant Professor Panichakorn Jaiyong, Ph.D.
Academic Year	2024

ABSTRACT

Phytocannabinoids have been studied for their medicinal purposes. This study examines their binding affinity to cyclooxygenase-2 (COX-2) and cannabinoids receptor type 2 (CB2), which are key therapeutic targets for inflammation. Semiempirical quantum mechanical (SQM) approaches hold promise for accurately describing noncovalent interactions in protein–ligand complexes, though calculating binding free energy for large complexes remains challenging. In this research, molecular docking simulations using AutoDock4 were initially employed to sampling ligand poses. False negative errors generated by AutoDock4 for non-steroidal anti-inflammatory drugs (NSAIDs) were identified using GFN2-xTB, a tight-binding SQM method. This approach, coupled with the ALPB solvation model, was used to compute the binding free energy of fully relaxed receptor-cannabinoid complexes in implicit aqueous solvation. This study also reports the performance of selected SQM methods in modeling noncovalent interaction of benchmark datasets. In addition to the solvation effect, thermostatistical contributions were included to obtain a more accurate binding free energy ($\Delta G_{\text{bind,solv}}$). Results showed that non-psychoactive acid derivatives such as cannabichromenic acid (CBCA), cannabinolic acid (CBNA), and cannabielsoic acid (CBEA) exhibited strong affinities for COX-2 and CB2. To enhance their anti-inflammatory potency, a sulfonamide group was incorporated to interact with Arg499 of COX-2. This modification of the CBCA analog yielded a novel anti-inflammatory

compound with a computed binding free energy of −48.41 kcal/mol for COX-2, which is lower than that of celecoxib (−32.02 kcal/mol), a known NSAID. The predicted drug-like properties of the modified cannabinoid analogs provide valuable insights for developing novel oral anti-inflammatory leads.

Keywords*:* tight-binding semiempirical quantum mechanical method, molecular docking, noncovalent interactions, anti-inflammation, cannabinoids, binding free energy

ACKNOWLEDGEMENTS

I would like to express the deepest appreciation to my advisor, Assistant Professor Dr. Panichakorn Jaiyong for the opportunity to me to do interesting research. The completion of this thesis could not have been possible without his invaluable guidance, continuous support, motivation, kindness, and encouragement.

I would like to thank the thesis committees, Associate Professor Dr. Yuthana Tantirungrotechai in Department of Chemistry, Faculty of Science and Technology, Thammasat University for their knowledge and good comments throughout the study.

I also would like to thank the external committee, Associate Professor Dr. Piyarat Nimmanpipug, in Department of Chemistry, Faculty of Science, Chiang Mai University for their encouragement and constructive comments.

I am truly grateful for the scholarship for talent student to study graduate program in Faculty of Science and Technology Thammasat University, Contract No. TB 23/2020.

Finally, I would like to thank my family for encouraging me to follow my dreams and I would like to thank my friends for sharing experiences.

Watcharin Kumaeum

TABLE OF CONTENTS

LIST OF TABLES

LIST OF FIGURES

LIST OF ABBREVIATIONS

Symbols/Abbreviations	Terms
Δ^9-THC	Delta-9-tetrahydrocannabinol
$\Delta G'_{bind,solv}$	Uncorrected binding free energy
$\Delta G_{bind,solv}$	Corrected binding free energy
µM	Micromolar
Å	Angstrom
ALPB	Analytical linearized Poisson-Boltzmann model
AM11542	Tetrahydrocannabinol
BE	Binding energy
CB1	Cannabinoid receptor type 1
CB2	Cannabinoid receptor type 2
CBC	Cannabichromene
CBD	Cannabidiol
CBDA	Cannabidiolic acid
CBE	Cannabielsoin
CBG	Cannabigerol
CBL	Cannabicyclol
CBN	Cannabinol
CBT	Cannabitriol
CNS	Human central nervous system
COX-1	Cyclooxygenase-1
COX-2	Cyclooxygenase-2
D	Dispersion correction
DFTB3	Density functional tight binding method version 3
D_{MAX}	Maximum deviation
D_{MIN}	Minimum deviation

Symbols/Abbreviations	**Terms**
ECS	Endocannabinoid system
E_{vac}	Total gas-phase energy
FEP	Free energy perturbation
$G_{complex}$	Free energy of complex
GCPRs	G-protein coupled receptors
GFN2-xTB	Acronym for geometries, frequencies, and noncovalent interactions version 2
GFN-FF	GFN force-field
G_{ligand}	Free energy of ligand
$T\Delta S_{mRRHO}$	Thermostatistical contribution
$G_{receptor}$	Free energy of receptor
H	Hydrogen bonding correction
HBA	Hydrogen bond acceptors
HBD	Hydrogen bond donors
IC_{50}	Half-maximal inhibitory concentration
IE	Interaction energy
K_i	Inhibitory constants
LogP	Partition coefficient
MAD	Mean absolute deviation
MD	Molecular dynamics
MM	Molecular mechanics
MM/GBSA	Molecular mechanics generalized Born surface area
MM/PBSA	Molecular mechanics Poisson–Boltzmann surface areas
mRRHO	Modified rigid-rotor-harmonic-oscillator approximation
MSE	Mean signed error
Mw	Molecular weigh

Symbols/Abbreviations	**Terms**
nM	Nanomolar
NSAIDs	Non-steroidal anti-inflammatory drugs
PDB	Protein databank
PGE_2	Prostaglandins
PGI_2	Prostacyclin
QM	Quantum mechanical method
RMSD	Root mean square deviation
RMSE	Root mean square errors
SI	Selectivity index
SQM	Semiempirical quantum mechanical
WIN55 212-2	Aminoalkylindole derivative
X	Halogen bonding correction
δG_{solv}	Solvation free energy

CHAPTER 1
INTRODUCTION

1.1 Statement of the problem

Cyclooxygenases play a role in producing prostaglandins (PGE_2) and prostacyclin (PGI_2) for inflammation. There are two isoforms of cyclooxygenase, cyclooxygenase-1 (COX-1) and cyclooxygenase-2 (COX-2) [1, 2]. The patterns of expression of both COX isoforms are different. COX-1 is a housekeeping enzyme expressed in many tissues whereas COX-2 is a key therapeutic target for inflammation [3]. Although the crystal structures of the COX-1 and COX-2 are similar and share 60% identical sequences of amino acid, the active site of both receptors is partially different. COX-1 and COX-2 contain three different residues of amino acid in the active site. COX-1 is bordered by Ile523 and His513, while COX-2 is surrounded by Val523 and Arg513 [4]. According to the protein structure of COX-2 (PDB code: 3LN1, as explored in this study), the valine and arginine residues are, respectively, numbered 509 and 499 [5].

Non-steroidal anti-inflammatory drugs (NSAIDs) are commonly used to treat pain and inflammation by inhibiting COX enzymes. Based on selectivity, diclofenac, ibuprofen, flurbiprofen, and naproxen are non-selective NSAIDs, inhibiting both COX-1 and COX-2. Aspirin is COX-1 selective NSAID whereas celecoxib is COX-2 selective NSAID [6]. However, traditional NSAIDs have gastrointestinal and renal adverse effects in humans [7]. Morphine derived from the opium plant has previously been used as an alternative to synthetic drugs for treating severe pain [8]. Recent evidence indicates that cannabis could be an alternative to opium usage for the treatment of chronic pain due to its fewer risks and side effects [9]. Thus, developing a new inhibitor that can bind to a particular COX isoform with less adverse effects has been a challenge.

Cannabis contains almost a hundred phytocannabinoids, including the psychoactive delta-9-tetrahydrocannabinol (Δ^9-THC) and the non-psychoactive cannabidiol (CBD) [10]. Recently, cannabis has been legalized for medicinal purposes. CBD has been used to treat inflammatory bowel diseases such as Crohn's disease [11].

The half-maximal inhibitory concentration (IC_{50}) of Δ^9-THC, CBD, cannabidiolic acid (CBDA), and cannabigerol (CBG) on COX-2 receptor has been reported in a millimolar unit [12]. Additionally, it has been mentioned that cannabinoids are interrelated with the endocannabinoid system (ECS), including cannabinoid receptor type 1 (CB1) and cannabinoid receptor type 2 (CB2) [13]. CB1 is found in the human central nervous system (CNS) and linked to the psychotropic effects of Δ^9-THC [14], while CB2 plays a role in the inflammatory response without the psychoactivity [15]. The inhibitory constants (K_i) of cannabinoids with CB2 receptors in a nanomolar unit has been reported in the previous study [16]. Nevertheless, the use of cannabinoids as a pure substance for medical treatment is limited due to the complexity of their mechanisms of action at a cellular level. This process not only requires advanced analysis tools and laboratory studies, but also consumes the time for drug development. Therefore, computational studies have emerged as a promising approach for investigating protein–ligand binding affinities.

Noncovalent interactions, e.g., dispersion, hydrogen bonding, halogen bonding, salt bridge, and π–π stacking, play a role in the binding affinity of protein–ligand complexes [17]. A common technique for exploring the binding affinity of protein–ligand interaction is molecular docking. The success of docking approaches relies on both search algorithm and scoring function [18, 19]. The binding affinities of docking poses are estimated and ranked by the scoring function. The scoring functions, including the force field-based, knowledge-based, and empirical scoring functions, are available in various docking engines [20]. Discriminating between false-positive and false-negative docking results, as well as identifying the correct ones, remains a significant challenge for docking techniques [21].

Semiempirical quantum mechanical (SQM) methods offer the advantage of reducing computational costs while improving the quantitative description of noncovalent interactions through empirical corrections for dispersion and hydrogen-bonding interactions. PM6-DH2 method has shown promise by accurately reproducing interaction energies for noncovalent geometries obtained from high-level quantum mechanical calculations [22] and identifying correct binding modes and bioactive conformations of bound ligands [23]. Furthermore, the development of the atom pairwise D3H4 formalism has enhanced the robustness of SQM methods, with errors

lower than 1 kcal/mol for benchmark datasets [24, 25]. Notably, a tight-binding semiempirical quantum mechanical method, GFN2-xTB, including the electrostatic and exchange-correlation Hamiltonian terms without specific corrections has reported a small error of noncovalent interaction energies for different benchmark sets [26]. The use of SQM potentials as scoring functions are still challenging due to solvation effects.

Solvation plays a key role in protein–ligand interactions for many biochemical applications and has a strong impact on the calculation of binding free energies. Free energy perturbation (FEP) [27] has the highest accuracy in calculating the accurate binding free energy but is computationally costly and difficult to converge a large number of the protein–ligand complexes. Alternatively, molecular mechanics Poisson–Boltzmann surface areas (MM/PBSA) [28] and molecular mechanics generalized Born surface areas (MM/GBSA) [29] are low computational cost while providing the approximate binding free energy with whole protein–ligand complexes. Notably, SQM methods have shown the performance for calculating the binding free energy in thousands of atoms of protein–ligand complexes with low-time-cost and good accuracy. With the implementation of COSMO solvation model, both PM6-D3H4X and DFTB3-D3H4X methods have demonstrated reductions in the occurrence of false-positive ligand poses in diverse classes of protein–ligand complexes [30]. GFN force-field (GFN-FF) method [31] and GBSA solvation model has simulated the dynamics of a met-myoglobin mutant and reproduces the experimental EPR-distance measurements excellently [31]. GFN-FF method has performed good performance in whole protein–ligand complexes, considering Pearson correlation coefficient (r_p) [32]. Furthermore, GFN2-xTB method and analytical linearized Poisson–Boltzmann (ALPB) solvation model outperformed GFN2-xTB (GBSA) and GFN-FF (ALPB), with a small MAD of hydration free energy for the neutral molecules of the FreeSolv database [33]. In comparison, the performance of GFN2-xTB is much better than the GFN-FF in truncated protein–ligand complexes. Additionally, the GFN2-xTB has shown a better performance than the PM6-D3H4 method in terms of binding free energy [32].

In this work, we explore the binding affinity of cannabinoids at the active sites of COX-2 and CB2 receptors by using SQM and molecular docking methods. Validations of SQM method with noncovalent benchmark dimers and complexes are presented to evaluate parameter sets and performance of SQM methods. The use of

outperforming GFN2-xTB methods for improving docking results are discussed. The ALPB solvation model and GFN2-xTB method are used to compute the binding free energy of receptor/cannabinoids complexes, considering both unrelaxed and fully relaxed geometry of receptors. Furthermore, cannabinoid analogs are modified to enhance the highest binding affinity comparable to that of NSAIDs. Druglike properties are used to predict a lead identification as novel oral anti-inflammatory drugs.

1.2 Research objectives

1.2.1 To explore the binding affinity of cannabinoids at the active sites of COX-2 and CB2 receptors by using SQM and molecular docking methods.

1.2.2 To explore the use of SQM potentials as scoring functions for improving docking results.

1.2.3 To identify potential novel analogs of cannabinoids with anti-inflammatory activities.

CHAPTER 2
REVIEW OF LITERATURE

2.1 Inflammation

Inflammation is an essential immune response which allows survival during infection or injury. Redness and swelling with heat and pain can occur at the site of tissue injury. The inflammatory pathway shown in **Figure 2.1** consists of inducers, sensors, mediators, and target tissues. After infection, inducers initiate the inflammatory response, followed by sensors such as Toll-like receptors (TLRs). The sensor induces the production of mediators, including tumor-necrosis factor-α (TNF-α), interleukin (IL-1 and IL-6), and cyclooxygenases (COX-1 and COX-2). These inflammatory mediators then act on various target tissues [1, 2].

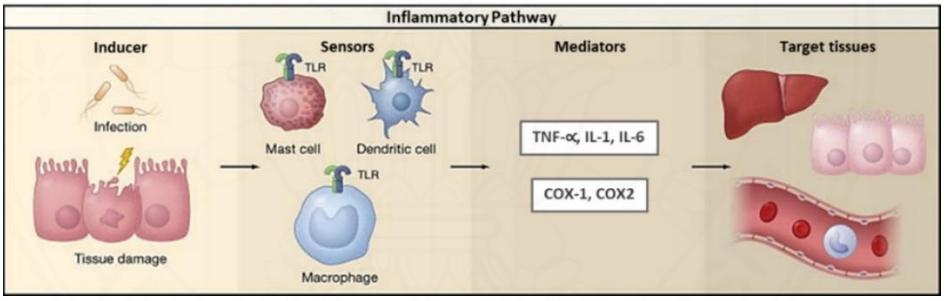

Figure 2.1 Inflammatory pathway [2].

2.2 Cyclooxygenase (COX) enzyme

Two isoforms of the cyclooxygenase-1 (COX-1) and cyclooxygenase-2 (COX-2) engage in the biosynthetic mechanism of transforming arachidonic acid into mediators such as prostaglandins (PGE_2), prostacyclin (PGI_2), and thromboxane (TXA_2) **(Figure 2.2)**. COX-1 is constitutively expressed as a housekeeping enzyme in many tissues whereas COX-2 is a major therapeutic target for inflammation [3].

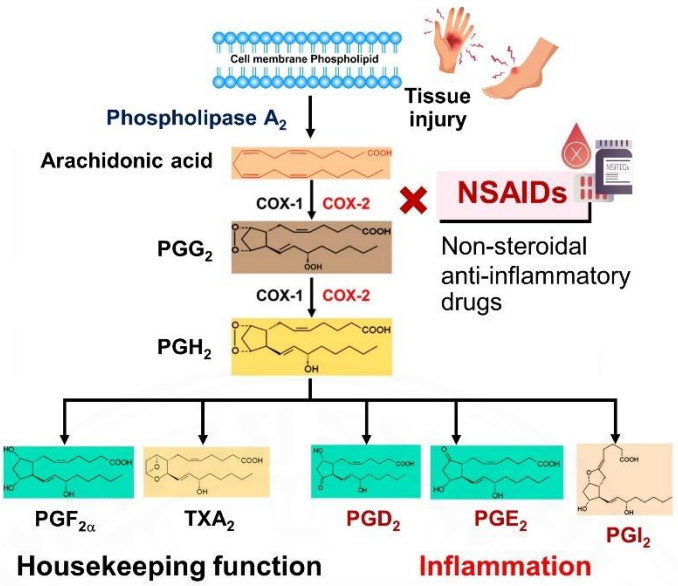

Figure 2.2 Schematic presentation of COX-1 and COX-2 pathways [3].

2.3 Non-steroidal anti-inflammatory drugs (NSAIDs)

Non-steroidal anti-inflammatory drugs (NSAIDs) are commonly used to treat pain and inflammation by inhibiting COX enzymes. NSAIDs are typically divided into groups based on their selectivity and chemical structures**.** For instance, aspirin is COX-1 selective NSAID, celecoxib is COX-2 selective NSAID, and ibuprofen is non-selective NSAID [6] **(Table 2.1)**.

Table 2.1 NSAIDs selectivity [6].

COX-1 selective	Non-selective	COX-2 selective
Aspirin	Diclofenac Naproxen Ibuprofen	Celecoxib Etoricoib Valdecoxib Meloxicam

Table 2.2 shows the half-maximal inhibitory concentration (IC_{50}) of NSAIDs with cyclooxygenase enzyme in micromolar unit reported in the previous study [34-36].

Table 2.2 *In vitro* IC_{50} of NSAIDs tested as inhibitors of prostanoid formation determined in the COX-1 and COX-2 assays.

NSIADs	IC_{50} / (μM)	
	COX-1	**COX-2**
Etoricoxib	162.00	0.47
Celecoxib	16.00	0.54
Diclofenac	0.08	0.04
Naproxen	9.30	28.00
Ibuprofen	7.60	20.00
Flurbiprofen	0.08	5.50
Aspirin	1.70	7.5

Based on their chemical structure, as shown in **Figure 2.3**, NSAIDs can be classified into diverse types such as salicylic acid, heteroaryl acetic acid and enolic acid derivatives. The hydroxyl and carboxylic acid groups are attached to an aromatic structure. Additionally, nitrogen and sulfur atoms are mostly found in the structure of NSAIDs. For example, ibuprofen and naproxen are aryl and heteroaryl acetic acid derivatives whereas meloxicam and piroxicam are enolic acid derivatives [37, 38].

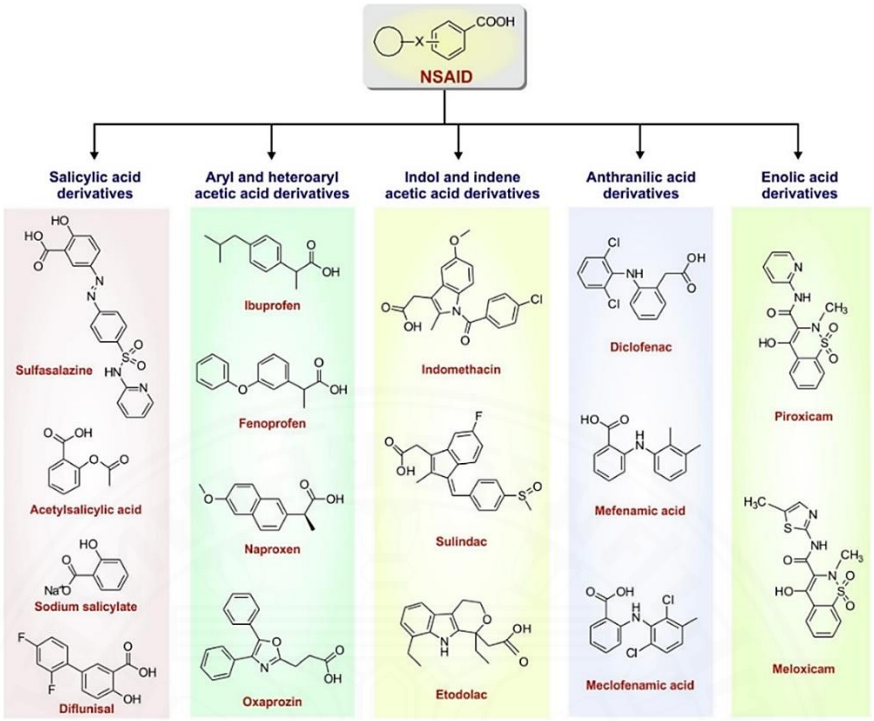

Figure 2.3 Classification of NSAIDs based on a chemical structure [37].

2.4 Cannabinoids and cannabinoid (CB) receptors

Cannabis sativa L. or marijuana is in Cannabaceae family. The active compound of cannabis is called cannabinoids. Among their diverse structure, natural cannabinoids can be classified into eight general types [39], presented in **Figure 2.4.** Δ^9-THC, CBD, CBDA and CBG could exhibit COX enzymes with the half-maximal inhibitory concentration (IC_{50}) values ranging from 0.2 to 1.7 mM [12]. CBDA could also inhibit COX-2 selectively with an IC_{50} of approximately 2 µM [40].

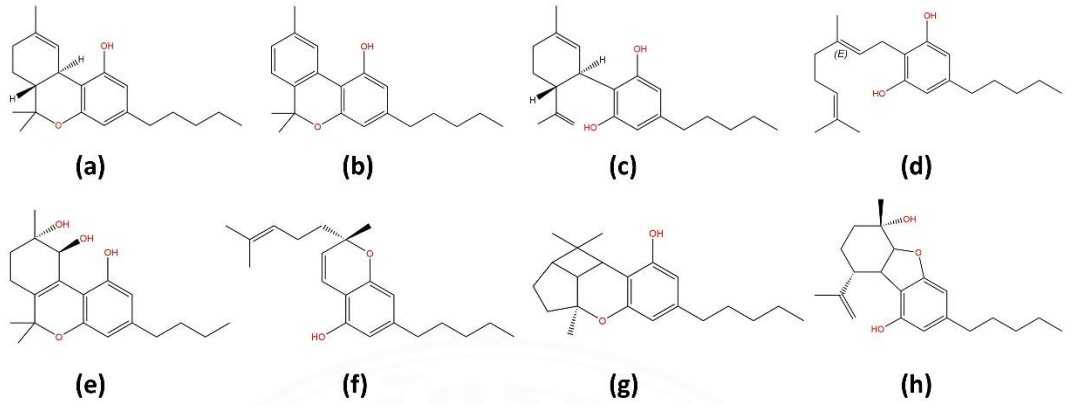

Figure 2.4 Chemical structures of cannabinoids: (a) Δ^9-tetrahydrocannabinol (Δ^9-THC), (b) cannabinol (CBN), (c) cannabidiol (CBD), (d) cannabigerol (CBG), (e) cannabitriol (CBT), (f) cannabichromene (CBC), (g) cannabicyclol (CBL), and (h) cannabielsoin (CBE).

Cannabinoids are related to the endocannabinoid system, cannabinoid receptor types 1 (CB1) and cannabinoid receptor types 2 (CB2). Cannabinoid receptors are identified as G-protein coupled receptors (GPCRs) [41, 42]. GPCRs are a diverse family of eukaryote-specific membrane receptors which translate external signals into specific cellular responses. GPCR ligands can classified into four categories depending on their interactions: agonists, antagonists, partial agonists, and inverse agonists **(Figure 2.5)**. Agonists bind to the receptor, producing a full response. Antagonists bind to the receptor without a response. Partial agonists bind and activate to the receptor with only partial response. Inverse agonists bind to a receptor but produce a response opposite to an agonist [43].

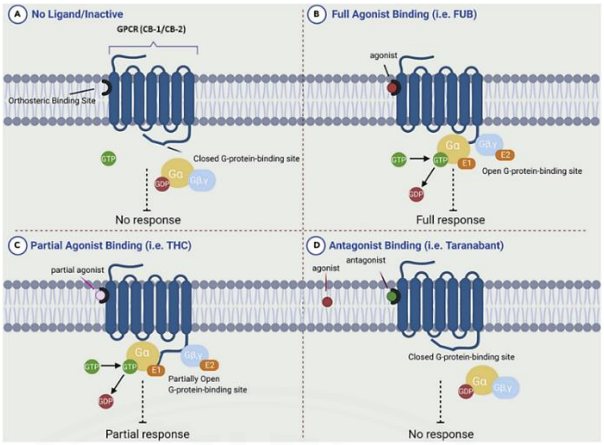

Figure 2.5 Schematic representation of signal transduction by ligand interactions with the cannabinoid receptors [43].

Dongchen, *et. al*. reported that the psychoactive Δ^9-THC acts as an agonist of CB1 and CB2 whereas CBD is a non-psychoactive antagonist or inverse agonist [44]. CB1 is expressed in the central nervous system and associated with the psychotropic effects of Δ^9-THC [14]. In contrast, CB2 is expressed in the immune system and regulates inflammatory response without psychoactivity [45] **(Figure 2.6)**.

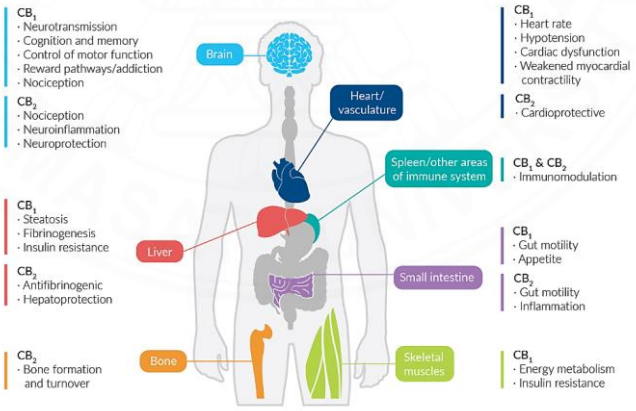

Figure 2.6 Distribution of CB1 and CB1 and their associated functions [46].

Cannabinoids can reduce inflammation by acting on the CB2 receptor, leading to downregulation of enzymes involved in the production of prostaglandins, COX-2, inducible nitric oxide synthase (iNOS), and TNF-α [13] **(Figure 2.7).**

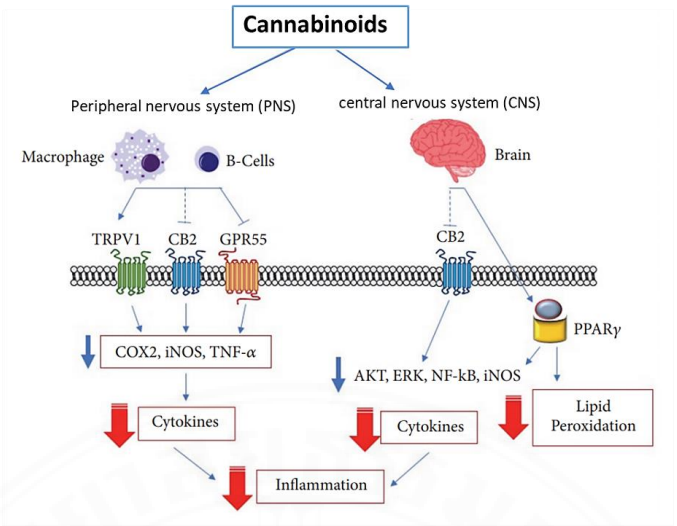

Figure 2.7 Schematic presentation of the signaling pathways for anti-inflammatory effects [13].

The inhibitory constants (K_i) of cannabinoids including Δ^9-THC, Δ^9-THCA, CBD, CBG, and CBN with cannabinoid receptors in a nanomolar unit have been reported in the previous study [16] (**Table 2.3**).

Table 2.3 The K_i values (in nM) of cannabinoids with cannabinoid (CB) receptors.

Cannabinoids	CB1 / (K_i, nM)	CB2 / (K_i, nM)	Ref.
Δ^9-THC	5.05	3.13	[47]
	35.6	8.5	[48]
	21	36.4	[49]
	53.3	75.3	[50]
Δ^9-THCA	23.5	56.1	[48]
CBD	1458.5	372.4	[48]
	4350	2860	[49]
	4900	4200	[51, 52]
CBG	896.8	153.4	[48]
CBN	12.7	16.4	[48]
	120.2	100	[53]
	326	96.3	[49]

2.5 Protein–ligand interactions

A drug (or ligand) is a small molecule which can interact with protein receptors (e.g., enzymes and hormones) for various biological processes. Protein–ligand (P–L) interactions play a key role in the binding affinity of a protein–ligand complex, such as signal transduction, cell regulation, and immune response [54]. Noncovalent interactions, e.g., dispersion, hydrogen bonding, halogen bonding, salt bridge, and π–π stacking, pi-alkyl, pi-pi, and hydrophobic force can be observed between bound ligand and amino acid residues of receptor [55]. The Protein Data Bank (PDB) is the primary source for the data of X-ray crystallographic structure [56].

2.5.1 COX binding pockets

Although the three-dimensional structures of the COX-1 and COX-2 are similar and share 60% identical sequence of amino acid [16], the active sites of both receptors are partially different. **Figure 2.8** shows the key residues of amino acids at the active sites of COX-1 and COX-2. Tyr385 and Ser530 are at the apex of the channel whereas Arg120 and Tyr355 are at the bottom of the active sites for both COX isoforms. The COX-2 binding pockets are bordered by Val523 and Arg513, while COX-1 is surrounded by Ile523 and His513 at the base of the pockets [57, 58]. According to the protein structure of COX-2 (PDB code: 3LN1, as explored in this study), the valine and arginine residues are, respectively, numbered 509 and 499 [5].

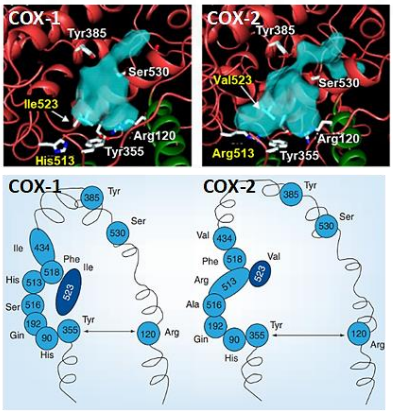

Figure 2.8 Comparison of the key amino acid residues of COX-1 and COX-2 binding pockets [57, 58].

Binding interactions with key amino acid residues can be found in NSAIDs. The hydrogen bonding interactions between the carboxyl group of ibuprofen and amino acid Tyr355 and Arg120 could be observed within 3 Å **(Figure 2.9)**. In contrast, pi-alkyl interaction occurs with Val349 [59].

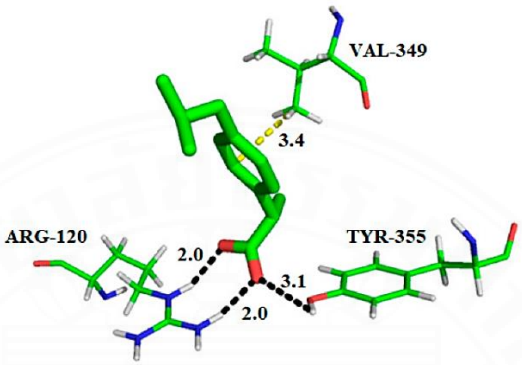

Figure 2.9 Binding interaction of ibuprofen with COX-2 active site. The hydrogen bonds are displayed as black dashed lines, and hydrophobic interactions are in yellow dashed lines. All distances are measured in angstroms.

Cannabigerol (CBG) has showed strong binding interactions with key amino acid residues, Arg120, Tyr355, and Val523 at the active sites of COX-2. The oxygen atom of the phenyl group interacted with Leu352 via hydrogen bonding in 3.32 Å. The carbon-5 (C5) of pentyl side chain showed hydrophobic contact with Leu384, while the carbon-3 (C3) interacted with Trp387 and Met522 [60] **(Figure 2.10)**.

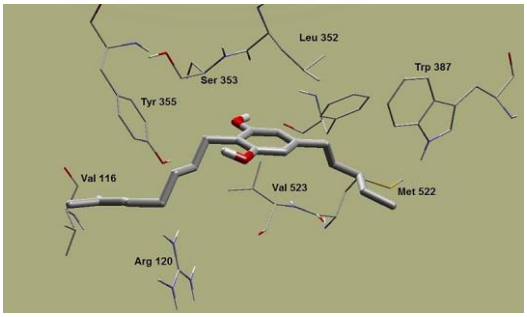

Figure 2.10 Molecular interactions of CBG with key amino acid residues inside binding pocket of COX-2 enzyme [60].

2.5.2 CB binding pockets

Cannabinoid receptors, CB1 and CB2, share 44% amino acid similarity and 68% homology in the transmembrane regions [61, 62]. CB1 with a tetrahydrocannabinol (AM11542) has been reported at a high resolution of 2.80 Å with the PDB code of 5XRA. The chemical structure of AM11542 contains a tricyclic ring system and the hydroxyl group, greatly resemble the structure of Δ^9-THC. The key binding interactions of Δ^9-THC are similar to that of co-crystallized tetrahydrocannabinol **(Figure 2.11a)**. Hydrogen bonding interactions are observed between the hydroxyl group of Δ^9-THC and Ser383 of CB-1. Pi-pi interactions also occur with Phe177, Phe189, Phe200, Phe268, and Phe379 residues. Additionally, the alkyl side chain extended into the long channel and interacts with Leu193, Val196, Tyr275, Leu276, L359, and Met363 [14]. CB2 bound to the potent aminoalkylindole derivative (WIN 55,212-2) with a resolution of 3.20 Å (PDB ID: 6PT0) **(Figure 2.11b)**. The naphthalene moiety of WIN 55,212-2 forms strong pi-pi interactions with Phe91 and Phe94, while hydrophobic interactions occurred with Phe87, His95, Pro184, and Phe281. In addition, the core structure of WIN 55,212-2 engages the pi-pi interactions with Ile110, Val113, Phe117, Phe183, Trp258, Val261, and Met265 [15].

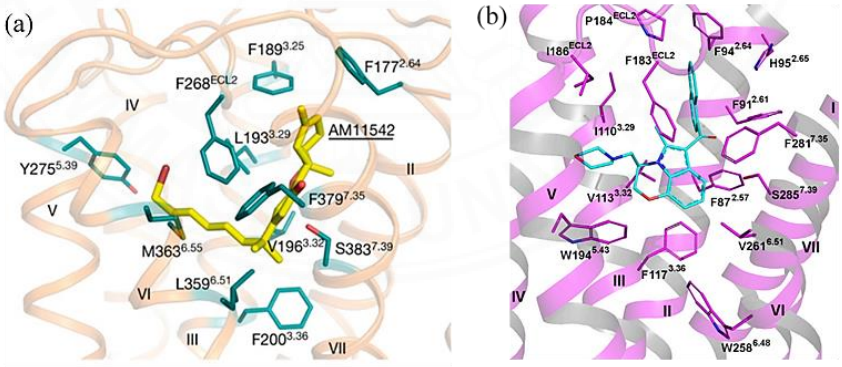

Figure 2.11 Comparison of the key amino acid residues (deep teal and magenta sticks) of (a) CB-1 receptors with AM11542 (yellow sticks) and (b) CB-2 receptors with WIN 55,212-2 (cyan sticks). The water is shown as a red sphere. The hydrogen bonds are shown as dashed lines [14, 15].

Ring systems and hydroxyl groups of cannabinoids play a key role for their binding affinity at the active sites of cannabinoid receptors. **Figure 2.12** shows the binding interactions of (−)-*trans*-Δ^9-THC and their derivatives with CB1 receptor. The ring of cannabinoid analogs made pi-pi interaction with Phe170 and Phe268 whereas the hydroxy group formed a hydrogen bond with Ser383 [63]. The other amino acid residues were observed at the position of the aliphatic side chain listed in **Table 2.4**.

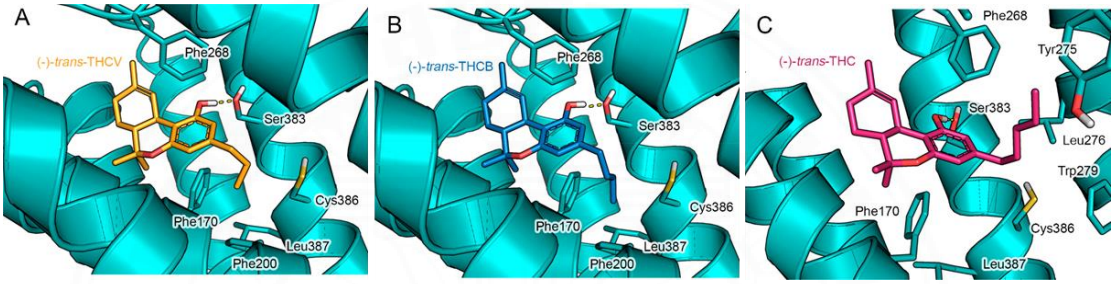

Figure 2.12 Binding interactions of (a) (−)-*trans*-Δ^9-THCV, (b) (−)-*trans*-Δ^9-THCB, and (c) (−)-*trans*-Δ^9-THC in complex with CB-1 (PDB ID 5XRA) [63].

Table 2.4 List of the binding interactions of cannabinoids.

	(-)-*trans*-Δ^9-THCV	**(-)-*trans*-Δ^9-THCB**	**(-)-*trans*-Δ^9-THC**
	Propyl side chain	Butyl side chain	Pentyl side chain
Hydrogen bond		Ser383	
pi–pi interaction		Phe170 and Phe268	
Hydrophobic interactions	Phe170, Phe200, Leu387, Met363, Leu359, and Cys386	Phe170, Phe200, and Leu387	Leu193, Val196, Tyr275, Leu276, Trp279, and Met363

Hydrogen bonding interactions and pi-pi interactions at the active sites of CB1 and CB2 receptors with various PDB codes have been reported in the previous study **(Table 2.5 and Table 2.6)**.

Table 2.5 Information of ligand binding interactions with CB1.

CB1 receptor					
PDB ID	6KPG	5XR8	5XRA	6N4B	5TGZ
Ligand	AM12033	AM841	AM11542	FUB	AM6538
Hydrogen bond	Ser385	Ser383 Ile267 Tyr275	Ser383	Ser383 His178	
pi-pi interaction	Phe94 Phe183 Phe281	Phe170 Phe268 Phe379 Phe189 Phe177	Phe170 Phe268 Phe379 Phe189 Phe177	Try279 Phe170 Phe268	Phe170 Phe268 Phe102 Try356
Ref.	[64]	[14]	[14]	[65]	[66]

Table 2.6 Information of ligand binding interactions with CB2.

CB2 receptor		
PDB ID	6PT0	5ZTY
Ligand	WIN 55,212-2	AM10257
Hydrogen bond	-	Ser165
pi-pi interaction	Phe91 Phe94 Phe117 Try258	Phe117 Phe183 Try258
Ref.	[15]	[45]

2.6 Challenge in protein–ligand binding affinity predictions

2.6.1 Molecular docking algorithm

Molecular docking technique is used to propose the orientations of ligands (or drugs) within the protein binding sites, visualize the protein–ligand interactions, and estimate binding free energies. A docking scheme requires X-ray crystallographic structure of a protein receptor determined by a biophysical technique such as X-ray crystallography and NMR spectroscopy. Docking engines, such as Glide XP [67], UCSF Dock [68], GOLD Suite [69], DOCK [70], FlexX [71], Discovery Studio [72], AutoDock Vina [73], and AutoDock4 [74] have different algorithms for solving chemical problems. The success of docking approaches relies on both the search algorithm and the scoring function. The former is responsible for exploring various ligand conformations within a specific target protein. The latter is responsible for estimating the binding affinities of the generated poses.

The search algorithm can be divided into three fundamental classes: deterministic (or systematic search), stochastic (or random search), and simulation methods [18]. *Deterministic method* is an algorithm which explores all the degrees of freedom in a molecule. Thus, ligands are incrementally grown into active sites. *Stochastic methods* are useful for flexible molecules [19]. This method performs by making a population of ligands. The popular random approaches are Monte Carlo (MC) and genetic algorithms (GA). *Simulation methods* is an approach in which the temperature of a system is adjustable. Molecular dynamics (MD) is the most popular simulation [75].

Scoring functions are derived by the approximate mathematical methods. Binding free energy is estimated by the strength of noncovalent interactions in protein –ligand complexes. The best candidate ligand should have the strongest binding affinity [20]. Scoring functions can be divided into three classes: the force-field-based, the empirical, and the knowledge-based scoring functions. *Force-field-based scoring functions* depend on classical molecular mechanics (MM) methods, representing the force fields. *Empirical scoring functions* are based on the parameterization of several types of interactions contributed to energy terms. The energy terms can be approximated by a sum of individual interactions, e.g., hydrogen

bonding, binding entropy, ionic and lipophilic interactions [20]. *Knowledge-based scoring* functions are derived from statistical analysis of the known 3D structures of protein–ligand complexes. The binding free energy of docking is the sum of the intermolecular forces acting upon the protein–ligand complex [76], as shown in **Equation 2.1**.

$$\Delta G_{bind} = \Delta G_{vdw} + \Delta G_{hbond} + \Delta G_{elec} + \Delta G_{tor} + \Delta G_{sol} \quad \text{(Equation 2.1)}$$

where the molecular mechanics terms are dispersion/repulsion, hydrogen bonding, and electrostatics. ΔG_{tor} is rotation and translation. ΔG_{sol} is hydrophobic effect (solvent-entropy changes at solute-solvent interfaces).

2.6.2 Dispersion corrected methods for modelling noncovalent interactions

Noncovalent interactions, e.g., dispersion, hydrogen bonding, pi-alkyl, pi-pi and hydrophobic force involve in protein–ligand (P-L) binding interactions. These interactions play a role in contributing to binding affinity. Scoring functions of docking are limited to correct noncovalent interactions due to approximate term in energy calculation. High-level quantum mechanical (QM) methods can be used to describe noncovalent interactions. However, accurate QM calculations are high computational cost with small-sized system. To address this concern, semiempirical quantum mechanical (SQM) methods offer the advantage of reducing computational costs with thousands of atoms while improving the description of noncovalent interactions. The classical SQM methods, e.g., AM1 [77], PM6 [78], PM7 [79], SCC-DFTB [80], are based on the neglect of differential diatomic overlap approximations [81]. To enhance the accuracy of SQM, dispersion corrections (D, D3) have been added to semiempirical methods [82, 83] Additionally, corrections of hydrogen bonding (H, H+, H2, H4, H5) [84] and halogen bonding (X) have been improved the potential SQM methods [85]. SQM parameter sets have been parametrized to reproduce accurate interaction energies using CCSD(T)/CBS tested against benchmark dimers and complexes [24, 26, 86-90] (**Table 2.7**).

Table 2.7 The root mean square errors (RMSEs) in kcal/mol of the SQM methods tested against the benchmark datasets.

Data set	PM6		DFTB3		GFN2-xTB
	D3H4	D3H4X	D3H4	D3H5	
S66	0.67 [86]	0.68 [87]	0.66 [24]	0.58 [86]	0.65 [26]
X40	2.59 [87]	2.32 [87]	-	-	-
HB375	1.09 [89]	-	1.23 [89]	1.05 [89]	1.22 [89]
HB300SPX	3.95 [90]	4.44 [90]	2.79 [90]	2.71 [90]	1.58 [90]
PLA15	21.00 [88]	-	21.40 [88]	15.20 [88]	13.40 [88]

PM6-DH2 method [22] has shown promise by accurately reproducing interaction energies for noncovalent geometries obtained from high-level quantum mechanical calculations and identifying correct binding modes and bioactive conformations of bound ligands. **Table 2.8** shows the calculated binding free energy of the top-ranked poses by using AutoDock4 and PM6-DH2. It was found that PM6-DH2 optimization can identify the bound pose of carboxamide ligand that suggested a false negative error, with the recomputed BE of -24.9 kcal/mol. The orientation of the false negative pose was close to the X-ray crystallographic ligand. Additionally, The PM6-DH2 single point energy calculation can identify the bound pose of carboxamide ligand that suggested a false positive error, with the positive BE value of +10.2 kcal/mol [23].

Table 2.8 Calculated binding free energies in kcal/mol of the top-ranked poses from Autodock Vina and PM6-DH2 calculations [23].

Ligand	Protein code	Autodock Vina	PM6-DH2	
		E_{vina} (rank)	Single point E_{sp} (rank)	Optimization E_{opt} (rank)
Carboxamide derivative (d11)	1P44	–7.3 (3)	–2.7 (1)	–24.9 (1)
	3FNE	–7.7 (1)	10.2 (10)	–3.6 (10)

The performance of SQM method has been explored and tested with 15 protein-ligand active site complexes (PLA15 dataset) [88]. PM6-D3H4, DFTB3-D3H4, DFTB3-D3H5, and GFN2-xTB outperformed other SQM methods with small error of interaction energy (**Figure 2.13**).

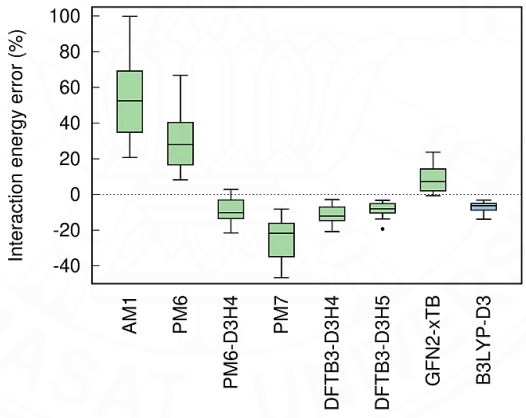

Figure 2.13 Distribution of the relative errors of interaction energies obtained from the tested methods using the PLA15 data [88].

GFN-xTB includes the electrostatic and exchange-correlation Hamiltonian terms without dispersion, hydrogen, and halogen bond specific corrections. It has been reported that the error of GFN-xTB [91] and DFTB3-D3(BJ) [92] were much smaller in magnitude compared to PM6-D3H4X for PL24 protein-ligand binding set [91]. Furthermore, GFN2-xTB outperforms GFN-xTB, DFTB3-

D3(BJ), and PM6-D3H4X with a small error of MAD for the noncovalent interaction energies of different benchmark sets from the GMTKN55 database [26] (**Figure 2.14**).

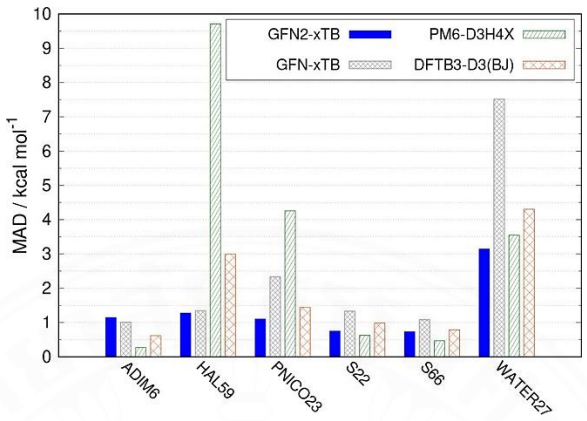

Figure 2.14 Mean absolute deviations (MADs) in kcal/mol for the noncovalent energies of different benchmark sets.

2.6.3 Solvation model and predicted binding free energy

Solvation plays a key role in protein–ligand interactions for many biochemical applications and has a strong impact on the calculation of binding free energies. Free energy perturbation (FEP) [27] has the highest accuracy in calculating the accurate binding free energy. FEP refers to an ensemble of rigorous statistical mechanical methods for calculating the free energy in an alchemical process [93]. **Figure 2.15** shows alchemical free-energy calculations according to the thermodynamic cycle. The binding free energy of a compound consists of four different states: the protein–ligand complexes of molecules A and B, as well as A and B in a water box. **Figure 2.16** shows the transformation from A to B by varying a number of alchemical intermediates characterized by intermediate λ values [94]. The binding free energy (ΔG_{bind}) of A–B are calculated using **Equation 2.1**.

$$\Delta G_{bind,A} - \Delta G_{bind,B} = \Delta G_{bound} - \Delta G_{solvated} \quad \text{(Equation 2.1)}$$

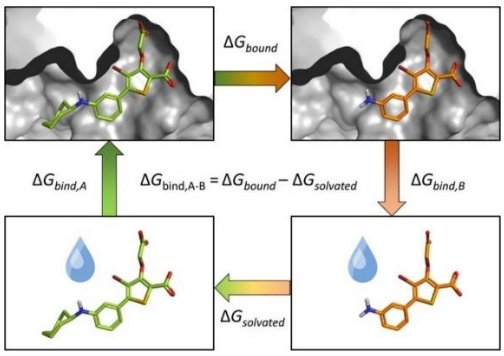

Figure 2.15 Schematic representation of alchemical free-energy calculations [93].

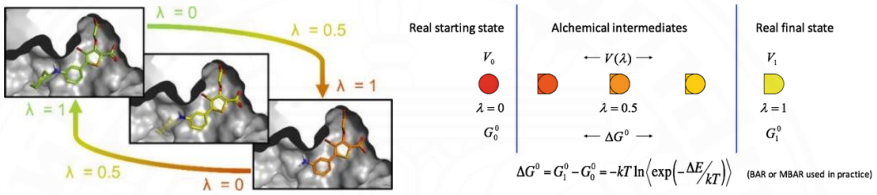

Figure 2.16 Schematic representation of alchemical intermediates [93, 94].

Free energy perturbation has predicted the binding free energy (ΔG_{FEP}) of protein–ligand complexes, with the mean absolute deviations $|\Delta G_{FEP} - \Delta G_{EXP}|$ lower than 2 kcal/mol [95]. However, FEP is computationally costly and difficult to converge a large number of the protein–ligand complexes.

Molecular mechanics Poisson–Boltzmann surface areas (MM/PBSA) [28] and molecular mechanics generalized Born surface areas (MM/GBSA) [29] are low computational cost while providing the approximate binding free energy with whole protein–ligand complexes. These methods employ ensembles derived from molecular dynamic simulation and force field. The binding free energy (ΔG_{bind}) of the protein–ligand complex [96] is calculated using **Equation 2.2**.

$$\Delta G_{bind} = G_{complex} - (G_{receptor} + G_{ligand}) \quad \text{(Equation 2.2)}$$

where $G_{complex}$ is the free energy of protein–ligand complex and $G_{receptor}$ and G_{ligand} are the free energy of the protein and ligand respectively.

The binding free energy of protein–ligand can also be calculated in terms of thermodynamics using **Equation 2.3** and **2.4**.

$$\Delta G_{bind} = \Delta H - T\Delta S \qquad \text{(Equation 2.3)}$$

$$\Delta G_{bind,solv} = \Delta G_{bind,vac} + \Delta G_{solv,complex} - (\Delta G_{solv,ligand} - \Delta G_{solv,receptor}) \qquad \text{(Equation 2.4)}$$

where ΔG_{solv} is solvation free energy, which can be either polar or non-polar components ($\Delta G_{solv} = \Delta G_{polar} + \Delta G_{nonpolar}$) and ΔG_{vac} is the free energy in vacuum which constitute of electrostatic energy ($\Delta E_{electrostatic}$) and entropy ($T\Delta S$) ($\Delta G_{vac} = \Delta E_{(MM)} - T\Delta S$). **Figure 2.17a** shows protein–ligand binding free energy in solvation (ΔG_{bind}). **Figure 2.17b** shows thermodynamic cycle for estimating the binding free binding energy of protein–ligand complexes. $\Delta G_{solv,ligand}$ and $\Delta G_{solv,receptor}$ is difference in binding energy in vacuum and solvation of ligand and protein, respectively. $\Delta G_{bind,vac}$ and $\Delta G_{bind,solv}$ is binding energy of protein and ligand in vacuum and solvation, respectively. $\Delta G_{solv,complex}$ is difference in binding energy of protein–ligand complex in solvation.

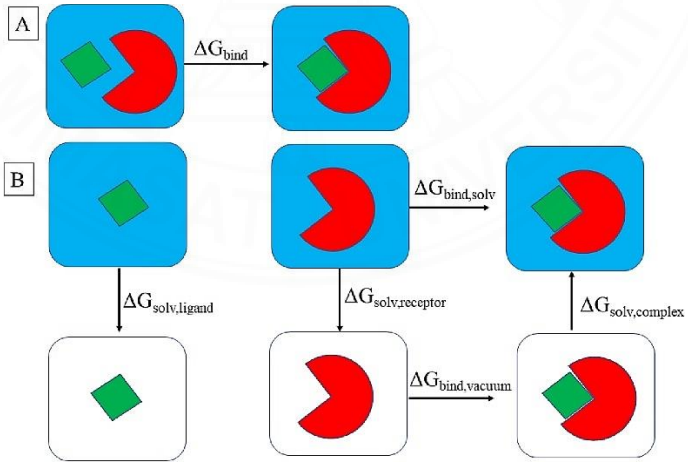

Figure 2.17 (a) protein–ligand binding free energy in solvation. (b) thermodynamic cycle for estimating the binding free energy of protein–ligand complexes. Ligand is presented in green. Protein is presented in red. Solvent is presented in blue [96].

SQM methods have shown the performance for calculating the binding free energy in thousands of atoms of protein–ligand complexes with low-time-cost and good accuracy. With the implementation of COSMO solvation model, both PM6-D3H4X and DFTB3-D3H4X methods have demonstrated reductions in the occurrence of false-positive ligand poses in diverse classes of protein–ligand complexes [30] (**Figure 2.18**).

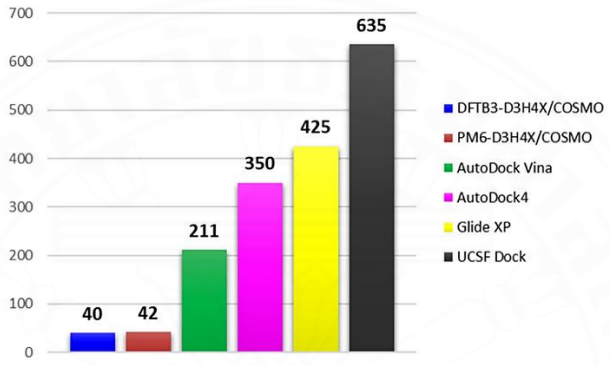

Figure 2.18 Number of false positive poses for the six methods across all the 17 protein–ligand complexes [30].

GFN force-field (GFN-FF) [31] is designed to combine high force-field speed with the accuracy of QM methods with low computational cost. GFN-FF introduces an approximation to the remaining quantum mechanics by replacing the extended Hückel theory with molecular mechanics for the description of covalent bonds. The total GFN-FF energy is calculated using **Equation 2.5**.

$$E_{\text{GFN-FF}} = E_{\text{cov}} + E_{\text{NCI}} \qquad \text{(Equation 2.5)}$$

where E_{cov} refers to the bonded FF energy and E_{NCI} describes the intra- and intermolecular noncovalent interactions.

In the covalent part, as shown in **Equation 2.6**, interactions are described by correcting bond stretch, bond angle, and torsional terms. Repulsive terms are added for bonded and non-bonded interactions. A new three-body bonding correction is the sum of pairwise interactions.

$$E_{cov} = E_{bond} + E_{bend} + E_{tors} + E_{bond,rep} + E_{bond,abc} \quad \text{(Equation 2.6)}$$

In the non-covalent part, as shown in **Equation 2.7,** electrostatic interactions are described by the EEQ model. The correction terms of dispersion hydrogen bonding, and halogen bonding correction are accounted to the energy.

$$E_{NCI} = E_{IES} + E_{disp} + E_{HB} + E_{XB} + E_{NCI,rep} \quad \text{(Equation 2.7)}$$

GFN-FF method and GBSA solvation model has simulated the dynamics of a met-myoglobin mutant and reproduces the experimental EPR-distance measurements excellently [31]. Furthermore, the performance of the GFN-FF method is quite good in a neutral–ligand system since the Pearson correlation coefficient (r_p) is 0.70 and the mean absolute error (MAE) is 5.49 kcal/mol. However, it may fail in a charge–ligand system (the MAE is 18.98 kcal/mol) [32].

To enhance the accuracy, GFN2-xTB method has been used to compute the binding free energy of truncated protein–ligand complexes [32]. The binding free energy ($\Delta G_{bind,solv}$) of the protein–ligand complex is calculated using **Equation 2.2**. For a more detailed, the binding free energy can be described in three contributions shown in **Equation 2.8**. The free energy (G) consists of three contributions: the total gas-phase energy (E_{vac}), the solvation free energy (δG_{solv}), and the thermostatistical contribution to the free energy $(-T)\Delta S_{solv,mRRHO}$. G_{mRRHO} is modified rigid-rotor-harmonic-oscillator approximation at 298.15K, including translation, rotation, vibration of molecule.

$$\Delta G_{bind,solv} = \Delta E_{vac(GFN2\text{-}xTB)} + \Delta\delta G_{solv} + (-T)\Delta S_{solv,mRRHO} \quad \text{(Equation 2.8)}$$

GFN2-xTB method and analytical linearized Poisson–Boltzmann (ALPB) solvation model outperformed GFN2-xTB with GBSA solvation model and GFN-FF with ALPB solvation model, with a small MAD of hydration free energy for the neutral molecules of the FreeSolv database [33] (**Figure 2.19**).

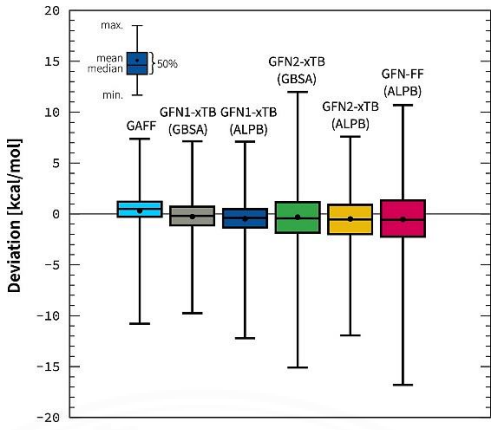

Figure 2.19 Mean deviation in kcal/mol of hydration free energies for the neutral species of the FreeSolv database [33].

In comparison, the performance of GFN2-xTB is much better than the GFN-FF in truncated protein–ligand complexes. (MAE is 4.91 kcal/mol in neutral–ligand system and 10.25 kcal/mol in the charged–ligand systems). The Pearson correlation coefficient was not increased when using the GFN2-xTB. As shown in **Figure 2.20**, the GFN2-xTB had a smaller error than the PM6-D3H4 for accurate binding free energy in most cases of truncated protein–ligand complexes [32].

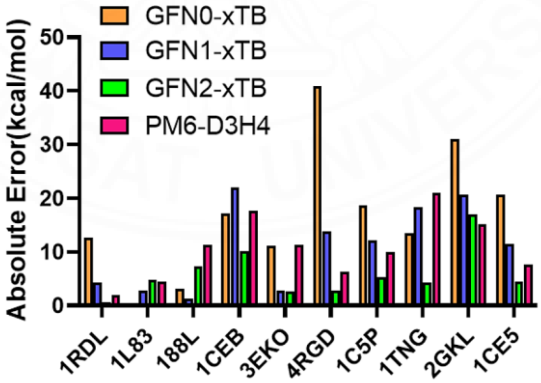

Figure 2.20 Absolute error (i.e., |ΔGexp-ΔGcal|) for the binding free energy of the truncated systems with the PM6-D3H4 and GFNn-xTB methods.

CHAPTER 3
RESEARCH METHODOLOGY

In this study, the protein receptors and studied NSAIDs and cannabinoids were prepared for molecular docking simulations. The noncovalent datasets were used to benchmark the parameters used for semiempirical quantum mechanical (SQM) method and the solvation model. Docked poses of cannabinoids were then reoptimized at the prepared active site of protein receptor using the outperforming SQM method. The binding free energy of fully relaxed protein-ligand complexes was computed in implicit aqueous solvation at the same level of theory. The highest-scored complex with a more negative binding energy is predicted to be more stable. The binding affinity and selectivity index of calculated inhibitory constant of the highest-scored complex were examined and compared with NSAIDs. Finally, 3D graphic representations of the protein-ligand complexes were generated for analysis of the binding interactions**.**

3.1 Preparation of receptors

Structures of COX-1 and COX-2 with co-crystallized ligand in **Table 3.1** were used for validation of docking and GFN2-xTB. The multiple structures of COX-1 and COX-2 were used due to having difference co-crystallized ligand. The X-ray crystallographic structures of COX-1 (PDB code: 3KK6 [97], 3N8Y [98], 1EQG [99], 1EQH [99]), COX-2 (PDB code: 3LN1 [100], 1PXX [101], 4PH9 [102], 3PGH [103]), CB1 (PDB code: 5XRA [14]), and CB2 (PDB code: 6PT0 [15]) receptors with a resolution < 3.50 Å were downloaded from the RCSB protein data bank (PDB) [56]. Only chain A of the receptor was selected. Water molecules and other heteroatoms were removed from the protein-ligand complexes. Hydrogen atoms were then added to the complexes. The protonation states of amino acids were adjusted at pH of 7.4 using the PROPKA plugin under the APBS-PDB2PQR software suite [104]. We noted that COX-1 with the PDB code of 1EQH and COX-2 with the PDB code of 3LN1 were used for molecular docking and GFN2-xTB optimization.

Table 3.1 X-ray crystallographic structures of protein receptors.

Protein	PDB code	Res (Å)	Co-crystallized ligand	Source
COX-1	3KK6	2.75	Celecoxib	*Ovis aries*
	3N8Y	2.60	Diclofenac	*Ovis aries*
	1EQG	2.61	Ibuprofen	*Ovis aries*
	1EQH	2.70	Flurbiprofen	*Mus musculus*
COX-2	3LN1	2.40	Celecoxib	*Mus musculus*
	1PXX	2.90	Diclofenac	*Mus musculus*
	4PH9	1.81	Ibuprofen	*Mus musculus*
	3PGH	2.50	Flurbiprofen	*Mus musculus*
CB1	5XRA	2.80	Tetrahydrocannabinol (AM11542)	*Homo sapiens*
CB2	6PT0	3.20	Aminoalkylindole derivative (WIN 55212-2)	*Homo sapiens*

The key residues of amino acids at the binding region for each receptor (COX-1, COX-2 [5, 57, 58], CB1 [14], and CB2 [15]) were selected based on the binding interaction of protein-ligand complex, as listed in **Table 3.2.** The binding pockets of these protein receptors were subjected to determining binding affinity using SQM theory, either in their native form or in a fully relaxed pose.

Table 3.2 The list of amino acid residues in the pocket of protein receptors.

Protein	PDB code	Amino acid residues in the pocket
COX-1	3KK6, 3N8Y, 1EQG, 1EQH	His90, Leu93, Thr94, Met113, Arg114, Val116, Arg120, Gln192, Phe198, Phe205, Val344, Ile345, Tyr348, Val349, Gln351, Leu352, Ser353, Gly354, Tyr355, Leu357, Leu359, Phe381, Leu384, Tyr385, Trp387, Ile434, His513, Asn515, Ser516, Ile517, Phe518, Gly519, Met522, Ile523, Glu524, Met525, Gly526, Ala527, Ser530, Leu531, Leu534

Table 3.2 The list of amino acid residues in the pocket of protein receptors. (cont.)

Protein	PDB code	Amino acid residues in the pocket
COX-2	3LN1	His75, Leu78, Thr79, Met99, Val102, Leu103, Arg106, Gln178, Phe191, Thr192, Phe195, Val330, Ile331, Tyr334, Val335, Leu338, Ser339, Gly340, Tyr341, Leu345, Phe367, Leu370, Tyr371, Trp373, Val420, Arg499, Ala502, Ile503, Phe504, Met508, Val509, Glu510, Leu511, Gly512, Ala513, Ser516, Leu517, Leu520
	1PXX	His90, Leu93, Thr94, Met113, Val116, Leu117, Arg120, Gln192, Phe205, Thr206, Phe209, Val344, Ile345, Tyr348, Val349, Leu352, Ser353, Gly354, Tyr355, Leu359, Phe381, Leu384, Tyr385, Trp387, Val434, Arg513, Ala516, Ile517, Phe518, Met522, Val523, Glu524, Leu525, Gly526, Ala527, Ser530, Leu531, Leu534
	4PH9	His90, Leu93, Thr94, Met114, Val117, Leu118, Arg121, Gln193, Phe206, Thr207, Phe210, Val345, Ile346, Tyr349, Val350, Leu353, Ser354, Gly355, Tyr356, Leu360, Phe382, Leu385, Tyr386, Trp388, Val435, Arg514, Ala517, Ile518, Phe519, Met523, Val524, Glu525, Leu526, Gly527, Ala528, Ser531, Leu532, Leu535
	3PGH	His90, Leu93, Thr94, Met113, Val116, Leu117, Arg120, Gln192, Phe205, Thr206, Phe209, Val344, Ile345, Tyr348, Val349, Leu352, Ser353, Gly354, Tyr355, Leu359, Phe381, Leu384, Tyr385, Trp387, Val434, Arg513, Ala516, Ile517, Phe518, Met522, Val523, Glu524, Leu525, Gly526, Ala527, Ser530, Leu531, Leu534

Table 3.2 The list of amino acid residues in the pocket of protein receptors. (cont.)

Protein	PDB code	Amino acid residues in the pocket
CB1	5XRA	Phe108, Ile169, Phe170, Ser173, Phe174, Phe177, His178, Phe189, Lys192, Leu193, Val196, Thr197, Phe200, Ile267, Phe268, Pro269, Ile271, Tyr275, Leu276, Trp279, Ile280, Trp356, Leu359, Met363, Phe379, Ala380, Ser383, Cys386
CB2	6PT0	Tyr25, Val86, Phe87, Ser90, Phe91, Phe94, His95, Phe106, Lys109, Ile110, Gly111, Val113, Thr114, Phe117, Ser165, Pro168, Leu182, Phe183, Pro184, Ile186, Tyr190, Leu191, Trp194, Leu195, Trp258, Val261, Met265, Phe281, Ala282, Ser285, Cys288

To complete the binding pockets, all dangling bonds of the cleaved amino acid residues were then capped with the hydrogen atoms. The number of amino acid residues in the binding site was, respectively, 41, 38, 28, and 31 for COX-1, COX-2, CB1, and CB2 receptors. The size of protein pocket ranges from 494 to 657 atoms with their total charge of +1 and +2 (**Table 3.3**).

Table 3.3 The number of amino acid residue, atoms, and total charge at the pocket of protein receptors.

Protein	The binding site		
	Residues	Atoms	Charge
COX-1	41	657	+1
COX-2	38	607	+1
CB1	28	504	+1
CB2	31	494	+2

3.2 Preparation of ligands

The Simplified Molecular-Input Line-Entry System (SMILES) of 7 NSAIDs (etoricoxib, celecoxib, diclofenac, naproxen, ibuprofen, flurbiprofen, and aspirin) were retrieved from ChEMBL database [105] and converted to the 3D structures using OpenBabel [106]. The 2D structure of NSAIDs are shown in **Figure 3.1**.

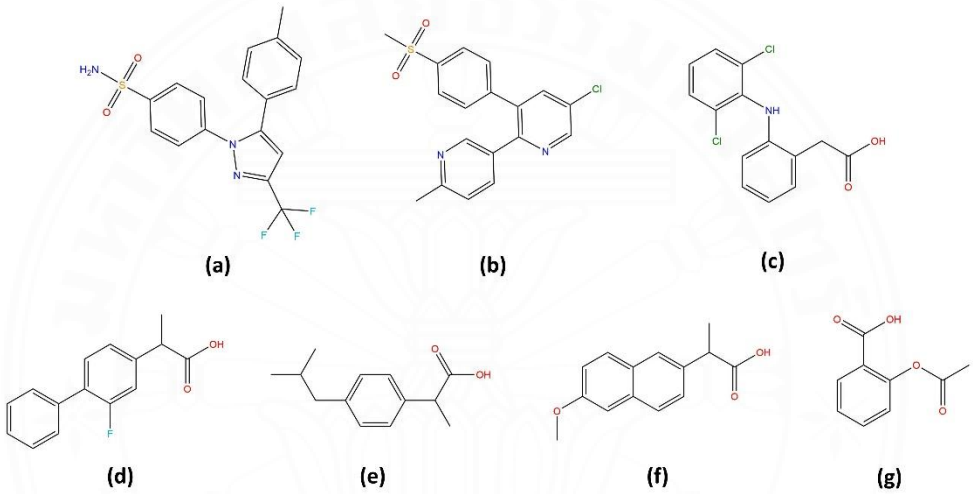

Figure 3.1 Chemical structures of NSAIDs: (a) celecoxib, (b) etoricoxib, (c) diclofenac, (d) flurbiprofen, (e) ibuprofen, (f) naproxen, and (g) aspirin.

The 3D structures of 54 phytocannabinoids were retrieved from cannabis database [107]. We note that CBTA was built by using IQmol [108] because its structure cannot be found in the database. All structures were manually checked and minimized using MMFF94s force field in IQmol. The compliance of all studied ligands with Lipinski's rules of five [109] was checked by using the additional information in the cannabis database and Swiss ADME [110] online tool. According to diverse structure of cannabinoids, our selected cannabinoids can be classified into 16 main classes, including their acid analogs **(Figure 3.2)**: Δ^9-tetrahydrocannabinol (Δ^9-THC-type), cannabinol (CBN-type), cannabidiol (CBD-type), cannabigerol (CBG-type),

cannabitriol (CBT-type), cannabichromene (CBC-type), cannabicyclol (CBL-type), and cannabielsoin (CBE-type).

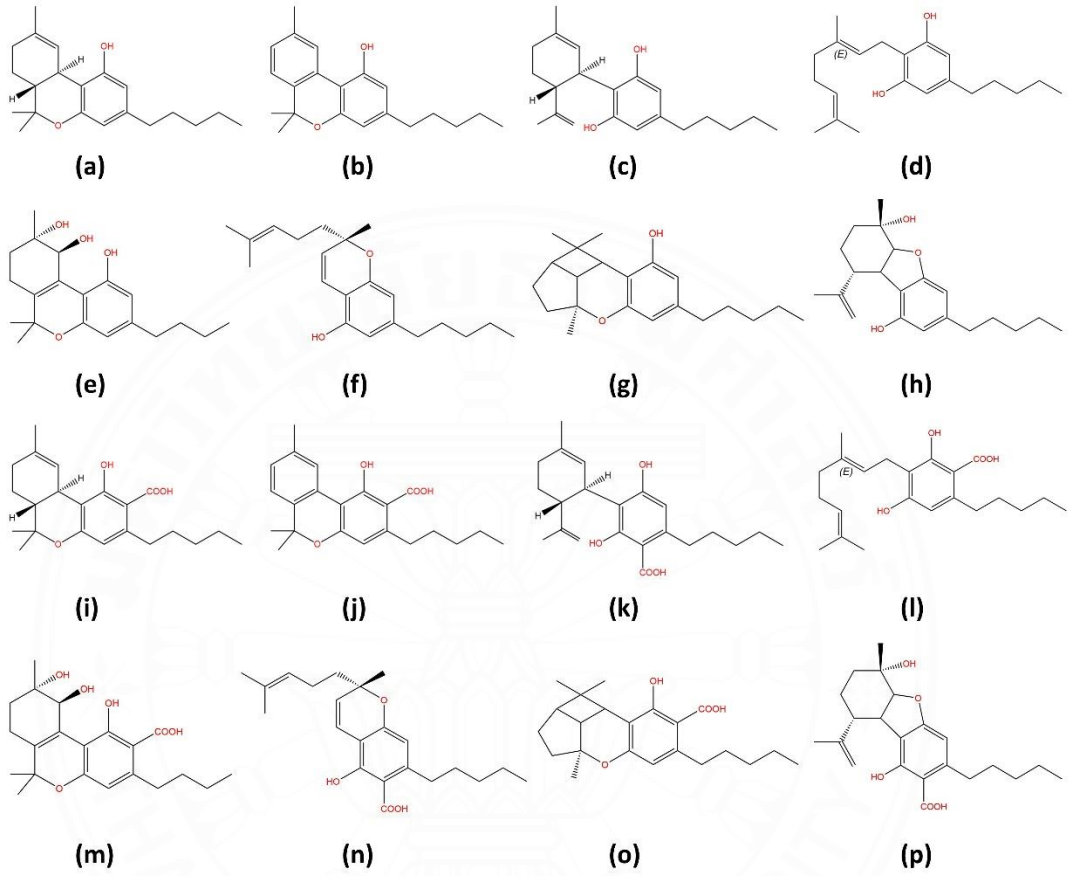

Figure 3.2 Chemical structures of cannabinoids: (a) Δ^9-tetrahydrocannabinol (Δ^9-THC), (b) cannabinol (CBN), (c) cannabidiol (CBD), (d) cannabigerol (CBG), (e) cannabitriol (CBT), (f) cannabichromene (CBC), (g) cannabicyclol (CBL), (h) cannabielsoin (CBE), (i) Δ^9-tetrahydrocannabinolic acid (Δ^9-THCA), (j) cannabinolic acid (CBNA), (k) cannabidiolic acid (CBDA), (l) cannabigerolic acid (CBGA), (m) cannabitriolic acid (CBTA), (n) cannabichromenic acid (CBCA), (o) cannabicyclolic acid (CBLA), and (p) cannabielsoic acid (CBEA).

3.3 Molecular docking protocols

The docking process was applied to NSAIDs and cannabinoids at the active sites of each receptor by using the Lamarckian genetic algorithm (LGA) in the AutoDock4 version 4.2.6 [111]. To validate docking parameters, co-crystallized ligands were docked into the active sites of their receptors. The grid box used for all four receptors was $50 \times 50 \times 50$ Å in size with 0.375 Å grid spacing, covered the binding region of all protein-ligand systems: COX-1/flurbiprofen, COX-2/celecoxib, CB1/tetrahydrocannabinol (AM11542), and CB2/aminoalkylindole derivative (WIN55 212-2), as shown in **Figure 3.3.**

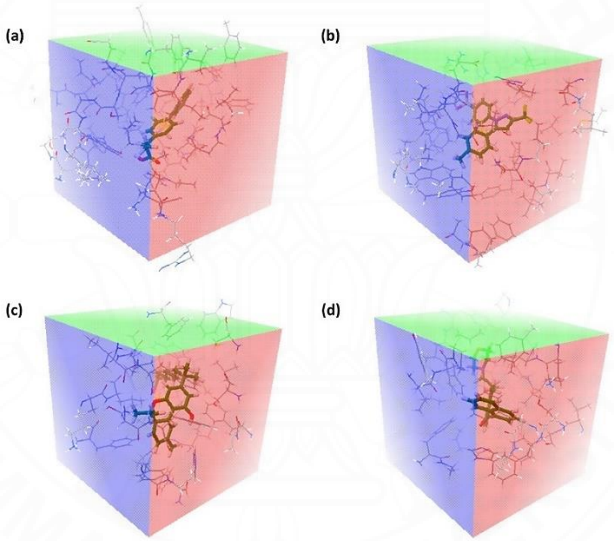

Figure 3.3 The size of a grid box at the binding regions of (a) COX-1, (b) COX-2, (c) CB1, and (d) CB2.

The docking scheme was run with 150 individuals in the population, 250,000 for maximum energy evaluations and 27,000 for maximum generation. The top-ten docked poses were ranked based on their binding energy, computed using AutoDock4 scoring function. AutoDock4 can reproduce bound ligand poses for all four receptors with an RMSD value ranging from approximately 1.0 - 2.0 Å (**Table 3.4**). Note that the best-aligned pose corresponds to the lowest binding energy pose for COX-1, COX-2, and CB1, but it is the third-ranked pose for CB2.

Table 3.4 RMSD of the best-docked poses of co-crystallized ligands with protein receptors.

Protein-ligand system	RMSD / (Å)
COX-1/flurbiprofen	1.05
COX-2/celecoxib	0.84
CB1/AM11542	0.89
CB2/WIN55 212-2	1.55

All studied ligands were then docked into the validated grid box at the binding sites of protein receptors. Protein-ligand interactions were visualized using Discovery Studio (DS) visualizer [72].

3.4 Benchmark datasets

We performed benchmarking of the SQM methods and the ALPB solvation model using noncovalent dimers and complexes listed in **Table 3.5.**

Table 3.5 Description of noncovalent benchmark datasets.

Dataset	Entries	Description
S66	66	Organic noncovalent dimers
X40	40	Organic noncovalent dimers with halogen atoms
HB375	262	Hydrogen bonding in organic dimers
HB300SPX	300	Hydrogen bonding extended to S, P, and halogens in organic dimers
PLA15	15	Protein-ligand active site complexes
MNSOL	533	Neutral and ionic solutes including the elements H, C, N, O, F, Si, P, S, Cl, Br, and I.
SAMPL2	21	Organic molecule and drug

The S66 dataset consists of 66 organic noncovalent dimers. This dataset represents a wide distribution of electrostatic and dispersion interaction; however, it does not contain the halogen atoms in system [112]. Thus, we used X40 dataset to describe noncovalent interactions of molecular dimers containing halogen atoms. This dataset includes electrostatic, dispersion, hydrogen bonding and halogen bonding interactions [87]. For a more detailed analysis of hydrogen bonding, we used HB375 dataset, which comprises six different types of hydrogen bonds: OH−O, NH−O, OH−N, NH−N, CH−O and CH−N [89]. Moreover, HB300SPX dataset was used to investigate the hydrogen and halogen bonding interactions. This dataset covers hydrogen bonds to sulfur, phosphorus, and halogens (F, Cl, Br, and I), and classified into eight groups labeled XH−N, XH−O, XH−P, XH−S, XH−F, XH−Cl, XH− Br, and XH−I [90]. For the dataset to be more relevant for the large system, we selected the PLA15 dataset, built from 15 protein-ligand active-site complexes with systems of sizes ranging from 259 to 584 atoms. Their ligands in these complexes have a net charge of either 1, 0, or +1, and range in size from 37 to 95 atoms [88]. With ALPB solvation model, MNSOL and SAMPL2 datasets were used to validate our computed solvation free energies. The MNSOL dataset contains 533 experimental solvation free energies for 390 neutral and 143 ionic solutes. The reference solvation free energies of this dataset refer to the process of transferring the molecule from the gas phase to the liquid phase [113]. The SAMPL2 dataset consists of 23 organic molecules and drugs [114]. It is worth noting that we focused only on 20 molecules, which include the NSAIDs: ibuprofen, flurbiprofen, ketoprofen, and naproxen.

3.5 SQM methods

The performance of SQM methods with dispersion (D), hydrogen bonding (H), and halogen bonding (X) corrections—specifically PM6-D3H4, PM6-D3H4X, DFTB3-D3H4, DFTB3-D3H5, and GFN2-xTB—was examined using noncovalent complexes from benchmark datasets. For the PM6 method, the MOZYME keyword was applied to speed up the SCF calculations in large protein-ligand complexes. For Grimme's D3 dispersion correction, the scaling coefficient s_6 of 0.88 was used for PM6 [25] whereas the scaling coefficient s_6 of 1.0 with Becke–Johnson damping (BJ) was

used for DFTB3 [24]. Detailed parameter sets for dispersion, hydrogen-bonding corrections, H4 [24] and H5 [86], and halogen bonding corrections [115] are provided in **Table 3.6**, **Table 3.7**, and **Table 3.8**, respectively. The PM6 calculations were carried out using MOPAC2016 [116]. DFTB3 calculations were performed using DFTB+ program version 21.2 [117].

Table 3.6 The parameters for dispersion correction used in the PM6 and DFTB3.

Parameter	PM6	DFTB3
a_1	-	0.746
a_2	-	4.191
s_6	0.88	1.0
s_8	-	3.209
s_r	1.18	-
a	22	-

Table 3.7 The parameters for hydrogen-bonding correction used in the PM6 and DFTB3.

Correction term	Parameter	PM6	DFTB3
H4	c_{OO}	2.32	1.28
	c_{ON}	3.10	3.84
	c_{NO}	1.07	0.88
	c_{NN}	2.01	2.83
	c_{wat}	0.42	1.00
	$c_{S,\ COO^-}$	1.41	1.75
	$c_{S,\ NH4}$	3.61	4.01
	$c_{S,\ gua}$	1.26	2.68
	$c_{S,\ imz}$	2.29	3.44
H5	s_r	-	0.714
	s_w	-	0.25
	k_{OH}	-	0.06
	k_{NH}	-	0.18
	k_{SH}	-	0.21

Table 3.8 The parameters for halogen-bonding correction used in the PM6 method.

Halogen bond	a (kcal/mol)	b ($Å^{-1}$)
Cl-O	1.871×10^{9}	7.44
Br-O	2.160×10^{4}	3.30
I-O	2.436×10^{6}	4.71
Cl-N	1.049×10^{12}	9.95
Br-N	5.560×10^{4}	3.04
I-N	5.237×10^{8}	6.77

The parameter sets of GFN2-xTB method [26] are shown in **Table 3.9.** Implicit aqueous solvation was implemented using the ALPB solvation model and a water solvent with the P16 interaction kernel [33]. The GFN2-xTB method and ALPB solvation model were executed using the xtb program, version 6.6.0 [118].

Table 3.9 The parameter sets used in GFN2-xTB method.

Correction term	Parameter	Value
	k_{ss}	1.85
	k_{pp}, k_{dd}	2.23
	k_{sp}	2.04
	k_{sd}, k_{pd}	2.00
	k_{rep}	1.5
	K_s	1.0
	K_p	0.5
	K_d	0.25
	k_{EN}	0.02
Multipole	D_{val}	1.2
	R_{max}	5.0
	a_3	3.0
	a_5	4.0

Table 3.9 The parameter sets used in GFN2-xTB method. (cont.)

Correction term	Parameter	Value
Dispersion	a_1	0.52
	a_2	5.0
	s_6	1.0
	s_8	2.7
	s_9	5.0

3.6 Computation of binding energy and binding free energy

To validate the SQM methods, the interaction energy (IE) of noncovalent dimers from S66, X40, HB375, and HB300 datasets was calculated using **Equation 3.1.** Similarly, the binding energy (BE) of protein-ligand complexes from PLA15 dataset was calculated using **Equation 3.2.**

$$IE = E_{dimer} - (E_{monomer\_a} + E_{monomer\_b}) \quad \text{(Equation 3.1)}$$

$$BE = E_{complex} - (E_{receptor} + E_{ligand}) \quad \text{(Equation 3.2)}$$

The hydration free energy (δG_{hyd}) for the SAMPL2 and MNSOL datasets was computed, as shown in **Equation 3.3**, by evaluating the difference between the total Gibbs free energy (G) in the two states: vacuum and solvation. This computation requires both full geometry optimizations and Hessian calculations.

$$\delta G_{hyd} = G_{solv} - G_{vac} \quad \text{(Equation 3.3)}$$

The statistical values of computed IEs and BEs of benchmark datasets including root mean square errors (RMSE), mean signed error (MSE), mean absolute deviation (MAD), maximum deviation (D_{MAX}), and minimum deviation (D_{MIN}) were then evaluated and analyzed.

To determine the binding affinity of receptor-cannabinoid complexes, the corrected binding free energy (ΔG_{bind}) of receptor and ligand was calculated by using GFN2-xTB method, as shown in **Equation 3.4**., where $G_{complex}$ is the free energy of the protein–ligand complex, $G_{receptor}$ is the free energy of the protein receptor and G_{ligand} is the free energy of the ligand.

$$\Delta G_{bind} = G_{complex} - (G_{receptor} + G_{ligand}) \quad \text{(Equation 3.4)}$$

The free energy (G) consists of three contributions: the total gas-phase energy (E_{vac}), the solvation free energy (δG_{solv}), and the thermostatistical contribution to the free energy ($T\Delta S_{mRRHO}$). To obtain the three contributions, each of ten docked poses ranked by using AutoDock4 scoring function was reoptimized at the native pockets of the receptors in vacuum by using GFN2-xTB method. This step provided the total gas-phase energy (ΔE_{vac}). Next, the ten optimized poses in vacuum were then reoptimized in implicit aqueous solvation with ALPB solvation model. The solvation free energy ($\Delta\delta G_{solv}$) was included in the calculation. Therefore, the free energy is defined by the uncorrected binding free energy ($\Delta G'_{bind,solv}$). Third, the lowest-energy complexes suggested by computed $\Delta G'_{bind,solv}$ were fully optimized at the same level of theory at 298.15 K. This step provided the energy in terms of the corrected binding free energy ($\Delta G_{bind,solv}$), included the thermostatistical contribution $(-T)\Delta S_{solv,mRRHO}$. All terms of computed energy were clarified in **Equation 3.5.**

$$\begin{aligned}\Delta G_{bind,solv} &= \Delta E_{vac(GFN2\text{-}xTB)} + \Delta\delta G_{solv} + (-T)\Delta S_{solv,mRRHO} \\ &= \Delta G'_{bind,solv} + (-T)\Delta S_{solv,mRRHO}\end{aligned} \quad \text{(Equation 3.5)}$$

3.7 Calculation of inhibitory constant (K_i) and selectivity index (SI)

The corrected binding free energy ($\Delta G_{bind,solv}$) and the uncorrected binding free energy ($\Delta G'_{bind,solv}$) in a unit of cal/mol can be converted to the inhibitory constant (K_i), as shown in **Equation 3.6.**

$K_i = \exp(\Delta G_{bind,solv} / RT)$ (Equation 3.6)

The gas constant, R, is 1.98 cal/K mol and T is the absolute temperature of 298.15 K. The inhibitory constant (K_i) was then used to estimate the selectivity index (SI) for COX-2/COX-1 ratio in **Equation 3.7** and CB2/CB1 ratio in **Equation 3.8.** The experimental selectivity index from literature was calculated from 50% inhibitory concentration (IC_{50}), as in **Equation 3.9.**

Calculated $SI_{COX\text{-}2/COX\text{-}1}$ = Log (K_i of COX-2 / K_i of COX-1) (Equation 3.7)

Calculated $SI_{CB2/CB1}$ = Log (K_i of CB2 / K_i of CB1) (Equation 3.8)

Experimental $SI_{COX\text{-}2/COX\text{-}1}$ = Log (IC_{50} of COX-2 / IC_{50} of COX-1) (Equation 3.9)

CHAPTER 4
RESULTS AND DISCUSSION

4.1 NSAIDs

This section explores the binding energies of the top-ten docked poses of NSIADs with COX-1 and COX-2. The ALPB solvation model and GFN2-xTB method were then used to compute the binding free energy of COX/NSAID complexes, considering unrelaxed geometry of receptors. Additionally, the selectivity index of COX-2 to COX-1 ratio was estimated to predict the anti-inflammatory potency of NSAIDs.

4.1.1 The binding affinity of protein-ligand complexes

The binding affinity of ligand in the pockets of studied protein receptors can be estimated using binding energies. First, we docked seven NSAIDs into the binding sites of COX-1 and COX-2 receptors by using AutoDock4. **Table 4.1** shows the top-ten docked poses of each NSAIDs ranked according to their binding energy. It was found that AutoDock4 can effectively predict the bound pose of NSAIDs with COX-1 and COX-2 receptors, displaying strong binding affinity comparable to that of the co-crystallized poses. As the COX-2 selective NSAIDs, etoricoxib and celecoxib showed the highest affinity with COX-2 with the binding energies (BEs) of −10.93 and −10.83 kcal/mol, respectively. In contrast, non-selective NSAIDs such as diclofenac, ibuprofen, naproxen, and flurbiprofen exhibited the binding affinity with both COX-1 and COX-2. Their BEs of the non-selective NSAIDs were ranging from −7.65 to −8.93 kcal/mol for COX-1 and −6.47 to −7.56 kcal/mol for COX-2. It is noteworthy that the difference in BE of NSAIDs from AutoDock4 was within a few kcal/mol.

Table 4.1 Binding energy (BE) in kcal/mol of top-ten docked poses of NSAIDs from AutoDock4.

NSAIDs	COX-1		COX-2	
	Rank	$BE_{autodock4}$ / (kcal/mol)	Rank	$BE_{autodock4}$ / (kcal/mol)
Etoricoxib	1	–6.83	1	–10.93
	2	–6.27	2	–10.90
	3	–5.38	3	–10.85
	4	–5.38	4	–10.83
	5	–5.28	5	–10.83
	6	–5.21	6	–10.80
	7	–5.05	7	–10.69
	8	–4.95	8	–10.69
	9	–3.62	9	–10.45
	10	–2.77	10	–10.05
Celecoxib	1	–6.89	1	–10.83
	2	–5.54	2	–10.81
	3	–5.39	3	–10.71
	4	–3.97	4	–10.65
	5	–5.02	5	–10.62
	6	–4.69	6	–10.61
	7	–4.41	7	–10.60
	8	–5.01	8	–10.59
	9	–4.96	9	–10.54
	10	–4.61	10	–10.51
Diclofenac	1	–7.65	1	–7.43
	2	–7.32	2	–7.32
	3	–7.26	3	–7.31

Table 4.1 Binding energy (BE) in kcal/mol of top-ten docked poses of NSAIDs from AutoDock4. (cont.)

NSAIDs	COX-1		COX-2	
	Rank	$BE_{autodock4}$ / (kcal/mol)	Rank	$BE_{autodock4}$ / (kcal/mol)
Diclofenac	4	–7.23	4	–7.31
	5	–7.08	5	–7.19
	6	–6.98	6	–7.08
	7	–7.44	7	–7.32
	8	–6.92	8	–7.19
	9	–7.40	9	–7.18
	10	–7.13	10	–7.08
Ibuprofen	1	–7.73	1	–6.47
	2	–7.68	2	–6.29
	3	–7.65	3	–6.08
	4	–7.63	4	–6.01
	5	–7.52	5	–5.87
	6	–7.45	6	–5.68
	7	–7.32	7	–5.91
	8	–7.13	8	–5.70
	9	–6.78	9	–5.51
	10	–6.53	10	–5.53
Naproxen	1	–8.58	1	–7.17
	2	–8.58	2	–6.70
	3	–8.56	3	–6.67
	4	–8.55	4	–6.75
	5	–8.54	5	–6.41
	6	–8.51	6	–6.71

Table 4.1 Binding energy (BE) in kcal/mol of top-ten docked poses of NSAIDs from AutoDock4. (cont.)

NSAIDs	COX-1		COX-2	
	Rank	$BE_{autodock4}$ / (kcal/mol)	Rank	$BE_{autodock4}$ / (kcal/mol)
Naproxen	7	–8.51	7	–6.69
	8	–8.45	8	–6.52
	9	–8.32	9	–5.96
	10	–8.28	10	–5.87
Aspirin	1	–5.80	1	–5.95
	2	–5.72	2	–5.85
	3	–5.67	3	–5.73
	4	–5.40	4	–5.71
	5	–5.53	5	–5.61
	6	–5.48	6	–5.57
	7	–5.33	7	–5.55
	8	–5.06	8	–5.51
	9	–5.02	9	–5.35
	10	–4.95	10	–5.30
Flurbiprofen	1	–8.93	1	–7.56
	2	–8.87	2	–7.50
	3	–8.83	3	–7.34
	4	–8.78	4	–7.32
	5	–8.75	5	–7.50
	6	–8.72	6	–7.50
	7	–8.57	7	–7.40
	8	–8.49	8	–7.19
	9	–8.35	9	–7.18
	10	–8.29	10	–6.87

The GFN2-xTB method coupled with the ALPB solvation model effectively discriminates between the top-ranked poses obtained from the Autodock4 scoring function with a wide range of binding free energies. **Table 4.2** shows the lowest-energy optimized pose of each NSAIDs, considering the uncorrected binding free energy in implicit aqueous solvation ($\Delta G'_{bind,solv}$). For the non-selective NSAIDs, their $\Delta G'_{binding}$ ranged from –24.13 to –26.73 kcal/mol for COX-1 and –21.70 to –25.26 kcal/mol for COX-2. In contrast, etoricoxib and celecoxib exhibited stronger binding to the active sites of COX-2, with the uncorrected binding free energy ($\Delta G'_{binding}$) of –39.75 and –43.86 kcal/mol, respectively. In addition, the binding affinities of etoricoxib and celecoxib with COX-1 were +3.01 and +2.56 kcal/mol, respectively, indicating weaker binding compared to COX-2. It is evident that COX-2 selective NSAIDs exhibit lower affinity for COX-1.

Table 4.2 Uncorrected binding free energy ($\Delta G'_{bind,solv}$) in kcal/mol of the lowest-energy optimized pose by using GFN2-xTB method with ALPB solvation model.

NSAIDs	COX-1	COX-2
Celecoxib	+2.56	–43.86
Etoricoxib	+3.01	–39.75
Flurbiprofen	–25.29	–25.26
Diclofenac	–24.13	–23.81
Aspirin	–17.26	–19.02
Ibuprofen	–24.73	–21.70
Naproxen	–26.73	–24.21

4.1.2 The performance of AutoDock4 and GFN2-xTB for predicting the correct conformations

The geometry optimization of docked poses using the GFN2-xTB method provides lowest-energy poses comparable to their co-crystallized conformations. Each of top-ten docked poses obtained from AutoDock4 was solely

reoptimized within the binding pocket of the prepared receptors. The deviation of these optimized poses was then compared to their corresponding X-ray crystallographic poses. **Table 4.3** shows the root mean square deviations of the optimized poses for all four receptors, with a range of 1.0 - 2.0 Å. Note that the analyzed poses were the lowest-energy optimized poses for flurbiprofen, celecoxib, and tetrahydrocannabinol, with the exception of the fifth-ranked pose for aminoalkylindole derivative.

Table 4.3 Root mean square deviations (RMSD) of lowest-energy optimized poses of co-crystallized ligands of protein receptors.

Protein-ligand system	Average RMSD / (Å)
COX-1/flurbiprofen	1.01
COX-2/celecoxib	1.04
CB1/tetrahydrocannabinol	1.95
CB2/aminoalkylindole derivative	1.76

The binding interactions of the optimized NSAID poses at the active sites of COX-1 and COX-2 were examined and compared with those of the best-docked poses. **Figure 4.1** shows the binding interactions between the best-docked poses and the lowest-energy-optimized poses of aspirin and diclofenac at the active site of COX-1. GFN2-xTB method gave the lowest-energy optimized pose of aspirin, while AutoDock4 suggested a false negative. The orientations of both lowest-energy optimized poses were closely aligned with their X-ray crystallographic poses. This can be seen from the carboxyl group of the lowest-energy optimized pose of aspirin (pink in **Figure 4.1a**) aligned at the same position as its X-ray crystallographic pose. Hydrogen bonding interactions of the lowest-energy optimized pose of aspirin included bonds between the carboxylic acid group and Tyr355 (1.65 Å), the ester group and Ser353 (2.79 Å), and the ester group and Ala527 (2.97 Å) with COX-1 (**Figure 4.1a**). Similarly, the carboxyl groups of the lowest-energy optimized pose and the X-ray crystallographic pose of diclofenac also aligned at the same position, displaying hydrogen bonding interactions with Arg120 within 2 Å (**Figure 4.1b**). It is noteworthy that the best-docked poses of aspirin and diclofenac were flipped compared to their X-

ray crystallographic poses. Arg120 and Tyr355 were identified as key amino acids at the binding entrance of COX-1, agreed with previous study [58]. **Figure 4.2** shows the binding interactions of the best-docked poses and the lowest-energy-optimized poses of flurbiprofen at the active sites of COX-2. The carboxyl group of the lowest-energy optimized pose of flurbiprofen aligned with the same position as the sulfonamide group of celecoxib, an NSIAD. Hydrogen bonding interactions between the carboxyl group of flurbiprofen and the amino group of Arg499 and Phe504 were observed within 3 Å. This agreed well with the crucial amino acids of COX-2 [5].

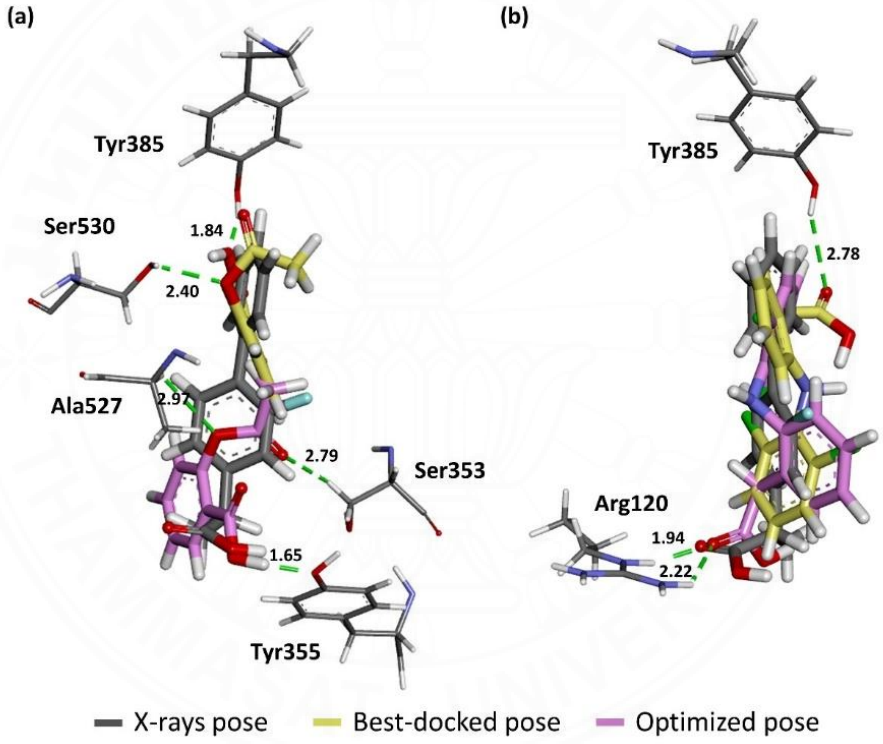

Figure 4.1 Hydrogen bonding interactions between the best-docked pose (stick representation in yellow) and the lowest-energy optimized pose (stick representation in pink) of (a) aspirin and (b) diclofenac at the active sites of COX-1.

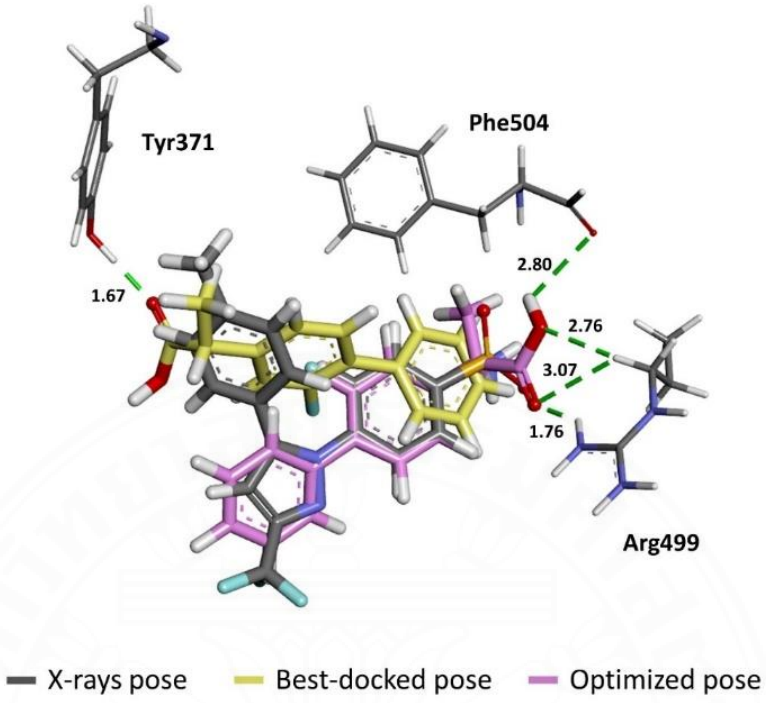

Figure 4.2 Hydrogen bonding interactions between the best-docked pose (stick representation in yellow) and the lowest-energy optimized pose (stick representation in pink) of flurbiprofen at the active sites of COX-2.

4.1.3 Validation of calculated selectivity index

The binding stability of an active compound with its target receptor can be evaluated by examining the binding free energy. The more negative binding free energy indicates that the ligand can bind strongly to its receptor. Considering the non-competitive mechanism of protein-ligand inhibition, the inhibitory constant (K_i) value is directly proportional to the 50% inhibitory concentration (IC_{50}). Thus, the higher affinity of inhibitors corresponds to lower value of K_i and IC_{50}.

The selectivity index (SI) is typically derived from the ratio of IC50 value for COX-2 to that for COX-1, reflecting the anti-inflammatory potency of NSAIDs. In our study, the uncorrected binding free energy ($\Delta G'_{bind,solv}$) calculated using GFN2-xTB method with the ALPB solvation model was converted to the inhibitory constant (K_i). This K_i value was then used to calculate the selectivity index. **Table 4.4** shows the calculated and experimental selectivity indexes [34, 35] of NSAIDs for

COX-2 to COX-1 ratio, determined using Spearman rank correlation [119]. We found that our calculated and the experimental selectivity indexes of four NSAIDs in **Table 4.4** were closely matched (r = 1, P-value = 0.083). Thus, when a ligand specifically binds to the anti-inflammatory COX-2 and CB2 receptors, the SI value is low. Conversely, when a ligand binds to COX-1 and psychoactive CB1 receptors, the SI value is high. Consequently, the calculated selectivity index in this study was used to predict the anti-inflammatory potency of cannabinoids.

Table 4.4 Experimental selectivity index (Exp. SI) and calculated selectivity index (Calc. SI) of NSIADs.

NSAIDs	Experimental value [1]			GFN2-xTB (ALPB)		
	IC_{50} (μM) COX-1	IC_{50} (μM) COX-2	Exp. SI	Calc. K_i COX-1	Calc. K_i COX-2	Calc. SI
Celecoxib	16.00	0.54	–1.47	2.20×10^{-5}	2.38×10^{-22}	–16.97
Diclofenac	0.08	0.04	–0.30	2.57×10^{-17}	2.54×10^{-14}	3.00
Ibuprofen	7.60	20.00	0.42	1.41×10^{-17}	2.42×10^{-12}	5.23
Flurbiprofen	0.08	5.50	1.84	5.87×10^{-17}	5.40×10^{-6}	10.96

[1] Experimental value was obtained from [34, 35]

4.1.4 Validation of binding free energy

The GFN2-xTB method with ALPB solvation model can compute binding free energy values that agree with experimental data. The experimental binding free energy is estimated as $\Delta G = -RT\ln K_d = RT\ln K_a = RT\ln K_i$, where K_d is the equilibrium dissociation constant, K_a is the equilibrium association constant, and K_i is the inhibitory constant. The Pearson correlation coefficient (r_p) [120] was used to evaluate the correlation between the calculated binding free energy and the experimental binding free energy of seven NSAIDs. As shown in **Figure 4.3a**, the Pearson correlation coefficient (r_p) was approximately 0.40, indicating moderate performance of the computational method used. Additionally, the performance of the method improved significantly (r_p = 0.60), indicating strong performance, when using

the corrected binding free energy in implicit aqueous solvation ($\Delta G_{bind,solv}$) with fully-relaxed pocket protein-ligand geometries (**Figure 4.3b)**.

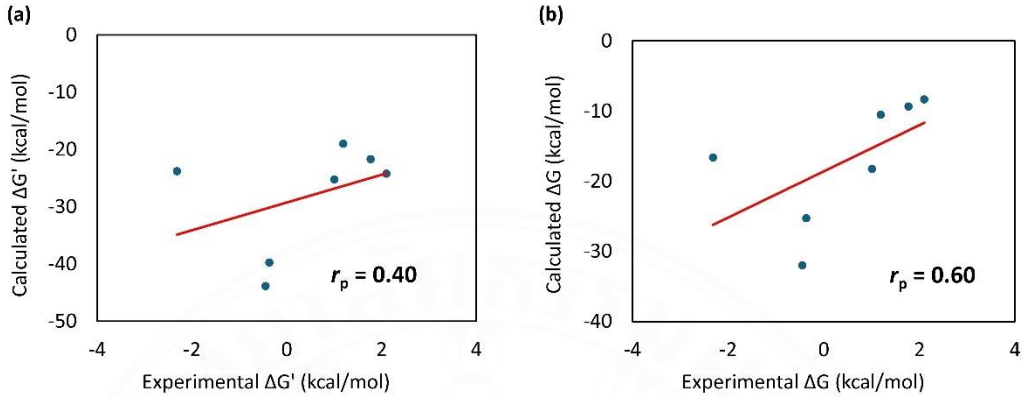

Figure 4.3. Pearson correlation between experimental binding free energy values and (a) uncorrected binding free energy ($\Delta G'_{bind,solv}$) and (b) corrected binding free energy in implicit aqueous solvation ($\Delta G_{bind,solv}$) by using the GFN2-xTB method with ALPB solvation model of NSAIDs.

4.2 Cannabinoids

This section examines the binding affinity of cannabinoids with COX-1, COX-2, CB1, and CB2. The ALPB solvation model and GFN2-xTB method were used to compute the binding free energy of receptors/cannabinoids complexes, considering both unrelaxed and fully relaxed geometries of the receptors. Additionally, the selectivity indexes of COX-2 to COX-1 and CB2 to CB1 ratios were estimated to predict the anti-inflammatory potency of cannabinoids. The predicted drug-like properties of modified cannabinoid analogs were compared to those of celecoxib.

4.2.1 The binding affinity of receptors/cannabinoids complexes

The GFN2-xTB method with the ALPB solvation model can differentiate the best-bound pose of a ligand. The binding enthalpy obtained from molecular docking and GFN2-xTB methods in a vacuum for 55 cannabinoids at the active sites of COX and CB receptors is reported in **Appendix A**. The binding free energy for all cannabinoids in native conformations of the studied receptors was

analyzed and is presented in **Table 4.5**. The number of bound-cannabinoids was clustered based on either the binding enthalpy obtained from the docking scheme or the uncorrected binding free energy in implicit aqueous solvation ($\Delta G'_{\mathrm{bind,solv}}$) obtained from the GFN2-xTB method. The GFN2-xTB method with the ALPB solvation model effectively differentiates the binding free energy of each optimized ligand pose, resulting in a wide range of MAX-MIN values, a higher RMSE, and a higher mean absolute deviation for all studied receptors. Considering the number of bound cannabinoids classified into three clusters, it was found that the GFN2-xTB method with the ALPB solvation model identified 7 cannabinoids with strong binding affinity to COX-1, ranging from −11 kcal/mol to −20 kcal/mol, out of 48 compounds. In addition, CB1 and CB2 receptors consistently showed the highest number of bound cannabinoids in the best cluster (number 1), with binding free energies more negative than −21 kcal/mol for both methods, as these receptors are well-known cannabinoid receptors.

Table 4.5 Statistical data of binding energies and uncorrected binding free energies in kcal/mol of 55 cannabinoids calculated by AutoDock4 and GFN2-xTB method with ALPB solvation model.

Receptor	Statistical data	Autodock4			GFN2-xTB (ALPB)		
		cluster 1 < –10	cluster 2 –8 to –9	cluster 3 –5 to –7	cluster 1 > –21	cluster 2 –11 to –20	cluster 3 < –10
COX-1	n	4	35	16	0	7	48
	Mean	–9.90	–8.32	–6.73	NA	–12.02	7.89
	RMSE	0.32	0.44	0.58	NA	1.31	7.59
	MAD	0.26	0.36	0.46	NA	1.11	6.05
	MIN	–0.49	–1.08	–0.68	NA	–2.55	–16.56
	MAX	0.38	0.80	1.33	NA	1.43	18.30
COX-2	n	10	36	9	5	18	32
	Mean	–9.97	–8.65	–6.50	–21.74	–14.57	–4.68
	RMSE	0.20	0.51	0.55	1.00	2.33	3.77
	MAD	0.17	0.44	0.48	0.80	1.83	3.03
	MIN	–0.30	–0.79	–0.89	–1.88	–5.83	–5.71
	MAX	0.26	1.04	0.69	0.95	3.96	7.67
CB1	n	37	14	4	39	15	1
	Mean	–10.38	–8.86	–6.33	–27.61	–16.76	–8.83
	RMSE	0.62	0.31	0.26	2.42	2.93	0.00
	MAD	0.52	0.24	0.21	1.87	2.38	0.00
	MIN	–1.49	–0.55	–0.42	–5.81	–3.56	0.00
	MAX	0.88	0.66	0.29	5.64	5.73	0.00
CB2	n	12	38	5	48	8	1
	Mean	–9.81	–8.52	–6.20	–25.15	–17.00	–10.44
	RMSE	0.36	0.55	0.68	2.81	2.02	0.00
	MAD	0.30	0.48	0.47	2.39	1.90	0.00
	MIN	–0.71	–0.88	–1.15	–5.57	–2.68	0.00
	MAX	0.36	1.07	0.97	4.71	2.89	0.00

Next, we examined the $\Delta G'_{bind,solv}$ of common parent cannabinoids and their acid derivatives. It was found that the studied cannabinoids exhibit strong binding affinity with cannabinoid receptors, CB1 and CB2 (**Table 4.6**). The $\Delta G'_{bind,solv}$ of the acid derivatives was more negative than that of the parent cannabinoids, indicating higher affinity. The $\Delta G'_{bind,solv}$ of the optimized poses of CBNA, Δ^9-THCA, Δ^9-THC, CBGA, CBDA, CBTA, CBG, and CBD with psychoactive CB1 were, respectively, –32.89, –31.11, –30.23, –29.69, –29.33, –28.36, –28.22, and –27.26 kcal/mol. Regarding the anti-inflammatory CB2 receptor, it was found that CBCA, CBEA, CBC, CBT, CBE, CBLA, CBL, and CBN showed strong affinity, with uncorrected binding free energy ranging from –22.34 to –29.13 kcal/mol.

Table 4.6 The uncorrected binding free energy ($\Delta G'_{bind,solv}$) in kcal/mol of the lowest-energy optimized pose of parent cannabinoids and acid derivatives with CB1 and CB2 using the GFN2-xTB method with the ALPB solvation model.

Cannabinoid	**$\Delta G'_{bind,solv}$ / (kcal/mol)**	
	CB1	**CB2**
CBNA	–32.89	–25.64
Δ^9-THCA	–31.11	–22.42
Δ^9-THC	–30.23	–25.43
CBGA	–29.69	–30.73
CBDA	–29.33	–22.36
CBTA	–28.36	–27.27
CBG	–28.22	–26.59
CBD	–27.26	–23.47
CBCA	–26.45	–29.13
CBEA	–25.23	–25.89
CBC	–23.47	–27.11
CBT	–19.76	–26.03

Table 4.6 The uncorrected binding free energy ($\Delta G'_{bind,solv}$) in kcal/mol of the lowest-energy optimized pose of parent cannabinoids and acid derivatives with CB1 and CB2 using the GFN2-xTB method with the ALPB solvation model. (cont.)

Cannabinoid	$\Delta G'_{bind,solv}$ / (kcal/mol)	
	CB1	CB2
CBE	–19.38	–27.61
CBLA	–19.12	–26.23
CBL	–17.91	–23.09
CBN	–17.16	–22.34

Furthermore, we explored the length of alkyl sidechains of parent cannabinoids and their acid derivatives upon their binding affinity. It was found that Δ^9-THC, Δ^9-THCA, CBD, CBDA, and CBGA containing three or four methylene groups still showed the highest affinity with CB1 (**Table 4.7**). The $\Delta G'_{bind,solv}$ of CBGA-C3, Δ^9-THC-C4, CBD-C4, Δ^9-THC-C3, CBDA-C3, Δ^9-THCA-C3, and CBG-C3 was, respectively, –33.42, –28.94, –28.72, –27.54, –27.37, –26.89, and –25.51 kcal/mol. However, CBN showed the high affinity with CB2 with the uncorrected binding free energy of –30.63, –28.93, and –27.67 kcal/mol, respectively, with C4, C3, and C2 alkyl sidechains (**Table 4.7**). Compared with CB2/CBCA ($\Delta G'_{bind,solv}$ = –29.13 kcal/mol), CBCA with three methylene groups showed the highest affinity with CB2 with the uncorrected binding free energy of –28.03 kcal/mol.

Table 4.7 The uncorrected binding free energy ($\Delta G'_{bind,solv}$) in kcal/mol of the lowest-energy optimized poses of parent cannabinoids and their acid derivatives with varying alkyl sidechain lengths using the GFN2-xTB method with ALPB solvation model.

Cannabinoid	$\Delta G'_{bind,solv}$ / (kcal/mol)	
	CB1	**CB2**
CBGA-C3	–33.42	–30.61
CBN-C4	–30.63	–23.83
Δ^9-THC-C4	–28.94	–23.12
CBN-C3	–28.93	–20.98
CBD-C4	–28.72	–24.06
CBN-C2	–27.67	–17.82
Δ^9-THC-C3	–27.54	–22.11
CBDA-C3	–27.37	–25.64
Δ^9-THCA-C3	–26.89	–23.49
CBC-C3	–26.74	–26.29
CBG-C3	–25.51	–24.62
CBCA-C3	–21.97	–28.03
CBD-C3	–20.31	–24.06

Apart from common parent cannabinoids, other cannabinoid derivatives were also examined. It was found that Δ^9-THCA, the acid derivative of Δ^9-THC, showed the highest affinity with CB1 ($\Delta G'_{bind,solv}$ = –30.69, **Table 4.8**). For other Δ^9-THC derivatives, the $\Delta G'_{bind,solv}$ values for Δ^8-THCA, OTHC, Δ^8-THC, TriOH-THC, 2-oxo-Δ3(4)-THC, cis-Δ^9-THC, Δ1(2)-THCM were –28.78, –28.62, –27.53, –26.42, –26.00, –23.39 kcal/mol, respectively (**Table 4.8**). However, 8,9-dihydroxy-Δ-6a-THC, Δ^9-THCA-B, 10-ethoxy-9-hydroxy-Δ-6a-THC, and Δ^7-cis-iso-THCV exhibited binding affinity with CB2 comparable to that of CB1. Other than Δ^9-THC derivatives,

CBND showed the highest affinity with CB1 with the uncorrected binding free energy of −28.42 kcal/mol.

Table 4.8 The uncorrected binding free energy ($\Delta G'_{bind,solv}$) in kcal/mol of the lowest-energy optimized pose of other cannabinoid derivatives using the GFN2-xTB method with ALPB solvation model.

Cannabinoid	$\Delta G'_{bind,solv}$ / (kcal/mol)	
	CB1	CB2
Δ^8-THCA	−30.69	−23.89
8,9-dihydroxy-Δ-6a-THC	−28.93	−30.59
OTHC	−28.78	−27.04
Δ^8-THC	−28.62	−22.89
CBND	−28.42	−20.77
TriOH-THC	−27.53	−19.52
H_2CBD	−26.99	−24.67
CBGAM	−26.90	−30.10
CBGM	−26.65	−29.08
CBDM	−26.59	−28.16
2-oxo-Δ3(4)-THC	−26.42	−22.12
cis-Δ^9-THC	−26.00	−24.30
CBCT	−25.40	−23.37
CBNM	−24.75	−24.27
CBCM	−24.24	−28.69
Δ1(2)-THCM	−23.39	−21.83
Δ^9-THCA-B	−19.99	−23.57
10-ethoxy-9-hydroxy-Δ-6a-THC	−17.75	−26.36
Terpenoids [a]	−17.29	−19.68
Hydronaphthalene	−16.55	−14.11
Δ^7-cis-iso-THCV	−16.21	−20.82

Table 4.8 The uncorrected binding free energy ($\Delta G'_{bind,solv}$) in kcal/mol of the lowest-energy optimized pose of other cannabinoid derivatives using the GFN2-xTB method with ALPB solvation model. (cont.)

Cannabinoid	$\Delta G'_{bind,solv}$ / (kcal/mol)	
	CB1	**CB2**
Terpenoids [b]	–14.56	–15.89
Terpenoids [c]	–12.71	–15.43
Terpenoids [d]	–11.59	–14.99
Terpenoids [e]	–11.03	–10.44
Terpenoids [f]	–8.83	–20.45

[a] CDB006348. [b] CDB006347. [c] CDB006349. [d] CDB006350. [e] CDB006346. [f] CDB006352.

Candidate cannabinoids with anti-inflammatory properties should have high binding affinity with COX-2 and/or CB2 receptors without psychoactive effects. It is noteworthy that CBC, CBL, and CBE and their acid derivatives showed a high affinity with CB2. Consequently, we examined the $\Delta G'_{bind,solv}$ of cannabinoids with COX-1 and COX-2 (**Table 4.9**). CBC, CBCA, and CBEA were the tightly bound cannabinoids with CB2 and COX-2. The $\Delta G'_{bind,solv}$ values of CBC, CBCA, and CBEA with COX-2 were respectively –14.72, –13.55, and –5.45 kcal/mol.

Table 4.9 The uncorrected binding free energy ($\Delta G'_{bind,solv}$) in kcal/mol of the lowest-energy optimized pose of parent cannabinoids and acid derivatives with COX-1 and COX-2 using the GFN2-xTB method with ALPB solvation model.

Cannabinoid	$\Delta G'_{bind,solv}$ / (kcal/mol)	
	COX-1	**COX-2**
CBG	–8.67	–16.38
CBC	0.50	–14.72

Table 4.9 The uncorrected binding free energy ($\Delta G'_{bind,solv}$) in kcal/mol of the lowest-energy optimized pose of parent cannabinoids and acid derivatives with COX-1 and COX-2 using the GFN2-xTB method with ALPB solvation model. (cont.)

Cannabinoid	$\Delta G'_{bind,solv}$ / (kcal/mol)	
	COX-1	**COX-2**
CBCA	4.97	–13.55
Δ^9-THC	7.44	–12.63
CBNA	1.41	–8.56
CBN	8.84	–8.03
Δ^9-THCA	15.54	–7.30
CBGA	–11.41	–6.01
CBEA	22.74	–5.45
CBTA	14.61	–3.51
CBD	7.45	–3.15
CBE	12.76	–2.37
CBT	14.43	–0.58
CBLA	20.45	2.14
CBDA	3.58	2.21
CBL	17.90	2.98

Furthermore, we explored the length of alkyl sidechains of parent cannabinoids and their acid derivatives upon their binding affinity. It was found that CBN showed the high affinity with CB2 with the uncorrected binding free energy of –21.87, –23.62, and –20.79 kcal/mol, respectively, with C4, C3, and C2 alkyl sidechains (**Table 4.10**).

Table 4.10 The uncorrected binding free energy ($\Delta G'_{bind,solv}$) in kcal/mol of the lowest-energy optimized pose of parent cannabinoids and acid derivatives with varying alkyl sidechain lengths using the GFN2-xTB method with ALPB solvation model.

Cannabinoid	$\Delta G'_{bind,solv}$ / (kcal/mol)	
	COX-1	**COX-2**
CBN-C3	–1.69	–23.62
CBN-C2	–1.01	–21.87
CBC-C3	–11.08	–21.30
Δ^9-THCA-C3	5.49	–21.13
CBN-C4	0.03	–20.79
Δ^9-THC-C3	9.03	–20.40
CBG-C3	–13.33	–17.86
Δ^9-THC-C4	8.09	–16.02
CBGA-C3	–11.77	–15.48
CBD-C3	4.66	–14.38
CBDA-C3	–0.01	–12.91
CBCA-C3	–14.57	–10.33
CBD-C4	4.66	-5.90

Apart from common parent cannabinoids, other cannabinoid derivatives were also examined. It was found that CBND and CBNM showed the highest affinity with COX-2 with the uncorrected binding free energy of −17.60 and −13.95 kcal/mol, respectively (**Table 4.11**).

Table 4.11 The uncorrected binding free energy ($\Delta G'_{bind,solv}$) in kcal/mol of the lowest-energy optimized pose of other cannabinoid derivatives using the GFN2-xTB method with ALPB solvation model.

Cannabinoid	$\Delta G'_{bind,solv}$ / (kcal/mol)	
	COX-1	COX-2
CBND	2.03	−17.60
8,9-dihydroxy-Δ-6a-THC	11.38	−14.03
CBNM	1.76	−13.95
Δ^8-THC	16.12	−13.92
TriOH-THC	8.22	−13.46
Δ^7-cis-iso-THCV	9.83	−12.37
CBGAM	−5.87	−11.99
Terpenoids [a]	−3.68	−10.61
Terpenoids [b]	−3.23	−10.39
CBCM	−10.59	−10.06
Δ^9-THCA-B	12.58	−9.99
Terpenoids [c]	6.11	−8.91
H_2CBD	5.61	−8.85
CBGM	−11.36	−6.56
Δ^8-THCA	9.88	−6.33
cis-Δ^9-THC	21.98	−5.42
2-oxo-Δ3(4)-THC	1.50	−5.19
Terpenoids [d]	4.84	−4.83
Hydronaphthalene	7.20	−4.30
10-ethoxy-9-hydroxy-Δ-6a-THC	26.19	−4.06
Δ1(2)-THCM	13.76	−3.92
CBCT	16.34	−3.46
CBDM	1.50	−3.17
OTHC	3.67	−1.81
Terpenoids [e]	8.01	−1.23
Terpenoids [f]	12.84	2.45

[a] CDB006347. [b] CDB006349. [c] CDB006346. [d] CDB006348. [e] CDB006350. [f] CDB006352.

4.2.2 The selectivity index

As mentioned in section 4.1.3, the calculated selectivity index (SI) was used to examine the anti-inflammatory potency of cannabinoids. The low SI of COX-2/COX-1 and CB2/CB1 ratios indicates high anti-inflammatory potency. On the other hand, the high SI of CB2/CB1 ratio suggests the psychoactive effects. It was clear that the $SI_{CB2/CB1}$ values of Δ^9-THC, CBN, CBD, CBG, and their acid derivatives were high **(Figure 4.4)** due to their high affinity with CB1**.** This agreed well with their low K_i values in µM unit of CB1 (Δ^9-THC = 0.02 µM [49], CBN = 0.33 µM [49], CBD = 4.90 µM [51, 52], CBG = 1.05 µM [48]). However, the $SI_{CB2/CB1}$ values for CBN and CBT were lower than those of their acid derivatives. Interestingly, the $SI_{CB2/CB1}$ and $SI_{COX\text{-}2/COX\text{-}1}$ were low in CBC, CBL, CBE, and their acid derivatives. The selectivity index of acid derivatives of these cannabinoids was lower than that of their parent compounds. From **Figure 4.4**, the $SI_{CB2/CB1}$ values of CBCA, CBLA, and CBEA were, respectively, –1.96, –5.22, and –0.49. The $SI_{COX\text{-}2/COX\text{-}1}$ values of CBCA, CBLA, and CBEA were, respectively, –13.59, –13.33, and –20.68. Therefore, we suggested that CBCA, CBLA, and CBEA were potential candidate compounds with anti-inflammatory properties targeting COX-2. However, as discussed in **Table 4.10** and **Table 4.11**, CBNA exhibited the highest affinity with COX-2; therefore, CBNA was also selected as a candidate compound.

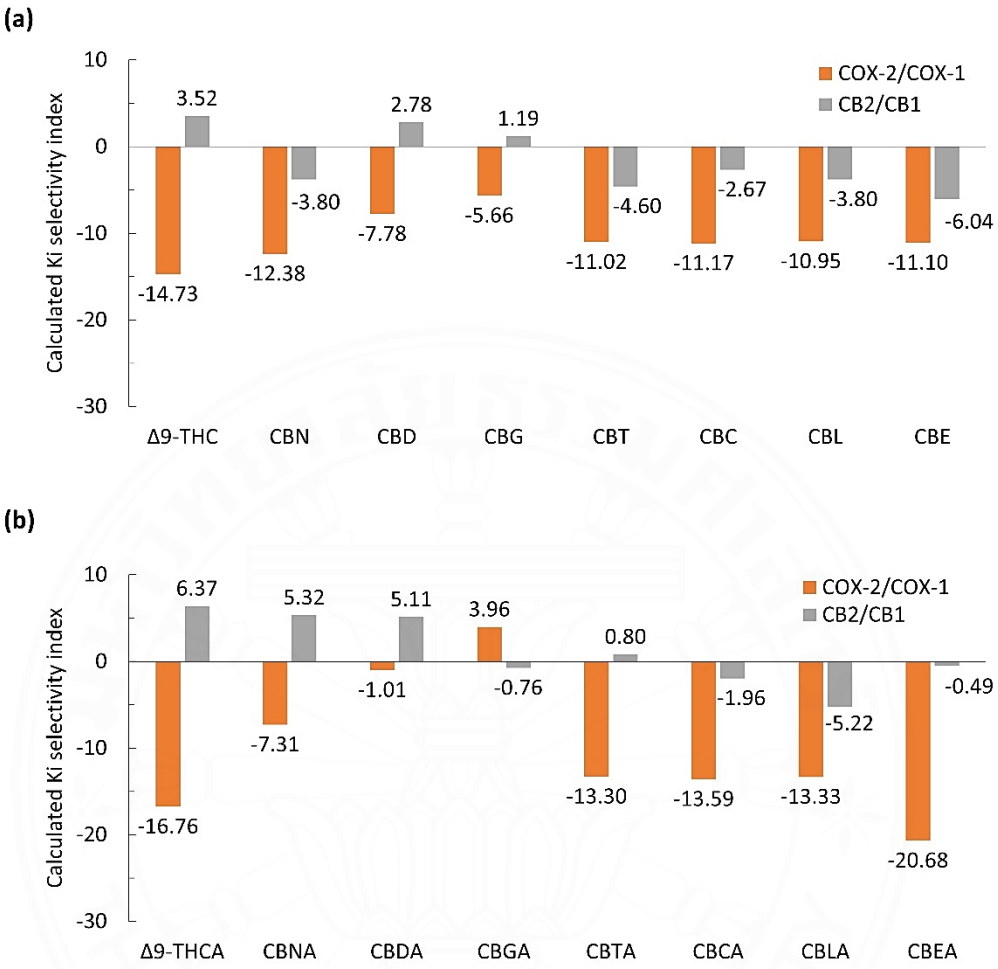

Figure 4.4 Selectivity index (SI) of COX-2/COX-1 ratio and CB2/CB1 ratio of (a) parent cannabinoids and (b) acid derivatives by using GFN2-xTB method with ALPB solvation model.

4.2.3 Geometry relaxation and binding interactions

The influence of thermal energy, entropy, and geometry relaxation plays an important role in the calculated binding free energy. The corrected binding free energy ($\Delta G_{\text{bind,solv}}$) consists of three contributions: the total gas-phase energy in a vacuum (ΔE_{vac}), the solvation free energy ($\Delta\delta G_{\text{solv}}$), and the thermostatistical contribution to the free energy ($T\Delta S_{\text{mRRHO}}$). To account for these contributions, the COX-2/candidate cannabinoids complexes were fully optimized by using GFN2-xTB

method with ALPB solvation model. **Table 4.12** shows the $\Delta G_{bind,solv}$ values of CBNA, CBCA, CBLA, and CBEA, which are comparable to those of NSAIDs.

Table 4.12 The corrected binding free energy ($\Delta G_{bind,solv}$) in kcal/mol of candidate cannabinoids and NSIADs at the active sites of COX-2 using GFN2-xTB method with ALPB solvation model.

Compound	**$\Delta G_{bind,solv}$ / (kcal/mol)**
celecoxib	–32.02
etoricoxib	–25.27
CBCA	–22.80
CBNA	–20.20
CBEA	–20.05
flurbiprofen	–18.26
diclofenac	–16.63
CBLA	–15.52
aspirin	–10.53
ibuprofen	–9.36
naproxen	–8.32

Compared to non-selective NSAIDs in **Table 4.12**, CBCA, CBNA, and CBEA showed higher affinities with COX-2. For the COX-2/CBCA complex ($\Delta G_{bind,solv}$ = –22.80 kcal/mol), hydrogen bonding interactions occurred between Tyr341 and the hydroxyl group of CBCA at a distance of 1.83 Å, as well as between Ser339 and Val509 with the carboxyl group of CBCA at distances of 1.83 Å and 2.44 Å, respectively (**Figure 4.5a**). Similarly, the higher binding affinity of CBNA ($\Delta G_{bind,solv}$ = –20.20 kcal/mol) compared to CBEA ($\Delta G_{bind,solv}$ = –20.05 kcal/mol) is attributed to hydrogen bonding interactions with Ser339 in 1.75 Å (**Figure 4.5b**) and Val509 in 1.76 Å (**Figure 4.5c**). Additionally, hydrogen bonding interactions between the carboxyl group of CBNA and Arg499 could be observed within 2.30 Å. In contrast, the COX-2/CBLA complex exhibits a lower affinity ($\Delta G_{bind,solv}$ = –15.52 kcal/mol)

compared to diclofenac, a non-selective NSAID, ($\Delta G_{bind,solv}$ = −16.63 kcal/mol), due to the presence of only two amino acids, Leu338 and Arg499 (**Figure 4.5d**). Our results agreed well with the findings previously reported [5].

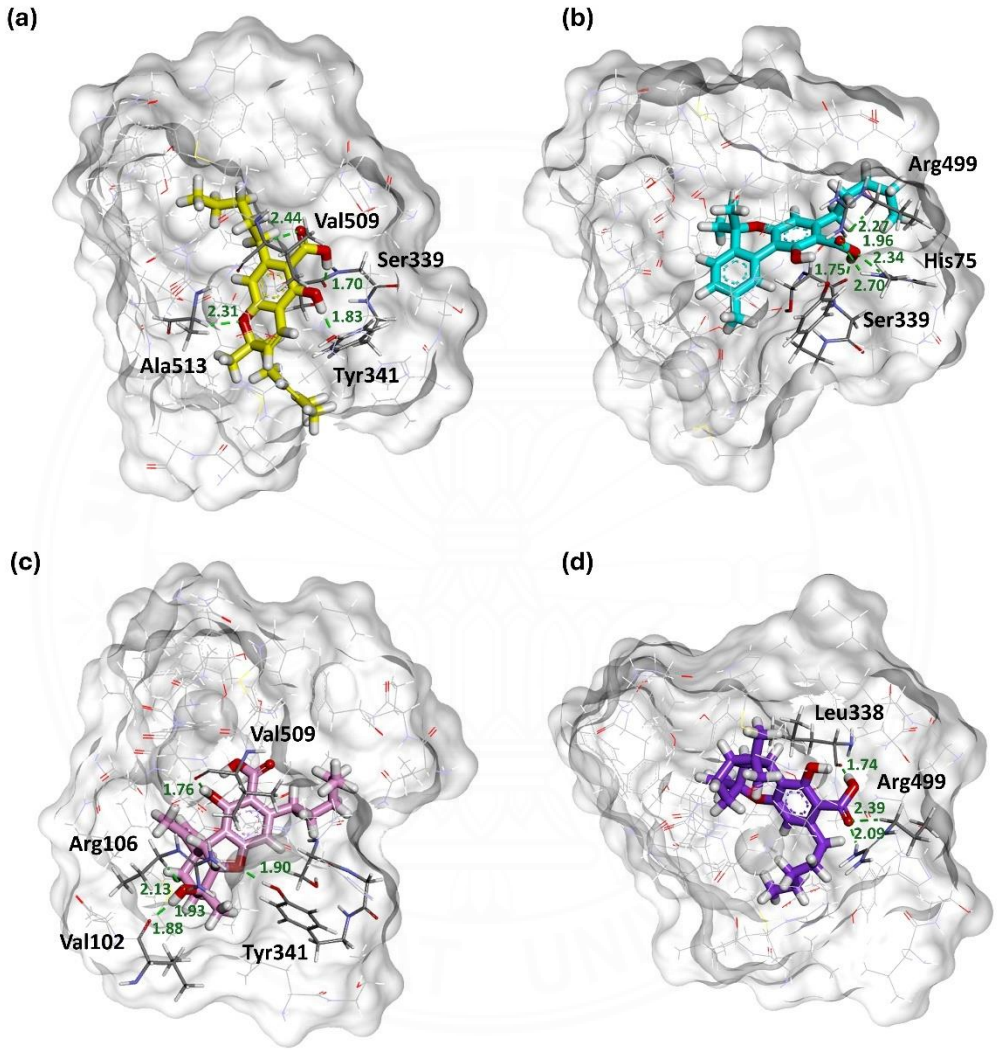

Figure 4.5 Binding interactions of (a) CBCA, (b) CBNA, (C) CBEA, and (d) CBLA with key amino acid at fully relaxed COX-2 complex. The hydrogen bonds are presented in green dashed lines. The unit of distance in proximity is angstrom.

It is noteworthy that the alkyl side chains of CBNA and CBEA were aligned in a similar position to the sulfonamide group of celecoxib, with interactions with Arg499 (**Figure 4.6a and 4.6b**). In addition, the alkyl side chain of CBCA (**Figure 4.6c**) could be modified and reoptimized for stronger binding affinity. Therefore, we anticipate that modification of the cannabinoid structure at the carbon side chains with the sulfonamide group could provide the higher affinity with COX-2.

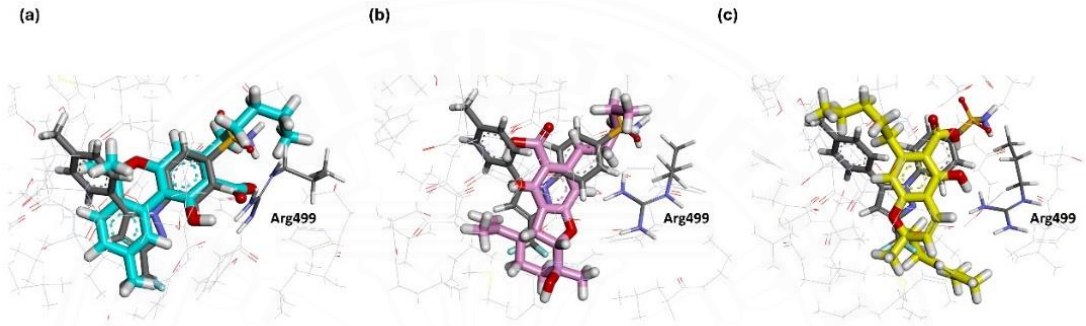

Figure 4.6 The optimized poses of (a) CBNA, (b) CBEA, and (C) CBCA aligned on celecoxib (gray stick) at fully relaxed COX-2 complex.

4.2.4 Modified cannabinoids analogs

As discussed in **Section 4.2.3**, structure modifications were made to the COX-2/cannabinoid complexes at the carbon side chains by introducing the sulfonamide group. **Figure 4.7** shows the 2D structures of these modified cannabinoid analogs.

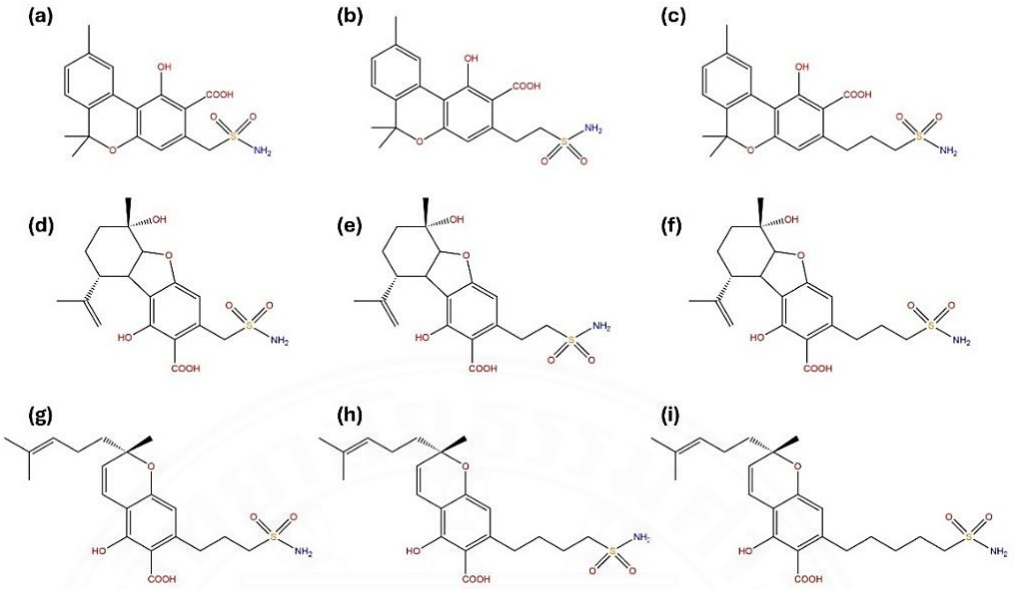

Figure 4.7 Chemical structures of modified cannabinoid analogs: (a) CBNA-C1, (b) CBNA-C2, (c) CBNA-C3 (d) CBEA-C1, (e) CBEA-C2, (f) CBEA-C3, (g) CBCA-C3, (h) CBCA-C4, and (i) CBCA-C5.

The complex of modified cannabinoid analogs was redocked and fully reoptimized using GFN2-XTB method with ALPB solvation model. It was found that the modified cannabinoid analogs of CBNA, CBEA, CBCA were the tightly bound cannabinoids with COX-2 (**Table 4.13)**. The modified CBCA at the C3 side chain showed the highest affinity ($\Delta G_{bind,solv}$ = −48.41 kcal/mol) compared to celecoxib ($\Delta G_{bind,solv}$ = −32.02 kcal/mol). The $\Delta G_{bind,solv}$ of modified CBEA at the C2 side chain and modified CBNA at the C3 side chain was respectively –45.82 and –45.62 kcal/mol.

Table 4.13 The corrected binding free energy ($\Delta G_{bind,solv}$) in kcal/mol of the modified cannabinoid analogs at the active sites of COX-2 by using GFN2-xTB method with ALPB solvation model.

Compound	**$\Delta G_{bind,solv}$ / (kcal/mol)**
CBCA-C3-SO_2NH_2	–48.41
CBEA-C2-SO_2NH_2	–45.82

Table 4.13 The corrected binding free energy ($\Delta G_{bind,solv}$) in kcal/mol of the modified cannabinoid analogs at the active sites of COX-2 by using GFN2-xTB method with ALPB solvation model. (cont.)

Compound	**$\Delta G_{bind,solv}$ / (kcal/mol)**
CBNA-C3-SO_2NH_2	–45.62
CBEA-C3-SO_2NH_2	–44.30
CBCA-C5-SO_2NH_2	–40.39
CBEA-C1-SO_2NH_2	–39.97
CBCA-C4-SO_2NH_2	–34.23
celecoxib	–32.02
CBNA-C2-SO_2NH_2	–25.42
CBNA-C1-SO_2NH_2	–24.00

For the fully relaxed COX-2 complexes, hydrogen bonding interactions were found at the sulfonyl group (-SO_2) of CBCA-C3-SO_2NH_2, CBNA-C3-SO_2NH_2, and CBEA-C2-SO_2NH_2 with Arg499, Ile503, and Phe504 within 3 Å. The sulfonamide group (-$SONH_2$) of those compounds occurred with His75 and Gln178 within 2 Å (**Figure 4.8**). Additionally, the carboxyl group of the CBCA-C3-SO_2NH_2 interacted with Met508 in 2.62 Å (**Figure 4.8a**) whereas that of CBNA-C3-SO_2NH_2 interacted with Ser339 in 2.09 Å (**Figure 4.8b**). Hydrogen bonding interactions with Val102 (in 1.85 Å) and Ala513 (in 2.56 Å) were observed at the hydroxyl group of CBEA-C2-SO_2NH_2 (**Figure 4.8c**).

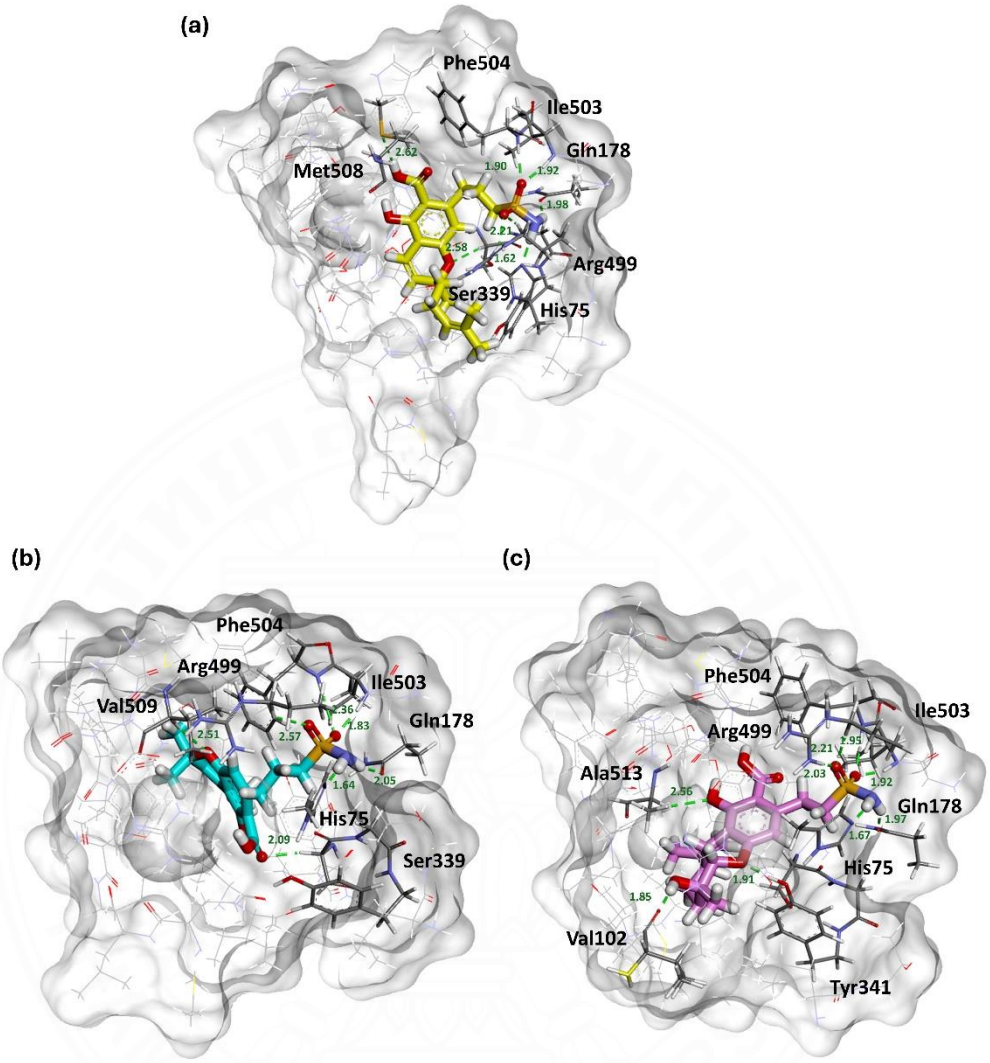

Figure 4.8 Binding interactions of modified (a) CBCA-C3-SO_2NH_2, (b) CBNA-C3-SO_2NH_2, and (C) CBEA-C2-SO_2NH_2 with key amino acid at fully relaxed COX-2 complex. The hydrogen bonds are presented in green dashed lines. The unit of distance in proximity is angstrom.

4.2.5 Drug-like properties

In drug development, it is important to ensure that drug candidates possess certain characteristics such as physicochemical properties, lipophilicity, water solubility, pharmacokinetics, and drug-likeness. In this study, drug-like properties of the modified cannabinoids were predicted by using Swiss ADME [110] online tool as presented in **Table 4.14.** It was found that CBCA, CBNA, CBEA, and their modified structures meet the Lipinski's rules of five, which state that the molecular weight should be less than 500 g/mol, with fewer than 5 hydrogen bond donors and fewer than 10 acceptors, and a partition coefficient (LogP) less than 5. This indicates that these compounds and their modified analogs have appropriate molecular weight, hydrogen bond counts, and partition coefficients.

Interestingly, the predicted LogP values of the modified cannabinoids were lower than those of their parent analogs and closed to that of celecoxib. According to log S, the CBEA-C2-SO_2NH_2 was found to be soluble. Conversely, CBCA, CBCA-C3-SO_2NH_2, CBNA, CBNA-C3-SO_2NH_2, and CBEA were moderately soluble. All compounds were suitable for oral drug availability, as indicated by their bioavailability scores falling within the range of 0−1.

In addition, we investigate their potential to inhibit cytochromes P450, a key factor in pharmacokinetics-related drug-drug interactions. It was found that none were found to inhibit CYP2D6 (**Table 4.14**). The modified cannabinoids had almost no effect to inhibit P450 inhibitors. These findings suggest that the modified compounds possess favorable physicochemical characteristics for oral bioavailability.

Table 4.14 Predicted drug-like properties of the modified cannabinoids and celecoxib.

	Mw[a] (g/mol)	HBA[b]	HBD[c]	Consensus Log $P_{o/w}$ (lipophilicity)	Log S (Water solubility)	Bioavailability Score	Cytochrome P450 inhibitor				
							CYP1A2	CYP2C19	CYP2C9	CYP2D6	CYP3A4
Celecoxib	381.37	7	1	3.40	-4.57	0.55	Yes	No	Yes	No	No
CBCA	358.47	4	2	4.98	-5.73	0.85	No	No	Yes	No	Yes
CBNA	354.44	4	2	4.48	-5.95	0.85	Yes	Yes	Yes	No	No
CBEA	374.47	5	3	4.04	-5.40	0.56	No	No	Yes	No	Yes
CBCA-C3-SO_2NH_2	409.50	7	3	2.71	-4.43	0.56	No	No	No	No	Yes
CBNA-C3-SO_2NH_2	405.46	7	3	2.64	-4.29	0.56	No	No	No	No	Yes
CBEA-C2-SO_2NH_2	411.47	8	4	1.61	-3.51	0.11	No	No	No	No	No

[a] Mw = Molecular weigh
[b] HBA = Hydrogen bond acceptors
[c] HBD = Hydrogen bond donors

4.3 Validation of SQM methods

The performance of the SQM methods in describing noncovalent interactions of protein-ligand systems was validated against five datasets of benchmark dimers and complexes as detailed in **Section 3.4**. To accurately describe these interactions, additional corrections were applied to the PM6 method including Grimme's dispersion (D) correction, a hydrogen bonding (H) correction, and a correction for extra repulsion in halogen atoms (X). For the DFTB3 method, Becke–Johnson damping function was employed to correct dispersion, along with a more advanced correction for hydrogen bonds. Lastly, the GFN2-xTB, an empirical tight binding approach, stands out as it does not require any ad-hoc corrections.

According to the nature of the benchmark dimers, the X correction had no effect on the S66 and HB375 datasets (**Table 4.15**) because these datasets include only H, C, O, and N atoms. Using the X40 dataset, PM6-D3H4 had a root mean square error (RMSE) of 2.59 kcal/mol, while PM6-D3H4X had a smaller RMSE of 2.31 kcal/mol. This indicates that the X correction improves the description of noncovalent interactions for specific element pairs, such as [O, N] – [Cl, Br, I] [121]. However, the X correction improves the description of noncovalent interactions in XH−I bonds but increases the error in XH−Cl and XH−Br groups in the HB300SPX dataset. This can be seen from the higher RMSE of 3.76 kcal/mol for PM6-D3H4X.

When the DFTB3-D3H4 was applied to S66, X40, and HB375 datasets, except for HB300SPX, the error remained large because H4 corrections apply only to H-bonds involving oxygen and nitrogen atoms [24]. For the DFTB3 methods, the DFTB3-D3H5 showed the lowest RMSE values for all five benchmark datasets. The H5 corrections provide more accurate interaction energy with fewer specific additional adjustments compared to the H4 corrections. H5 corrections also improved the overall description of hydrogen bonds involving oxygen, nitrogen, and sulfur atoms [86]. Among the studied SQM methods, GFN2-xTB was the most accurate method, reproducing the benchmark interaction energies with an RMSE of 1.06 kcal/mol for X40 and 1.40 kcal/mol for HB300SPX.

Table 4.15 RMSE, MAD, MSE, D_{MIN}, and D_{MAX} in kcal/mol of SQM methods tested against S66, X40, HB375, and HB300SPX data sets.

Dataset		PM6		DFTB3		GFN2-xTB
		D3H4	D3H4X	D3H4	D3H5	
S66	RMSE	0.69	0.69	1.26	0.60	0.95
	MAD	0.49	0.49	0.86	0.47	0.78
	MSE	–0.20	–0.20	–0.65	–0.19	–0.64
	D_{MIN}	–1.11	–1.11	–0.90	–1.18	–0.91
	D_{MAX}	2.51	2.51	3.60	1.94	2.44
X40	RMSE	2.59	2.31	2.65	2.32	1.06
	MAD	1.43	1.11	1.93	1.78	0.86
	MSE	–0.28	–0.70	0.90	0.97	–0.48
	D_{MIN}	–6.90	–1.12	–6.23	–5.45	–2.25
	D_{MAX}	11.39	11.39	7.40	4.56	2.57
HB375	RMSE	1.23	1.23	2.18	1.24	1.37
	MAD	0.96	0.96	1.71	0.94	1.18
	MSE	0.15	0.15	–1.67	–0.59	–1.12
	D_{MIN}	–3.74	–3.74	–1.22	–4.40	–1.55
	D_{MAX}	3.53	3.53	6.72	5.53	4.02
HB300SPX	RMSE	3.72	3.76	2.28	2.00	1.40
	MAD	2.57	2.63	1.50	1.37	1.00
	MSE	–2.21	–2.35	–0.96	–0.51	0.11
	D_{MIN}	–4.88	–2.40	–4.80	–4.90	–5.26
	D_{MAX}	13.27	13.27	12.71	11.06	4.40

The PLA15 benchmark dataset represents protein-ligand complexes with hundreds of atoms only at the binding region. The X correction had no effect on this dataset because it only addresses interactions between [O, N] – [Cl, Br, I] pairs of atoms, which are not presented in this dataset. For the PLA15 benchmark dataset, DFTB3-D3H5 outperformed best, with an RMSE of 15.58 kcal/mol (**Table 4.16**), compared to an RMSE of 13.27 kcal/mol from GFN2-xTB.

Table 4.16 RMSE, MAD, MSE, D_{MIN}, and D_{MAX} in kcal/mol of SQM methods tested against PLA15 data set.

Dataset		PM6		DFTB3		GFN2-xTB
		D3H4	D3H4X	D3H4	D3H5	
PLA15	RMSE	16.03	16.03	16.09	15.58	13.27
	MAD	13.30	13.30	12.47	12.47	10.52
	MSE	10.52	10.51	12.47	12.47	–10.23
	MIN	–30.74	–30.74	–38.23	–41.76	–2.18
	MAX	6.72	6.72	–2.78	–1.84	27.28

Figure 4.9 shows the mean absolute deviations (MADs) of GFN2-xTB across different datasets. Both the DFTB3-D3H5 and the GFN2-xTB methods outperformed the other SQM methods tested. The GFN2-xTB method is particularly notable because it has been developed to function without the need for specific, additional adjustments, making it user-friendly and straightforward to apply.

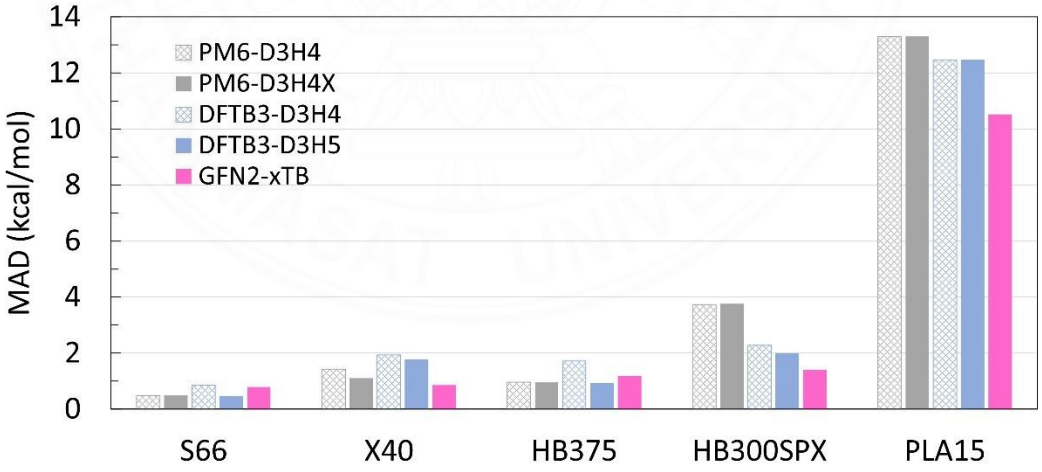

Figure 4.9 Mean absolute deviations (MADs) in kcal/mol for the noncovalent interaction energies of different benchmark datasets.

Figure 4.10 shows the distribution plot of the mean signed error (MSE) across different datasets. For S66, X40, HB375, and HB300SPX datasets, GFN2-xTB exhibited a narrow distribution with a significant peak height. However, all tested SQM methods displayed a broad distribution for the PLA15 dataset.

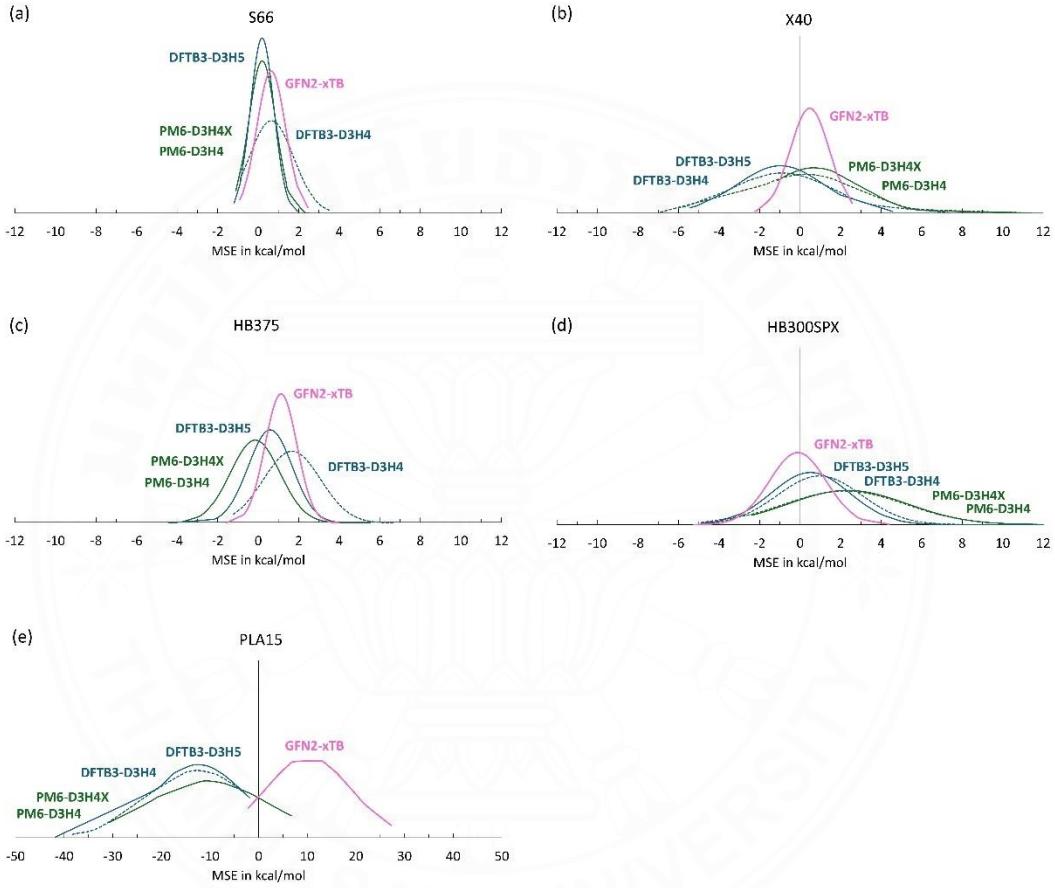

Figure 4.10 Distribution plots of the MSE in the computed interaction energies of (a) S66, (b) X40, (c) HB375, (d) HB300SPX, and (e) PLA15 benchmark datasets.

From the results of method validation, the DFTB3-D3H5 and GFN2-xTB methods outperformed other SQM methods testes, with lower RMSE, MAD, and MSE values. However, DFTB3-D3H5 failed to optimize the correct geometries of celecoxib, as it resulted in the breaking of the S-N bond in the sulfonamide group (**Figure 4.11**). This was evident from the hydrogen bonding observed between the amine group ($-NH_2$) of celecoxib and Gln178, Leu338, and Ser339 within 3 Å. Therefore, GFN2-xTB was used to examine the binding affinity of NSAIDs and cannabinoids in this study.

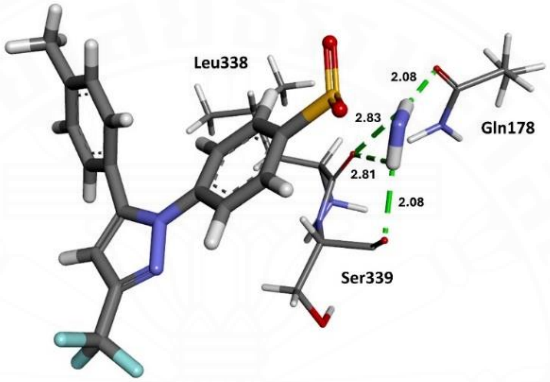

Figure 4.11 Hydrogen bonding interactions of the optimized pose of celecoxib at the pocket of COX-2 by using the DFTB3-D3H5 method.

To validate the accuracy of computing the solvation free energy (δG_{solv}) of small molecules, the MNSOL and SAMPL2 benchmark datasets, along with the ALPB solvation model, were used with the GFN2-xTB method. For the MNSOL dataset, the mean absolute deviation (MAD) of the computed hydration free energy was 3.35 kcal/mol for the given benchmark geometries, compared to 3.48 kcal/mol for their optimized geometries, with an error of less than 0.1 kcal/mol (**Table 4.17**). Notably, a smaller MAD within 2 kcal/mol and a Pearson correlation coefficient (r_p) of 0.99 were obtained for both given and optimized geometries of the neutral charge compounds (**Table 4.17, Figure 4.12**).

Table 4.17 Mean absolute deviation (MAD) for the computed hydration free energy in kcal/mol using the GFN2-xTB method, ALPB solvation model, and MNSOL benchmark datasets.

Subset	No. of entries	δG_{solv} / (kcal/mol)	
		Benchmark geometry	Optimized Geometry
neutral	390	1.89	2.04
positive	60	4.76	4.93
negative	83	9.17	9.16
all charged	143	7.32	7.38
all	533	3.35	3.48

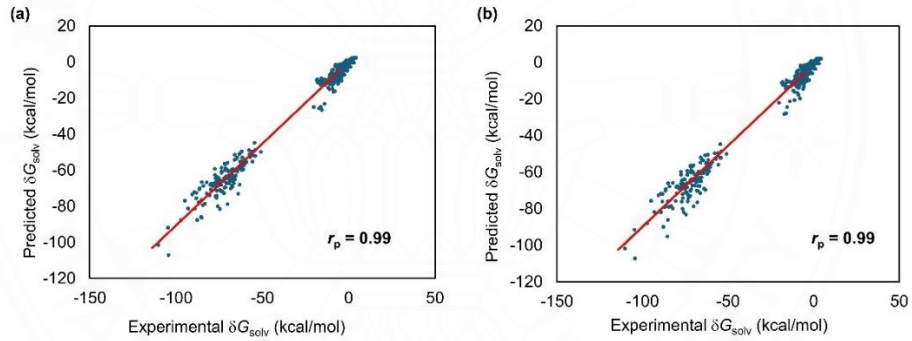

Figure 4.12 Pearson correlation between the experimental δG_{solv} values and the computed δG_{solv} for (a) benchmark geometries and (b) optimized geometries of MNSOL dataset using the GFN2-xTB method and ALPB solvation model.

Table 4.18 shows the computed hydration free energy of the SAMPL2 dataset using the GFN2-xTB method and the ALPB solvation model. The computed values of flurbiprofen, ibuprofen, ketoprofen, and naproxen closely matched the experimental values [114]. Using the GFN2-xTB method, the MAD value for all 20 compounds in the SAMPL2 dataset was within 3 kcal/mol, depending on the geometries and solvation model used [122]. Additionally, the Pearson correlation coefficient (r_p)

ranged from 0.3 to 0.4, indicating the moderate performance of the method used (**Figure 4.13**).

Table 4.18 The computed hydration free energy in kcal/mol of compounds in the SAMPL2 dataset using the GFN2-xTB method with the ALPB solvation model.

compound	δG_{solv} / (kcal/mol)			
	Exp.[1]	M05-2X/6-31G(d) (SMD)[2]	GFN2-xTB (ALPB)	
			Benchmark geometry	Optimized Geometry
Flurbiprofen	–8.42	–8.20	–10.27	–9.77
ibuprofen	–7.00	–6.10	–8.57	–8.55
ketoprofen	–10.78	–11.10	–11.74	–8.90
naproxen	–10.21	–9.70	–9.83	–9.51
MAD (20 compounds)		2.21	2.86	3.18

[1,2] The experimental and computed hydration free energy using SMD solvation model were obtained from [114] [122].

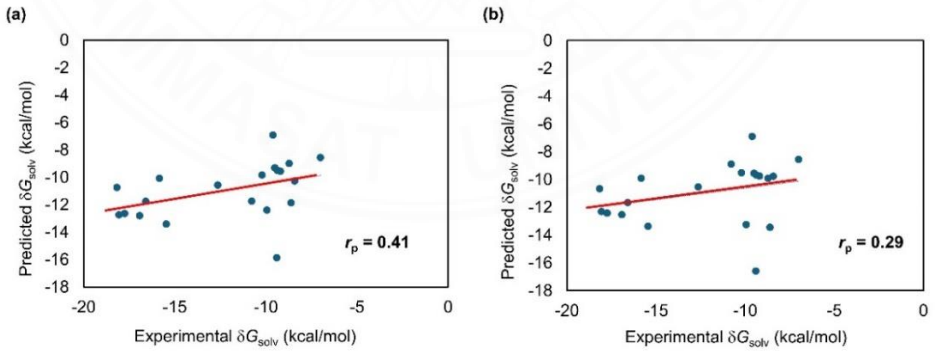

Figure 4.13 Pearson correlation between the experimental δG_{solv} values and the computed δG_{solv} for (a) benchmark geometries and (b) optimized geometries of SAMPL2 dataset using the GFN2-xTB method with ALPB solvation model.

CHAPTER 5
CONCLUSIONS AND RECOMMENDATIONS

5.1 Concluded remarks

In this work, AutoDock4 scoring function can predict the binding affinity of NSAIDs with COX-1 and COX-2 receptors, comparable to that of the co-crystallized poses. It is noteworthy that the difference in the binding enthalpy of NSAIDs from AutoDock4 was within a few kcal/mol. However, we found a false negative and false positive suggested by Autodock4, considering the X-ray crystallographic ligand pose, due to the absence of hydrogen bonding interaction with amino acid of receptor. To address this concern, semiempirical quantum mechanical (SQM) methods were validated with various benchmark datasets. The GFN2-xTB method showed the best performance among the tested SQM methods with small RMSE and MAD values of interaction energy of benchmark datasets. For the MNSOL and SAMPL2 datasets, the MAD for all compounds in the dataset was within 3.5 kcal/mol, depending on both given and optimized geometries. The Pearson correlation coefficient (r_p) ranged from 0.3 to 0.9, indicating the moderate and strong performance of the method used.

The GFN2-TB method along with the ALPB solvation model can discriminate the top-ranked poses obtained from Autodock4 scoring function by a wide range of computed binding free energies. Interestingly, this method can identify a false negative error from AutoDock4 considering the lowest-energy optimized pose of flurbiprofen at the active site of COX-2 and its co-crystallized pose. The carboxyl group of flurbiprofen were similarly positioned at the sulfonamide group of the co-crystallized pose of celecoxib, the commercially available NSAID.

Hydrogen bonding interactions of NSAIDs with Arg499 and Phe504, the crucial amino acids of COX-2 play a key role for their binding affinity. To examine the affinity of NSAIDs with their COX-1 and COX-2 receptors, we computed the binding free energy at the X-ray crystallographic and fully relaxed binding regions. The Pearson correlation coefficient (r_p) was used to compare the uncorrected binding free energy ($\Delta G'_{bind,solv}$) with the experimental binding free energy of NSAIDs. The r_p was 0.40,

indicating the moderate performance of the GFN2-xTB method used with the ALPB solvation model. The lowest-energy optimized pose of celecoxib showed the strongest binding affinity to the native pose of COX-2 with the uncorrected binding free energy ($\Delta G'_{\text{bind,solv}}$) of −43.86 kcal/mol. The influence of geometry relaxation of the candidate compounds was compared with NSAIDs. The Pearson correlation coefficient (r_p) between calculated corrected binding free energy ($\Delta G_{\text{bind,solv}}$) and experimental binding free energy of seven NSAIDs was 0.60, indicating the strong performance of the GFN2-xTB method used.

The GFN2-xTB method with ALPB solvation model can differentiate the difference in uncorrected binding free energy of cannabinoids, as it was evident by a wide range of the MAX and MIN errors as well as the high RMSE and MAD values. This method identified 7 lowest-optimized compounds out of 48 compounds as strong affinity ligands. According to the uncorrected binding free energy, Δ^9-THC, CBN, CBD, CBG, and their acid derivatives showed the highest affinity with CB1. CBCA, CBLA, CBEA, CBNA were tightly bound cannabinoids with CB2 and COX-2.

Conversion of the computed binding free energy for COX receptors to the inhibitory constant (K_i), the calculated selectivity index (SI) for K_i of COX-2 and K_i of COX-1 ratio was used to predict the anti-inflammatory potency of NSAIDs. The calculated selectivity index of selected NSAIDs was matched with the experimental selectivity index by the Spearman correlation (r = 1, P-value = 0.083). If cannabinoids can bind specifically to the anti-inflammatory COX-2 and CB2 receptors, their SI values are low. In contrast, if they specifically bind to COX-1 and psychoactive CB1 receptors, their SI value would be high. Consequently, the calculated selectivity index was used to predict the specific binding and anti-inflammatory potency of cannabinoids. It was clear that the $SI_{CB2/CB1}$ values of Δ^9-THC, CBN, CBD, CBG, and their acid derivatives were high due to their high affinity with psychoactive CB1. The $SI_{CB2/CB1}$ and $SI_{COX\text{-}2/COX\text{-}1}$ were low in CBC, CBL, CBE, and their acid derivatives. Notably, CBCA, CBLA, CBEA, and CBNA were suggested to be the candidate compounds with anti-inflammatory potency targeting the COX-2 receptor.

The influence of thermal energy, entropy, and geometry relaxation plays an important role in the calculated binding free energy. Compared to non-selective NSAIDs, CBCA, CBNA, and CBEA showed higher affinities with COX-2 due to hydrogen bonding interactions of their hydroxyl group and carboxyl group. Modification of the CBNA, CBEA, and CBCA structures at the carbon side chains with the sulfonamide group provided a higher affinity with COX-2. The modified CBCA at the C3 side chain exhibited the highest affinity with COX-2 with the corrected binding free energy of –48.41 kcal/mol and hydrogen bonding interactions with Arg499, Ile503, and Phe504 within 3 Å. Regarding the drug-like properties, it could be assumed that the best modified cannabinoids were favorable physicochemical characteristics for oral bioavailability.

5.2 Further suggestions

5.2.1 Experimental validation

To ensure the validity of our computational findings, further experimental studies should be carried out for therapeutic applications.

5.2.2 Exploration of active compounds

Other active compounds with anti-inflammatory properties can be further explored both experimentally and computationally.

REFERENCES

[1] Medzhitov, R., *Origin and physiological roles of inflammation.* Nature, 2008. **454**: p. 428-435.

[2] Medzhitov, R., *Inflammation 2010: New Adventures of an Old Flame.* Cell, 2010. **140**(6): p. 771-776.

[3] Zarghi, A. and S. Arfaei, *Selective COX-2 Inhibitors: A Review of Their Structure-Activity Relationships.* Iranian Journal of Pharmaceutical Research : IJPR, 2011. **10**: p. 655 - 683.

[4] Rouzer, C.A. and L.J. Marnett, *Structural and Chemical Biology of the Interaction of Cyclooxygenase with Substrates and Non-Steroidal Anti-Inflammatory Drugs.* Chem Rev, 2020. **120**(15): p. 7592-7641.

[5] Tavares, M.T., et al., *Using an in Silico Approach To Teach 3D Pharmacodynamics of the Drug–Target Interaction Process Focusing on Selective COX2 Inhibition by Celecoxib.* Journal of Chemical Education, 2017. **94**(3): p. 380-387.

[6] Brewer, C. and D. Waddell, *Role of Prostaglandin F2 alpha in Skeletal Muscle Regeneration.* Journal of Trainology, 2012. **1**: p. 45-52.

[7] Rayar, A.M., et al., *Update on COX-2 Selective Inhibitors: Chemical Classification, Side Effects and their Use in Cancers and Neuronal Diseases.* Curr Top Med Chem, 2017. **17**(26): p. 2935-2956.

[8] Mofidi, M., et al., *Comparing the efficacy of nebulized morphine with intravenous morphine in traumatic musculoskeletal pain management.* Journal of Research in Clinical Medicine, 2020. **8**(1): p. 21-21.

[9] Takakuwa, K.M., et al., *The Impact of Medical Cannabis on Intermittent and Chronic Opioid Users with Back Pain: How Cannabis Diminished Prescription Opioid Usage.* Cannabis and Cannabinoid Research, 2020. **5**(3): p. 263-270.

[10] Atakan, Z., *Cannabis, a complex plant: different compounds and different effects on individuals.* Ther Adv Psychopharmacol, 2012. **2**(6): p. 241-54.

[11] Esposito, G., et al., *Cannabidiol in Inflammatory Bowel Diseases: A Brief Overview.* Phytotherapy Research, 2013. **27**(5): p. 633-636.

[12] Ruhaak, L.R., et al., *Evaluation of the cyclooxygenase inhibiting effects of six major cannabinoids isolated from Cannabis sativa.* Biol Pharm Bull, 2011. **34**(5): p. 774-8.

[13] Pellati, F., et al., *Cannabis sativa L. and Nonpsychoactive Cannabinoids: Their Chemistry and Role against Oxidative Stress, Inflammation, and Cancer.* Biomed Res Int, 2018. **2018**: p. 1691428.

[14] Hua, T., et al., *Crystal structures of agonist-bound human cannabinoid receptor CB1.* Nature, 2017. **547**(7664): p. 468-471.

[15] Xing, C., et al., *Cryo-EM Structure of the Human Cannabinoid Receptor CB2-Gi Signaling Complex.* Cell, 2020. **180**(4): p. 645-654.e13.

[16] Pertwee, R.G., *The diverse CB1 and CB2 receptor pharmacology of three plant cannabinoids: Δ9-tetrahydrocannabinol, cannabidiol and Δ9-tetrahydrocannabivarin.* British Journal of Pharmacology, 2008. **153**(2): p. 199-215.

[17] Anighoro, A., *Underappreciated Chemical Interactions in Protein-Ligand Complexes.* Methods Mol Biol, 2020. **2114**: p. 75-86.
[18] Kitchen, D.B., et al., *Docking and scoring in virtual screening for drug discovery: methods and applications.* Nat Rev Drug Discov, 2004. **3**(11): p. 935-49.
[19] Agrafiotis, D.K., et al., *Conformational Sampling of Bioactive Molecules: A Comparative Study.* Journal of Chemical Information and Modeling, 2007. **47**(3): p. 1067-1086.
[20] Du, X., et al., *Insights into Protein-Ligand Interactions: Mechanisms, Models, and Methods.* International journal of molecular sciences, 2016. **17**(2): p. 144.
[21] Chen, Y.-C., *Beware of docking!* Trends in Pharmacological Sciences, 2015. **36**(2): p. 78-95.
[22] Korth, M., et al., *A Transferable H-Bonding Correction for Semiempirical Quantum-Chemical Methods.* Journal of Chemical Theory and Computation, 2010. **6**: p. 344-352.
[23] Stigliani, J.L., et al., *Cross-docking study on InhA inhibitors: a combination of Autodock Vina and PM6-DH2 simulations to retrieve bio-active conformations.* Org Biomol Chem, 2012. **10**(31): p. 6341-9.
[24] Miriyala, V.M. and J. Řezáč, *Description of non-covalent interactions in SCC-DFTB methods.* Journal of Computational Chemistry, 2017. **38**(10): p. 688-697.
[25] Řezáč, J. and P. Hobza, *Advanced Corrections of Hydrogen Bonding and Dispersion for Semiempirical Quantum Mechanical Methods.* Journal of Chemical Theory and Computation, 2012. **8**(1): p. 141-151.
[26] Bannwarth, C., S. Ehlert, and S. Grimme, *GFN2-xTB-An Accurate and Broadly Parametrized Self-Consistent Tight-Binding Quantum Chemical Method with Multipole Electrostatics and Density-Dependent Dispersion Contributions.* J Chem Theory Comput, 2019. **15**(3): p. 1652-1671.
[27] Zwanzig, R.W., *High-Temperature Equation of State by a Perturbation Method. I. Nonpolar Gases.* The Journal of Chemical Physics, 1954. **22**(8): p. 1420-1426.
[28] Srinivasan, J., et al., *Continuum Solvent Studies of the Stability of DNA, RNA, and Phosphoramidate−DNA Helices.* Journal of the American Chemical Society, 1998. **120**(37): p. 9401-9409.
[29] Bashford, D. and D.A. Case, *Generalized Born Models of Macromolecular Solvation Effects.* Annual Review of Physical Chemistry, 2000. **51**(Volume 51, 2000): p. 129-152.
[30] Ajani, H., et al., *Superior Performance of the SQM/COSMO Scoring Functions in Native Pose Recognition of Diverse Protein–Ligand Complexes in Cognate Docking.* ACS Omega, 2017. **2**(7): p. 4022-4029.
[31] Spicher, S. and S. Grimme, *Robust Atomistic Modeling of Materials, Organometallic, and Biochemical Systems.* Angew Chem Int Ed Engl, 2020. **59**(36): p. 15665-15673.
[32] Chen, Y.Q., et al., *Efficient calculation of protein-ligand binding free energy using GFN methods: the power of the cluster model.* Phys Chem Chem Phys, 2022. **24**(23): p. 14339-14347.
[33] Ehlert, S., et al., *Robust and Efficient Implicit Solvation Model for Fast Semiempirical Methods.* J Chem Theory Comput, 2021. **17**(7): p. 4250-4261.

[34] Capone, M.L., et al., *Pharmacodynamic of cyclooxygenase inhibitors in humans.* Prostaglandins Other Lipid Mediat, 2007. **82**(1-4): p. 85-94.
[35] Warner, T.D., et al., *Nonsteroid drug selectivities for cyclo-oxygenase-1 rather than cyclo-oxygenase-2 are associated with human gastrointestinal toxicity: a full in vitro analysis.* Proc Natl Acad Sci U S A, 1999. **96**(13): p. 7563-8.
[36] Patrignani, P., M.L. Capone, and S. Tacconelli, *Clinical pharmacology of etoricoxib: a novel selective COX2 inhibitor.* Expert Opin Pharmacother, 2003. **4**(2): p. 265-84.
[37] Bindu, S., S. Mazumder, and U. Bandyopadhyay, *Non-steroidal anti-inflammatory drugs (NSAIDs) and organ damage: A current perspective.* Biochemical Pharmacology, 2020. **180**: p. 114147.
[38] Cryer, B. and M. Feldman, *Cyclooxygenase-1 and cyclooxygenase-2 selectivity of widely used nonsteroidal anti-inflammatory drugs.* Am J Med, 1998. **104**(5): p. 413-21.
[39] Li, H., et al., *Overview of cannabidiol (CBD) and its analogues: Structures, biological activities, and neuroprotective mechanisms in epilepsy and Alzheimer's disease.* Eur J Med Chem, 2020. **192**: p. 112163.
[40] Takeda, S., et al., *Cannabidiolic acid as a selective cyclooxygenase-2 inhibitory component in cannabis.* Drug Metab Dispos, 2008. **36**(9): p. 1917-21.
[41] Paunescu, H., et al., *Cannabinoid system and cyclooxygenases inhibitors.* Journal of medicine and life, 2011. **4**: p. 11-20.
[42] Malek, N. and K. Starowicz, *Dual-Acting Compounds Targeting Endocannabinoid and Endovanilloid Systems-A Novel Treatment Option for Chronic Pain Management.* Front Pharmacol, 2016. **7**: p. 257.
[43] Shahbazi, F., et al., *Cannabinoids and Cannabinoid Receptors: The Story so Far.* iScience, 2020. **23**(7): p. 101301.
[44] An, D., et al., *Targeting Cannabinoid Receptors: Current Status and Prospects of Natural Products.* Int J Mol Sci, 2020. **21**(14).
[45] Li, X., et al., *Crystal Structure of the Human Cannabinoid Receptor CB2.* Cell, 2019. **176**(3): p. 459-467 e13.
[46] Cayman Chemical. https://www.caymanchem.com/news/cannabinoid-signaling-insights-to-future-pharmacotherapeutic-development (accessed 4 April 2022).
[47] Iwamura, H., et al., *In vitro and in vivo pharmacological characterization of JTE-907, a novel selective ligand for cannabinoid CB2 receptor.* J Pharmacol Exp Ther, 2001. **296**(2): p. 420-5.
[48] Rosenthaler, S., et al., *Differences in receptor binding affinity of several phytocannabinoids do not explain their effects on neural cell cultures.* Neurotoxicol Teratol, 2014. **46**: p. 49-56.
[49] Showalter, V.M., et al., *Evaluation of binding in a transfected cell line expressing a peripheral cannabinoid receptor (CB2): identification of cannabinoid receptor subtype selective ligands.* Journal of Pharmacology and Experimental Therapeutics, 1996. **278**(3): p. 989-999.
[50] Felder, C.C., et al., *Comparison of the pharmacology and signal transduction of the human cannabinoid CB1 and CB2 receptors.* Mol Pharmacol, 1995. **48**(3): p. 443-50.

[51] Thomas, A., et al., *6''-Azidohex-2''-yne-cannabidiol: a potential neutral, competitive cannabinoid CB1 receptor antagonist.* Eur J Pharmacol, 2004. **487**(1-3): p. 213-21.
[52] Thomas, A., et al., *Cannabidiol displays unexpectedly high potency as an antagonist of CB1 and CB2 receptor agonists in vitro.* Br J Pharmacol, 2007. **150**(5): p. 613-23.
[53] MacLennan, S.J., et al., *Evidence for inverse agonism of SR141716A at human recombinant cannabinoid CB1 and CB2 receptors.* Br J Pharmacol, 1998. **124**(4): p. 619-22.
[54] Dunn, M.F., *Protein–Ligand Interactions: General Description*, in *eLS*. 2010.
[55] Zhou, P., J. Huang, and F. Tian, *Specific noncovalent interactions at protein-ligand interface: implications for rational drug design.* Curr Med Chem, 2012. **19**(2): p. 226-38.
[56] Berman, H.M., et al., *The Protein Data Bank.* Nucleic Acids Research, 2000. **28**(1): p. 235-242.
[57] Rouzer, C.A. and L.J. Marnett, *Non-redundant functions of cyclooxygenases: oxygenation of endocannabinoids.* J Biol Chem, 2008. **283**(13): p. 8065-9.
[58] Knights, K.M., A.A. Mangoni, and J.O. Miners, *Defining the COX inhibitor selectivity of NSAIDs: implications for understanding toxicity.* Expert Rev Clin Pharmacol, 2010. **3**(6): p. 769-76.
[59] Bittencourt, J., et al., *In Silico Evaluation of Ibuprofen and Two Benzoylpropionic Acid Derivatives with Potential Anti-Inflammatory Activity.* Molecules, 2019. **24**(8).
[60] Shah, M.A., et al., *In silico molecular mechanism of cannabigerol as a cyclooxygenase-2 inhibitor.* Bangladesh Journal of Pharmacology, 2013. **8**(4).
[61] Munro, S., K.L. Thomas, and M. Abu-Shaar, *Molecular characterization of a peripheral receptor for cannabinoids.* Nature, 1993. **365**(6441): p. 61-5.
[62] Hryhorowicz, S., et al., *Allosteric Modulation of Cannabinoid Receptor 1—Current Challenges and Future Opportunities.* International Journal of Molecular Sciences, 2019. **20**(23): p. 5874.
[63] Linciano, P., et al., *Isolation of a High-Affinity Cannabinoid for the Human CB1 Receptor from a Medicinal Cannabis sativa Variety: Δ9-Tetrahydrocannabutol, the Butyl Homologue of Δ9-Tetrahydrocannabinol.* Journal of Natural Products, 2020. **83**(1): p. 88-98.
[64] Hua, T., et al., *Activation and Signaling Mechanism Revealed by Cannabinoid Receptor-Gi Complex Structures.* Cell, 2020. **180**(4): p. 655-665.e18.
[65] Krishna Kumar, K., et al., *Structure of a Signaling Cannabinoid Receptor 1-G Protein Complex.* Cell, 2019. **176**(3): p. 448-458.e12.
[66] Hua, T., et al., *Crystal Structure of the Human Cannabinoid Receptor CB₁*. Cell, 2016. **167**(3): p. 750-762.e14.
[67] Friesner, R.A., et al., *Glide: A New Approach for Rapid, Accurate Docking and Scoring. 1. Method and Assessment of Docking Accuracy.* Journal of Medicinal Chemistry, 2004. **47**(7): p. 1739-1749.
[68] Allen, W.J., et al., *DOCK 6: Impact of new features and current docking performance.* J Comput Chem, 2015. **36**(15): p. 1132-56.
[69] Jones, G., et al., *Development and validation of a genetic algorithm for flexible docking.* J Mol Biol, 1997. **267**(3): p. 727-48.

[70] Allen, W.J., et al., *DOCK 6: Impact of new features and current docking performance.* Journal of computational chemistry, 2015. **36**(15): p. 1132-1156.
[71] Rarey, M., et al., *A fast flexible docking method using an incremental construction algorithm.* J Mol Biol, 1996. **261**(3): p. 470-89.
[72] Biovia, D.S., *Discovery Studio Modeling Environment*. 2016, San Diego: Dassault Syst mes.
[73] Trott, O. and A.J. Olson, *AutoDock Vina: improving the speed and accuracy of docking with a new scoring function, efficient optimization, and multithreading.* J Comput Chem, 2010. **31**(2): p. 455-61.
[74] Morris, G.M., et al., *AutoDock4 and AutoDockTools4: Automated docking with selective receptor flexibility.* J Comput Chem, 2009. **30**(16): p. 2785-91.
[75] Di Nola, A., D. Roccatano, and H.J. Berendsen, *Molecular dynamics simulation of the docking of substrates to proteins.* Proteins, 1994. **19**(3): p. 174-82.
[76] Morris, G.M., et al., *Automated docking using a Lamarckian genetic algorithm and an empirical binding free energy function.* Journal of Computational Chemistry, 1998. **19**(14): p. 1639-1662.
[77] Dewar, M.J.S., et al., *Development and use of quantum mechanical molecular models. 76. AM1: a new general purpose quantum mechanical molecular model.* Journal of the American Chemical Society, 1985. **107**(13): p. 3902-3909.
[78] Stewart, J.J.P., *Optimization of parameters for semiempirical methods V: Modification of NDDO approximations and application to 70 elements.* Journal of Molecular Modeling, 2007. **13**(12): p. 1173-1213.
[79] Stewart, J.J.P., *Optimization of parameters for semiempirical methods VI: more modifications to the NDDO approximations and re-optimization of parameters.* Journal of Molecular Modeling, 2013. **19**(1): p. 1-32.
[80] Elstner, M., et al., *Hydrogen bonding and stacking interactions of nucleic acid base pairs: A density-functional-theory based treatment.* Chemical Physics - CHEM PHYS, 2001. **114**.
[81] Pecina, A., et al., *SQM/COSMO Scoring Function: Reliable Quantum-Mechanical Tool for Sampling and Ranking in Structure-Based Drug Design.* Chempluschem, 2020. **85**(11): p. 2362-2371.
[82] McNamara, J.P. and I.H. Hillier, *Semi-empirical molecular orbital methods including dispersion corrections for the accurate prediction of the full range of intermolecular interactions in biomolecules.* Physical Chemistry Chemical Physics, 2007. **9**(19): p. 2362-2370.
[83] Grimme, S., et al., *Dispersion-Corrected Mean-Field Electronic Structure Methods.* Chemical Reviews, 2016. **116**(9): p. 5105-5154.
[84] Rezac, J., *Empirical Self-Consistent Correction for the Description of Hydrogen Bonds in DFTB3.* J Chem Theory Comput, 2017. **13**(10): p. 4804-4817.
[85] Řezáč, J., *Description of halogen bonding in semiempirical quantum-mechanical and self-consistent charge density-functional tight-binding methods.* Journal of Computational Chemistry, 2019. **40**(17): p. 1633-1642.
[86] Řezáč, J., *Empirical Self-Consistent Correction for the Description of Hydrogen Bonds in DFTB3.* Journal of Chemical Theory and Computation, 2017. **13**(10): p. 4804-4817.

[87] Řezáč, J., K.E. Riley, and P. Hobza, *Benchmark Calculations of Noncovalent Interactions of Halogenated Molecules.* Journal of Chemical Theory and Computation, 2012. **8**(11): p. 4285-4292.
[88] Kříž, K. and J. Řezáč, *Benchmarking of Semiempirical Quantum-Mechanical Methods on Systems Relevant to Computer-Aided Drug Design.* Journal of Chemical Information and Modeling, 2020. **60**(3): p. 1453-1460.
[89] Rezac, J., *Non-Covalent Interactions Atlas Benchmark Data Sets: Hydrogen Bonding.* J Chem Theory Comput, 2020. **16**(4): p. 2355-2368.
[90] Rezac, J., *Non-Covalent Interactions Atlas Benchmark Data Sets 2: Hydrogen Bonding in an Extended Chemical Space.* J Chem Theory Comput, 2020. **16**(10): p. 6305-6316.
[91] Grimme, S., C. Bannwarth, and P. Shushkov, *A Robust and Accurate Tight-Binding Quantum Chemical Method for Structures, Vibrational Frequencies, and Noncovalent Interactions of Large Molecular Systems Parametrized for All spd-Block Elements (Z = 1–86).* Journal of Chemical Theory and Computation, 2017. **13**(5): p. 1989-2009.
[92] Christensen, A.S., M. Elstner, and Q. Cui, *Improving intermolecular interactions in DFTB3 using extended polarization from chemical-potential equalization.* J Chem Phys, 2015. **143**(8): p. 084123.
[93] Kuhn, M., et al., *Assessment of Binding Affinity via Alchemical Free-Energy Calculations.* Journal of Chemical Information and Modeling, 2020. **60**(6): p. 3120-3130.
[94] Wang, L., J. Chambers, and R. Abel, *Protein-Ligand Binding Free Energy Calculations with FEP*. Methods Mol Biol, 2019. **2022**: p. 201-232.
[95] Wu, D., et al., *Free energy perturbation (FEP)-guided scaffold hopping.* Acta Pharm Sin B, 2022. **12**(3): p. 1351-1362.
[96] Hans, N., et al., *Deciphering the role of fucoidan from brown macroalgae in inhibiting SARS-CoV-2 by targeting its main protease and receptor binding domain: Invitro and insilico approach.* Int J Biol Macromol, 2023. **248**: p. 125950.
[97] Rimon, G., et al., *Coxibs interfere with the action of aspirin by binding tightly to one monomer of cyclooxygenase-1.* Proc Natl Acad Sci U S A, 2010. **107**(1): p. 28-33.
[98] Sidhu, R.S., et al., *Comparison of cyclooxygenase-1 crystal structures: cross-talk between monomers comprising cyclooxygenase-1 homodimers.* Biochemistry, 2010. **49**(33): p. 7069-79.
[99] Selinsky, B.S., et al., *Structural Analysis of NSAID Binding by Prostaglandin H2 Synthase: Time-Dependent and Time-Independent Inhibitors Elicit Identical Enzyme Conformations.* Biochemistry, 2001. **40**(17): p. 5172-5180.
[100] Wang, J.L., et al., *The novel benzopyran class of selective cyclooxygenase-2 inhibitors. Part 2: The second clinical candidate having a shorter and favorable human half-life.* Bioorganic & Medicinal Chemistry Letters, 2010. **20**(23): p. 7159-7163.
[101] Rowlinson, S.W., et al., *A novel mechanism of cyclooxygenase-2 inhibition involving interactions with Ser-530 and Tyr-385.* J Biol Chem, 2003. **278**(46): p. 45763-9.

[102] Orlando, B.J., M.J. Lucido, and M.G. Malkowski, *The structure of ibuprofen bound to cyclooxygenase-2.* J Struct Biol, 2015. **189**(1): p. 62-6.
[103] Kurumbail, R.G., et al., *Structural basis for selective inhibition of cyclooxygenase-2 by anti-inflammatory agents.* Nature, 1996. **384**(6610): p. 644-8.
[104] Jurrus, E., et al., *Improvements to the APBS biomolecular solvation software suite.* Protein Sci, 2018. **27**(1): p. 112-128.
[105] Mendez, D., et al., *ChEMBL: towards direct deposition of bioassay data.* Nucleic Acids Research, 2018. **47**(D1): p. D930-D940.
[106] O'Boyle, N.M., et al., *Open Babel: An open chemical toolbox.* Journal of Cheminformatics, 2011. **3**(1): p. 33.
[107] Wishart DS, I.G., Cao X, Guo AC, Hiebert Giesbrecht M, LeVatte M, Liigand J, Wang F, Bhumireddy S, Wang Y, Zhang J, Mandal R, Dyck J. *Chemical composition of Cannabis*. Available from: https://cannabisdatabase.ca/.
[108] IQmol. *A molecular editor and visualization package.*; Available from: http://iqmol.org.
[109] Lipinski, C.A., et al., *Experimental and computational approaches to estimate solubility and permeability in drug discovery and development settings.* Advanced Drug Delivery Reviews, 1997. **23**(1): p. 3-25.
[110] Daina, A., O. Michielin, and V. Zoete, *SwissADME: a free web tool to evaluate pharmacokinetics, drug-likeness and medicinal chemistry friendliness of small molecules.* Scientific Reports, 2017. **7**(1): p. 42717.
[111] Morris, G.M., et al., *AutoDock4 and AutoDockTools4: Automated docking with selective receptor flexibility.* Journal of computational chemistry, 2009. **30**(16): p. 2785-2791.
[112] Řezáč, J., K.E. Riley, and P. Hobza, *S66: A Well-balanced Database of Benchmark Interaction Energies Relevant to Biomolecular Structures.* Journal of Chemical Theory and Computation, 2011. **7**(8): p. 2427-2438.
[113] Marenich, A.V.K., C. P.; Thompson, J. D.; Hawkins, G. D.; Chambers, C. C.; Giesen, D. J.; Winget, P.; Cramer, C. J.; Truhlar, D. G. *Minnesota Solvation Database-Version 2012*. 2020; Available from: https://hdl.handle.net/11299/213300.
[114] Geballe, M.T., et al., *The SAMPL2 blind prediction challenge: introduction and overview.* J Comput Aided Mol Des, 2010. **24**(4): p. 259-79.
[115] S. Brahmkshatriya, P., et al., *Quantum Mechanical Scoring: Structural and Energetic Insights into Cyclin-Dependent Kinase 2 Inhibition by Pyrazolo[1,5-a]pyrimidines.* Current Computer - Aided Drug Design, 2013. **9**(1): p. 118-129.
[116] Stewart, J.J.P. *MOPAC2016*. 2016; Available from: http://OpenMOPAC.net.
[117] Hourahine, B., et al., *DFTB+, a software package for efficient approximate density functional theory based atomistic simulations.* J Chem Phys, 2020. **152**(12): p. 124101.
[118] Bannwarth, C., et al., *Extended tight-binding quantum chemistry methods.* WIREs Computational Molecular Science, 2021. **11**(2): p. e1493.
[119] Wessa, P. *Free Statistics Software version 1.2.1*. 2024; Available from: https://www.wessa.net/.
[120] Sedgwick, P., *Pearson's correlation coefficient.* BMJ, 2012. **345**: p. e4483-e4483.

[121] Kubillus, M., et al., *Parameterization of the DFTB3 method for Br, Ca, Cl, F, I, K, and Na in organic and biological systems.* J Chem Theory Comput, 2015. **11**(1): p. 332-42.
[122] Marenich, A.V., C.J. Cramer, and D.G. Truhlar, *Generalized Born Solvation Model SM12.* Journal of Chemical Theory and Computation, 2013. **9**(1): p. 609-620.

APPENDIX

APPENDIX A

The binding energy and the uncorrected binding free energy in implicit aqueous solvation obtained from AutoDck4 and GFN2-xTB methods.

Table A1. Binding energy (ΔE_{vac}) and uncorrected binding free energy in implicit aqueous solvation ($\Delta G'_{bind,solv}$) in kcal/mol of the best poses of 55 cannabinoids with COX-1 and COX-2 using Autodock4 and GFN2-xTB method.

Protein	Cannabinoid		ΔE_{vac}	ΔE_{vac}	$\Delta G'_{bind,solv}$
	ID	Name	AutoDock4	GFN2-xTB	
COX-1	CDB000008	CBCVA	–8.22	–26.51	–14.57
	CDB000006	CBGV	–7.02	–28.78	–13.33
	CDB000005	CBGVA	–6.70	–24.76	–11.77
	CDB000018	CBGA	–6.84	–26.53	–11.41
	CDB000004	CBGM	–8.65	–24.41	–11.36
	CDB000009	CBCV	–7.23	–23.54	–11.08
	CDB000042	CBCM	–8.72	–20.42	–10.59
	CDB000003	CBG	–6.72	–21.27	–8.67
	CDB000011	CBGAM	–6.53	–20.07	–5.87
	CDB006347	Terpenoids	–6.14	–10.51	–3.68
	CDB006349	Terpenoids	–5.40	–8.82	–3.23
	CDB000032	CBNV	–8.43	–11.69	–1.69
	CDB000033	CBN-C2	–8.15	–10.92	–1.01
	CDB000014	CBDVA	–7.56	–14.23	–0.01
	CDB000031	CBN-C4	–8.43	–10.25	0.03
	CDB000007	CBC	–7.78	–10.90	0.50
	CDB000028	CBNA	–9.19	–12.94	1.41
	CDB000012	CBDM	–8.87	–9.50	1.50
	CDB000030	CBNM	–8.57	–7.51	1.76
	CDB000433	CBND	–6.74	–9.21	2.03
	CDB000010	CBDA	–7.39	–11.71	3.58

Table A1. Binding energy (ΔE_{vac}) and uncorrected binding free energy in implicit aqueous solvation ($\Delta G'_{bind,solv}$) in kcal/mol of the best poses of 55 cannabinoids with COX-1 and COX-2 using Autodock4 and GFN2-xTB method. (cont.)

Protein	Cannabinoid		ΔE_{vac}	ΔE_{vac}	$\Delta G'_{bind,solv}$
	ID	Name	AutoDock4	GFN2-xTB	
COX-1	CDB000037	OTHC	–9.93	–7.96	3.67
	CDB000015	CBDV	–8.09	–7.11	4.66
	CDB006348	Terpenoids	–7.86	–2.84	4.84
	CDB000398	CBCA	–7.96	–6.36	4.97
	CDB000020	Δ^9-THCVA	–9.40	–8.82	5.49
	CDB000043	H_2CBD	–7.24	–6.81	5.61
	CDB006346	Terpenoids	–6.14	2.20	6.11
	CDB000040	2-oxo-Δ3(4)-THC	–0.39	–5.43	7.20
	CDB000001	Δ^9-THC	–8.81	–3.87	7.44
	CDB000002	CBD	–7.41	–5.07	7.45
	CDB006350	Terpenoids	–5.74	3.46	8.01
	CDB000019	Δ^9-THC-C4	–8.47	–3.46	8.09
	CDB000039	TriOH-THC	–7.85	–6.39	8.22
	CDB000029	CBN	–8.52	–1.95	8.84
	CDB000021	Δ^9-THCV	–8.48	–1.72	9.03
	CDB000013	CBD-C4	–7.32	–2.95	9.65
	CDB000022	Δ^7-cis-iso-THCV	–8.67	–0.66	9.83
	CDB000023	Δ^8-THCA	–9.75	–8.33	9.88
	CDB000035	8,9-dihydroxy-Δ-6a-THC	–8.36	–4.70	11.38
	CDB000017	Δ^9-THCA-B	–7.94	3.68	12.58
	CDB000027	CBE	–7.60	0.50	12.76
	CDB006352	Terpenoids	–7.07	5.06	12.84
	CDB006351	Hydronaphthalene	–8.23	8.27	13.32
	CDB000041	Δ1(2)-THCM	–7.52	4.64	13.76

Table A1. Binding energy (ΔE_{vac}) and uncorrected binding free energy in implicit aqueous solvation ($\Delta G'_{bind,solv}$) in kcal/mol of the best poses of 55 cannabinoids with COX-1 and COX-2 using Autodock4 and GFN2-xTB method. (cont.)

Protein	Cannabinoid		ΔE_{vac}	ΔE_{vac}	$\Delta G'_{bind,solv}$
	ID	Name	AutoDock4	GFN2-xTB	
COX-1	CDB000435	CBT	–8.44	0.57	14.43
		CBTA	–7.73	–6.27	14.61
	CDB000016	Δ^9-THCA	–8.52	–0.39	15.54
	CDB000024	Δ^8-THC	–9.52	5.45	16.12
	CDB000036	CBCT	–8.36	8.50	16.34
	CDB000026	CBL	–8.73	7.57	17.90
	CDB000025	CBLA	–8.65	8.47	20.45
	CDB000038	cis-Δ^9-THC	–8.15	12.78	21.98
	CDB000423	CBEA	–7.96	8.49	22.74
	CDB000034	10-ethoxy-9-hydroxy-Δ-6a-THC	–8.39	14.44	26.19
COX-2	CDB000032	CBNV	–8.89	–34.73	–23.62
	CDB000033	CBN-C2	–8.61	–32.25	–21.87
	CDB000009	CBCV	–8.19	–32.66	–21.30
	CDB000020	Δ^9-THCVA	–10.16	–46.46	–21.13
	CDB000031	CBN-C4	–9.14	–31.23	–20.79
	CDB000021	Δ^9-THCV	–9.71	–31.39	–20.40
	CDB000006	CBGV	–7.72	–30.16	–17.86
	CDB000433	CBND	–9.04	–33.14	–17.60
	CDB000003	CBG	–7.82	–28.14	–16.38
	CDB000019	Δ^9-THC-C4	–10.02	–27.77	–16.02
	CDB000005	CBGVA	–7.01	–29.71	–15.48
	CDB000007	CBC	–8.42	–26.69	–14.72
	CDB000015	CBDV	–7.83	–25.67	–14.38

Table A1. Binding energy (ΔE_{vac}) and uncorrected binding free energy in implicit aqueous solvation ($\Delta G'_{bind,solv}$) in kcal/mol of the best poses of 55 cannabinoids with COX-1 and COX-2 using Autodock4 and GFN2-xTB method. (cont.)

Protein	Cannabinoid		ΔE_{vac}	ΔE_{vac}	$\Delta G'_{bind,solv}$
	ID	Name	AutoDock4	GFN2-xTB	
COX-2	CDB000035	8,9-dihydroxy-Δ-6a-THC	–8.95	–31.16	–14.03
	CDB000030	CBNM	–9.04	–24.14	–13.95
	CDB000024	Δ^8-THC	–9.44	–23.00	–13.92
	CDB000398	CBCA	–7.39	–28.94	–13.55
	CDB000039	TriOH-THC	–8.14	–29.07	–13.46
	CDB000014	CBDVA	–8.33	–28.86	–12.91
	CDB000001	Δ^9-THC	–9.74	–25.62	–12.63
	CDB000022	Δ^7-cis-iso-THCV	–9.04	–23.85	–12.37
	CDB000011	CBGAM	–6.13	–23.38	–11.99
	CDB006347	Terpenoids	–5.95	–6.27	–10.61
	CDB006349	Terpenoids	–5.81	–17.03	–10.39
	CDB000008	CBCVA	–8.35	–27.05	–10.33
	CDB000042	CBCM	–8.86	–20.46	–10.06
	CDB000017	Δ^9-THCA-B	–8.84	–28.55	–9.99
	CDB006346	Terpenoids	–6.39	–11.88	–8.91
	CDB000043	H_2CBD	–8.98	–22.60	–8.85
	CDB000028	CBNA	–9.14	–30.93	–8.56
	CDB000029	CBN	–9.16	–19.41	–8.03
	CDB000016	Δ^9-THCA	–10.27	–33.15	–7.30
	CDB000004	CBGM	–6.57	–21.36	–6.56
	CDB000023	Δ^8-THCA	–9.12	–32.73	–6.33
	CDB000018	CBGA	–9.11	–18.98	–6.01
	CDB000013	CBD-C4	–8.61	–17.61	–5.90
	CDB000423	CBEA	–8.77	–20.53	–5.45

Table A1. Binding energy (ΔE_{vac}) and uncorrected binding free energy in implicit aqueous solvation ($\Delta G'_{bind,solv}$) in kcal/mol of the best poses of 55 cannabinoids with COX-1 and COX-2 using Autodock4 and GFN2-xTB method. (cont.)

Protein	Cannabinoid		ΔE_{vac}	ΔE_{vac}	$\Delta G'_{bind,solv}$
	ID	Name	AutoDock4	GFN2-xTB	
COX-2	CDB000038	cis-Δ^9-THC	–9.38	–17.02	–5.42
	CDB000040	2-oxo-Δ3(4)-THC	–10.26	–21.73	–5.19
	CDB006348	Terpenoids	–7.96	–11.54	–4.83
	CDB006351	Hydronaphthalene	–8.34	–10.02	–4.30
	CDB000034	10-ethoxy-9-hydroxy-Δ-6a-THC	–8.53	–18.49	–4.06
	CDB000041	Δ1(2)-THCM	–9.44	–13.84	–3.92
		CBTA	–8.09	–32.08	–3.51
	CDB000036	CBCT	–9.71	–10.71	–3.46
	CDB000012	CBDM	–8.50	–13.62	–3.17
	CDB000002	CBD	–8.61	–15.41	–3.15
	CDB000027	CBE	–8.25	–14.98	–2.37
	CDB000037	OTHC	–9.27	–17.19	–1.81
	CDB006350	Terpenoids	–6.07	–7.32	–1.23
	CDB000435	CBT	–9.99	–16.53	–0.58
	CDB000025	CBLA	–9.92	–16.43	2.14
	CDB000010	CBDA	–7.22	–14.62	2.21
	CDB006352	Terpenoids	–7.61	–3.51	2.45
	CDB000026	CBL	–9.90	–8.48	2.98

Table A2. Binding energy (ΔE_{vac}) and uncorrected binding free energy in implicit aqueous solvation ($\Delta G'_{bind,solv}$) in kcal/mol of the best poses of 55 cannabinoids with CB1 and CB2 using Autodock4 and GFN2-xTB method.

Protein	Cannabinoid		ΔE_{vac}	ΔE_{vac}	$\Delta G'_{bind,solv}$
	ID	Name	AutoDock4	GFN2-xTB	
CB1	CDB000005	CBGVA	–8.94	–49.37	–33.42
	CDB000028	CBNA	–11.20	–47.47	–32.89
	CDB000016	Δ^9-THCA	–11.54	–45.58	–31.11
	CDB000023	Δ^8-THCA	–11.48	–42.18	–30.69
	CDB000031	CBN-C4	–9.74	–41.61	–30.63
	CDB000001	Δ^9-THC	–10.56	–40.45	–30.23
	CDB000018	CBGA	–9.07	–46.20	–29.69
	CDB000010	CBDA	–10.83	–46.19	–29.33
	CDB000019	Δ^9-THC-C4	–10.21	–39.01	–28.94
	CDB000032	CBNV	–9.41	–39.35	–28.93
	CDB000035	8,9-dihydroxy-Δ-6a-THC	–10.38	–46.49	–28.93
	CDB000037	OTHC	–10.97	–38.56	–28.78
	CDB000013	CBD-C4	–9.68	–39.99	–28.72
	CDB000024	Δ^8-THC	–10.69	–39.22	–28.62
	CDB000433	CBND	–8.95	–39.21	–28.42
		CBTA	–10.28	–46.96	–28.36
	CDB000003	CBG	–8.99	–40.17	–28.22
	CDB000033	CBN-C2	–9.01	–37.97	–27.67
	CDB000021	Δ^9-THCV	–9.83	–37.32	–27.54
	CDB000039	TriOH-THC	–10.41	–45.01	–27.53
	CDB000014	CBDVA	–8.99	–42.80	–27.37
	CDB000002	CBD	–9.52	–38.74	–27.26

Table A2. Binding energy (ΔE_{vac}) and uncorrected binding free energy in implicit aqueous solvation ($\Delta G'_{bind,solv}$) in kcal/mol of the best poses of 55 cannabinoids with CB1 and CB2 using Autodock4 and GFN2-xTB method. (cont.)

Protein	Cannabinoid		ΔE_{vac}	ΔE_{vac}	$\Delta G'_{bind,solv}$
	ID	Name	AutoDock4	GFN2-xTB	
CB1	CDB000043	H_2CBD	–9.97	–38.73	–26.99
	CDB000011	CBGAM	–8.77	–39.47	–26.90
	CDB000020	Δ^9-THCVA	–11.00	–40.19	–26.89
	CDB000009	CBCV	–9.86	–36.29	–26.74
	CDB000004	CBGM	–9.50	–38.85	–26.65
	CDB000012	CBDM	–10.58	–37.29	–26.59
	CDB000398	CBCA	–9.74	–38.66	–26.45
	CDB000040	2-oxo-Δ3(4)-THC	–11.87	–35.17	–26.42
	CDB000038	cis-Δ^9-THC	–10.01	–38.11	–26.00
	CDB000006	CBGV	–8.91	–37.81	–25.51
	CDB000036	CBCT	–11.09	–31.96	–25.40
	CDB000423	CBEA	–9.74	–36.21	–25.23
	CDB000030	CBNM	–9.62	–31.84	–24.75
	CDB000042	CBCM	–9.90	–32.62	–24.24
	CDB000007	CBC	–10.07	–34.22	–23.47
	CDB000041	Δ1(2)-THCM	–10.20	–30.17	–23.39
	CDB000008	CBCVA	–9.07	–38.16	–21.97
	CDB000015	CBDV	–8.92	–32.63	–20.31
	CDB000017	Δ^9-THCA-B	–10.15	–31.30	–19.99
	CDB000435	CBT	–9.81	–30.68	–19.76
	CDB000027	CBE	–10.19	–30.95	–19.38
	CDB000025	CBLA	–10.91	–32.41	–19.12
	CDB000026	CBL	–10.17	–25.38	–17.91

Table A2. Binding energy (ΔE_{vac}) and uncorrected binding free energy in implicit aqueous solvation ($\Delta G'_{bind,solv}$) in kcal/mol of the best poses of 55 cannabinoids with CB1 and CB2 using Autodock4 and GFN2-xTB method. (cont.)

Protein	Cannabinoid		ΔE_{vac}	ΔE_{vac}	$\Delta G'_{bind,solv}$
	ID	Name	AutoDock4	GFN2-xTB	
CB1	CDB000034	10-ethoxy-9-hydroxy-Δ-6a-THC	–11.46	–26.60	–17.75
	CDB006348	Terpenoids	–8.20	–25.60	–17.29
	CDB000029	CBN	–10.12	–28.99	–17.16
	CDB006351	Hydronaphthalene	–8.52	–21.27	–16.55
	CDB000022	Δ^7-cis-iso-THCV	–10.60	–25.00	–16.21
	CDB006347	Terpenoids	–6.04	–19.92	–14.56
	CDB006349	Terpenoids	–6.23	–16.74	–12.71
	CDB006350	Terpenoids	–6.75	–18.70	–11.59
	CDB006346	Terpenoids	–6.29	–14.87	–11.03
	CDB006352	Terpenoids	–8.26	–15.44	–8.83
CB2	CDB000018	CBGA	–7.82	–43.00	–30.73
	CDB000005	CBGVA	–7.69	–41.31	–30.61
	CDB000035	8,9-dihydroxy-Δ-6a-THC	–9.59	–41.24	–30.59
	CDB000011	CBGAM	–8.60	–40.36	–30.10
	CDB000398	CBCA	–9.32	–44.43	–29.13
	CDB000004	CBGM	–8.34	–36.23	–29.08
	CDB000042	CBCM	–9.18	–33.39	–28.69
	CDB000012	CBDM	–8.82	–35.69	–28.16
	CDB000008	CBCVA	–8.57	–46.11	–28.03
	CDB000027	CBE	–8.90	–38.49	–27.61
		CBTA	–10.21	–40.66	–27.27

Table A2. Binding energy (ΔE_{vac}) and uncorrected binding free energy in implicit aqueous solvation ($\Delta G'_{bind,solv}$) in kcal/mol of the best poses of 55 cannabinoids with CB1 and CB2 using Autodock4 and GFN2-xTB method. (cont.)

Protein	Cannabinoid		ΔE_{vac}	ΔE_{vac}	$\Delta G'_{bind,solv}$
	ID	Name	AutoDock4	GFN2-xTB	
CB2	CDB000007	CBC	–9.02	–33.98	–27.11
	CDB000037	OTHC	–9.82	–35.85	–27.04
	CDB000003	CBG	–7.77	–34.60	–26.59
	CDB000034	10-ethoxy-9-hydroxy-Δ-6a-THC	–10.41	–33.78	–26.36
	CDB000009	CBCV	–8.28	–32.46	–26.29
	CDB000025	CBLA	–9.62	–35.98	–26.23
	CDB000435	CBT	–9.51	–36.39	–26.03
	CDB000423	CBEA	–9.32	–38.14	–25.89
	CDB000014	CBDVA	–7.95	–42.12	–25.64
	CDB000028	CBNA	–9.40	–36.45	–25.64
	CDB000001	Δ^9-THC	–9.00	–32.21	–25.43
	CDB000043	H_2CBD	–8.18	–33.58	–24.67
	CDB000006	CBGV	–7.35	–33.45	–24.62
	CDB000038	cis-Δ^9-THC	–9.14	–32.95	–24.30
	CDB000030	CBNM	–8.67	–29.22	–24.27
	CDB000015	CBDV	–7.69	–35.83	–24.06
	CDB000023	Δ^8-THCA	–9.50	–35.87	–23.89
	CDB000031	CBN-C4	–8.47	–30.27	–23.83
	CDB000017	Δ^9-THCA-B	–8.86	–36.36	–23.57
	CDB000020	Δ^9-THCVA	–9.50	–31.52	–23.49
	CDB000002	CBD	–8.44	–34.18	–23.47
	CDB000036	CBCT	–9.68	–29.05	–23.37
	CDB000019	Δ^9-THC-C4	–8.62	–30.28	–23.12

Table A2. Binding energy (ΔE_{vac}) and uncorrected binding free energy in implicit aqueous solvation ($\Delta G'_{bind,solv}$) in kcal/mol of the best poses of 55 cannabinoids with CB1 and CB2 using Autodock4 and GFN2-xTB method. (cont.)

Protein	Cannabinoid		ΔE_{vac}	ΔE_{vac}	$\Delta G'_{bind,solv}$
	ID	Name	AutoDock4	GFN2-xTB	
CB2	CDB000026	CBL	–8.89	–28.88	–23.09
	CDB000024	Δ^8-THC	–9.45	–30.12	–22.89
	CDB000016	Δ^9-THCA	–9.29	–34.28	–22.42
	CDB000010	CBDA	–9.14	–34.44	–22.36
	CDB000029	CBN	–8.89	–28.61	–22.34
	CDB000040	2-oxo-Δ3(4)-THC	–10.52	–31.04	–22.12
	CDB000021	Δ^9-THCV	–8.54	–28.67	–22.11
	CDB000041	Δ1(2)-THCM	–8.99	–27.71	–21.83
	CDB000032	CBNV	–8.21	–26.40	–20.98
	CDB000022	Δ^7-cis-iso-THCV	–8.76	–25.94	–20.82
	CDB000433	CBND	–8.21	–27.27	–20.77
	CDB006352	Terpenoids	–7.45	–24.57	–20.45
	CDB006348	Terpenoids	–7.68	–23.90	–19.68
	CDB000039	TriOH-THC	–9.87	–33.19	–19.52
	CDB000013	CBD-C4	–7.86	–29.82	–18.59
	CDB000033	CBN-C2	–8.05	–22.45	–17.82
	CDB006347	Terpenoids	–5.23	–21.23	–15.89
	CDB006349	Terpenoids	–6.24	–21.13	–15.43
	CDB006350	Terpenoids	–6.09	–19.13	–14.99
	CDB006351	Hydronaphthalene	–7.70	–16.93	–14.11
	CDB006346	Terpenoids	–6.10	–12.50	–10.44

BIOGRAPHY

Name	Watcharin Kumaeum
Educational Attainment	2019: Bachelor of Science (Chemistry) Thammasat University, Thailand
Scholarship	2020-2022: Scholarship for Talent Student to Study Graduate Program in Faculty of Science and Technology Thammasat University, Contract No. TB 23/2020.

Presentations/conferences

1. W. Kumaeum and P. Jaiyong, “Lignin Model Compounds and Theoretical Study on Pyrolysis Mechanism of Biomass”, poster session of Pure and Applied Chemistry International Conference (PACCON) 2020: Chemistry for Catalyzing Sustainability and Prosperity, Bangkok, Thailand, February 13th - 14th, 2020.
2. W. Kumaeum and P. Jaiyong, “*In silico* studies of cannabinoids targeting COX-2 and CB-2 receptors: a screening of putative anti-inflammatory agents”, proceeding session of Pure and Applied Chemistry International Conference (PACCON) 2022. 771-776: Frontiers in Chemical Sciences for Health, Energy, and Sustainability, Bangkok, Thailand, June 30th - July1st, 2022.